University of Windsor
Scholarship at UWindsor

Electronic Theses and Dissertations | Theses, Dissertations, and Major Papers

2010

Study of Thickly and Thinly Sectioned Melanoma Skin Tissues with Mechanical Scanning Acoustic Reflection Microscopy

Yihan Tian
University of Windsor

Follow this and additional works at: https://scholar.uwindsor.ca/etd

Recommended Citation

Tian, Yihan, "Study of Thickly and Thinly Sectioned Melanoma Skin Tissues with Mechanical Scanning Acoustic Reflection Microscopy" (2010). *Electronic Theses and Dissertations*. 8209.
https://scholar.uwindsor.ca/etd/8209

This online database contains the full-text of PhD dissertations and Masters' theses of University of Windsor students from 1954 forward. These documents are made available for personal study and research purposes only, in accordance with the Canadian Copyright Act and the Creative Commons license—CC BY-NC-ND (Attribution, Non-Commercial, No Derivative Works). Under this license, works must always be attributed to the copyright holder (original author), cannot be used for any commercial purposes, and may not be altered. Any other use would require the permission of the copyright holder. Students may inquire about withdrawing their dissertation and/or thesis from this database. For additional inquiries, please contact the repository administrator via email (scholarship@uwindsor.ca) or by telephone at 519-253-3000ext. 3208.

www.manaraa.com

Study of Thickly and Thinly Sectioned Melanoma Skin Tissues with Mechanical Scanning Acoustic Reflection Microscopy

By

Yihan Tian

A Thesis
Submitted to the Faculty of Graduate Studies
Through the Department of Physics
In Partial Fulfillment of the Requirements for
The Degree of Master of Science at the
University of Windsor

Windsor, Ontario, Canada

2010

© 2010 Yihan Tian

Library and Archives Canada

Published Heritage Branch

395 Wellington Street
Ottawa ON K1A 0N4
Canada

Bibliothèque et Archives Canada

Direction du Patrimoine de l'édition

395, rue Wellington
Ottawa ON K1A 0N4
Canada

Your file Votre référence
ISBN: 978-0-494-70576-6
Our file Notre référence
ISBN: 978-0-494-70576-6

NOTICE:

The author has granted a non-exclusive license allowing Library and Archives Canada to reproduce, publish, archive, preserve, conserve, communicate to the public by telecommunication or on the Internet, loan, distribute and sell theses worldwide, for commercial or non-commercial purposes, in microform, paper, electronic and/or any other formats.

The author retains copyright ownership and moral rights in this thesis. Neither the thesis nor substantial extracts from it may be printed or otherwise reproduced without the author's permission.

AVIS:

L'auteur a accordé une licence non exclusive permettant à la Bibliothèque et Archives Canada de reproduire, publier, archiver, sauvegarder, conserver, transmettre au public par télécommunication ou par l'Internet, prêter, distribuer et vendre des thèses partout dans le monde, à des fins commerciales ou autres, sur support microforme, papier, électronique et/ou autres formats.

L'auteur conserve la propriété du droit d'auteur et des droits moraux qui protège cette thèse. Ni la thèse ni des extraits substantiels de celle-ci ne doivent être imprimés ou autrement reproduits sans son autorisation.

In compliance with the Canadian Privacy Act some supporting forms may have been removed from this thesis.

While these forms may be included in the document page count, their removal does not represent any loss of content from the thesis.

Conformément à la loi canadienne sur la protection de la vie privée, quelques formulaires secondaires ont été enlevés de cette thèse.

Bien que ces formulaires aient inclus dans la pagination, il n'y aura aucun contenu manquant.

Canada

DECLARATION OF ORIGINALITY

I hereby certify that I am the sole author of this thesis and that no part of this thesis has been published or submitted for publication.

I certify that, to the best of my knowledge, my thesis does not infringe upon anyone's copyright nor violate any proprietary rights and that any ideas, techniques, quotations, or any other material from the work of other people included in my thesis, published or otherwise, are fully acknowledged in accordance with the standard referencing practices. Furthermore, to the extent that I have included copyrighted material that surpasses the bounds of fair dealing within the meaning of the Canada Copyright Act, I certify that I have obtained a written permission from the copyright owner(s) to include such material(s) in my thesis and have included copies of such copyright clearances to my appendix.

I declare that this is a true copy of my thesis, including any final revisions, as approved by my thesis committee and the Graduate Studies office, and that this thesis has not been submitted for a higher degree to any other University or Institution.

ABSTRACT

The contents of the present study are organized into two parts: the first is focused on characterizing a thickly sectioned skin tissue with a mechanical scanning acoustic reflection microscopy (hereinafter simply called "SAM") of pulse-wave mode. The second part is focused on characterizing a thinly sectioned skin tissue with tone-burst-wave mode of SAM.

We showed analyses of optical and acoustical images, as well as developed mathematical models using an angular spectrum approach for predicting contrast and characterizing acoustic properties of both sections of tissue. Also, for thin specimens a reflectance function for the tissue located on a substrate was theoretically determined, and fitted into a mathematical model of the V(z) curve. Their leaky surface acoustic wave velocities were obtained from the experimentally formed V(z) curves through FFT analyses. Finally, a computer simulation with a parameter-fitting technique was implemented to obtain the longitudinal wave velocities and densities of the tissues.

Dedicated to my parents

Tian Geng and Fan Kui

ACKNOWLEDGEMENTS

I want to express my sincere thanks to the people who gave me direct or indirect support during my graduate study and my research at the University of Windsor and Pennsylvania State University.

My sincere appreciation first goes to Dr. E. Maeva for her constant and continued support which brought me the peace of mind to freely think, study and research. Her guidance both with respect to the science behind this project and academic pursuit as a whole has been indispensable.

I would especially like to thank Dr. C. Miyasaka who initiated the ideas, taught me advanced ultrasonic imaging and quantitative data acquisition techniques, and kept me in the right direction during my research.

Furthermore, I would like to thank Dr. B. R. Tittmann who kindly provided his facility and equipment, and gave useful advice for my research.

As well, I would also like to thank Dr. D. Shum for his great help to provide a biological specimen and pathological evaluation of an image formed from the specimen.

And finally, I would like to thank Dr. I. Seviaryn for teaching me how to appropriately operate a mechanical scanning acoustic reflection microscope (Pulse-Wave mode) for characterizing a thickly sectioned biological tissue.

TABLE OF CONTENTS

DECLARATION OF ORIGINALITY iii

ABSTRACT iv

DEDICATION v

ACKNOWLEDGEMENTS vi

LIST OF TABLES ix

LIST OF FIGURES x

CHAPTER

I. **INTRODUCTION**

..... 1

II. **REVIEW OF LITERATURE**

2.1 Brief History of SAM 6

2.2 Biological Applications for SAM 13

III. **THICK SECTIONED MELANOMA TISSUE**

3.1 Design and Methodology 21

3.1.1 Imaging Principle (Pulse-Wave Mode) 21

3.1.2 Resolution 26

3.1.3 Description of Specimen 28

3.1.4 Experimental Procedures and Results 29

3.1.4.1 Experimental Setup 29

3.1.4.2 Optical Images 31

3.1.4.3 Acoustic Images (C-Scan) 32

3.1.4.4 Acoustic Images (B-Scan) 34

3.1.4.5 Waveform Analysis 37

3.1.4.6 Frequency Analysis 43

3.2 Physical and Mathematical Modeling 48

IV. **THIN SECTIONED MELANOMA TISSUE**

4.1 Design and Methodology 56

4.1.1 Imaging Principle (Tone-Burst-Wave Mode) 60

4.1.2 Description of Specimen 63

4.1.3 Experimental Procedures and Results 65

4.1.3.1 Optical Image 65

4.1.3.2 Acoustic Image 70

4.1.3.3 TEM Image 74

4.1.3.4 Method for Visualizing Anisotropy.....76
4.2 Physical and Mathematical Modeling 78
4.3 Computer Simulation.....87

V. CONCLUSIONS AND RECOMMENDATIONS
.....93

APPENDICES

A - RAY TRACING OF ULTRASONIC WAVE PROPAGATION.....94
B - ACOUSTIC WAVES IN ISOTROPIC MEDIA.....95
C - REFLECTANCE FUNCTION 99
D - TRANSDUCER OUTPUT 105
E - DETERMINATION OF $u_1^+(x,y)$ 107
F - THEORY OF V(Z) CURVE (Ray Optic Model) 109

REFERENCES.....111

VITA AUCTORIS 118

LIST OF TABLES

Table 1. Comparison of acoustic impedance 29

Table 2. Amplitudes of waveforms 38

Table 3. Center frequency and acoustic signal loss 39

Table 4. Acoustic Properties of Some Biological Tissue and Water 40

Table 5. Parameters of Acoustic Lens 91

Table 6. Physical Parameters of the Biological Tissue 91

LIST OF FIGURES

Fig. 1. Schematic diagram of the experimental setup for the SAM (Pulse-Wave Mode) 23

Fig. 2. Schematic diagram showing reflected acoustic beams from each interface of a specimen system 24-25

Fig. 3. Optical images of thickly sectioned abnormal and normal skin tissues 28

Fig. 4. Setup of the specimen chamber 30

Fig. 5. Optical mosaic images of skin tissues 31

Fig. 6. Acoustic C-Scan images of thick skin tissues 33

Fig. 7. B-scan images of thickly sectioned abnormal and normal skin tissues 35-36

Fig. 8. Reference for waveform analysis 37

Fig. 9. Waveforms obtained from the thickly sectioned abnormal tissue. 38

Fig. 10. A-Scan images of thick melanoma tissue 40

Fig. 11. Setup of specimen in the chamber for attenuation measurement 42

Fig. 12. Schematic diagram showing acoustic reflected beams for attenuation Measurement 43

Fig. 13. FFT reference (FFT of water) 44-45

Fig. 14. FFT analysis of thick melanoma skin tissue 46

Fig. 15. The structure of the specimen and their periphery conditions 51

Fig. 16. Optical image of thinly sectioned melanoma tissue 57

Fig. 17. Acoustic image of the thinly sectioned melanoma tissue with reflected waveform and FFT analysis. (Pulse-Wave Mode) 57

Fig. 18. Resolution Comparison (Tone-Burst-Wave Mode) 59

Fig. 19. Schematic diagram of the SAM (Tone-Burst-Wave Mode) 60

Fig. 20. Interior observation with defocused lens (Tone-Burst-Wave Mode) 62

Fig. 21. Optical images of normal/abnormal specimens at low magnification 64

Fig. 22. Optical images of a thinly sliced normal skin tissue 66

Fig. 23. Montage optical image of abnormal skin tissue 68

Fig. 24. Optical images of melanoma tumor in the dermis 69

Fig. 25. Comparison of optical and acoustic images of normal skin specimen 71

Fig. 26. Comparison of optical and acoustic images of abnormal skin specimen 73

Fig. 27. Maturational stages of melanosomes 75

Fig. 28. Experimental TEM images of thinly sectioned melanoma skin tissue 75

Fig. 29. Schematic diagram of shear wave-buffer rod lens system 76

Fig. 30. Isotropic acoustic images of skin tissues 77

Fig. 31. The V(z) curve (experimental result) for fused quartz 79

Fig. 32. Schematic diagram of contrast mechanism in the spatial distribution 80

Fig. 33. The structure of the specimen and their periphery conditions 82

Fig. 34. SAW velocity acquisition with FFT 87

Fig. 35. V(z) curves obtained at abnormal/normal spot region of the melanoma tissue 88

Fig. 36. FFT analysis obtained at abnormal/normal spot region of the melanoma tissue 89

Fig. 37. V(z) curve simulation of abnormal/normal spot region of the melanoma tissue 92

CHAPTER I

INTRODUCTION

What is melanoma?

Melanoma is a form of cancer that begins in melanocytes (*i.e.*, cells that make the pigment melanin). It may start predominantly in a mole (*i.e.*, skin melanoma), but also may present itself in other pigmented tissues, such as in the eye or in the intestines. It is one of the less common types of skin cancer but causes the majority (75%) of skin cancer related deaths.

The skin is the body's largest organ. It protects the organs inside your body from injury, infection, heat and ultraviolet light from the sun. The skin has two main layers. The layer at the surface is called the *epidermis*. Below the epidermis is the inner layer, the *dermis*. Deep in the epidermis are cells called melanocytes. Melanocytes make melanin, which gives color to your skin. When skin is exposed to the sun, the melanocytes make more melanin and cause the skin to tan or darken. Sometimes melanocytes cluster together and form moles (*i.e.*, *nevi*).

There are three types of skin cancer:

- Squamous Cell Cancer (hereinafter simply called "SCC") starts in the squamous cells (*i.e.*, thin flat cells found on the surface of the skin)
- Basal Cell Cancer (hereinafter simply called "BCC") starts in the basal cells *(I.e.*, round cells that lie under the squamous cells).
- Melanoma starts in the melanocytes.

Melanoma is less common than squamous cell and basal cell skin cancers (sometimes called non-melanoma skin cancers). Melanoma can start in other places in the body where melanocytes are found, such as the eyes, the mouth, or under the fingernails.

Early signs of melanoma are changes in the shape or color of existing moles. A mole, whose medical name is a melanocytic nevus, is a common benign growth of the color cells of the skin called melanocytes. Moles that are irregular in color or shape are suspicious of malignant or premalignant melanoma. Melanoma needs to be detected as early as possible in order for patients to have the best possible prognosis due to its aggressive tendency to invade other tissues of the body. Treatment is much less successful if the cancer is well advanced or has already metastasized to other areas.

How is melanoma diagnosed?

To detect melanomas, it is recommended to be aware of moles and check for changes (*i.e.*, shape, size, color, itching, bleeding and the like). Furthermore, a popular method for remembering the signs and symptoms of melanoma is the so-called mnemonic "ABCDE":

- **A**symmetrical skin lesion. If the lesion was folded in half, the two sides would not match.
- **B**order of the lesion is irregular.
- **C**olors: melanomas usually have multiple colors.
- **D**iameter: moles greater than 6 mm are more likely to be melanomas than smaller moles.
- **E**nlarging: Enlarging or evolving. A mole or skin lesion that looks different from the rest or is changing in size, shape, or color.

Therefore, any moles that are found that have notably altered, or are asymmetric, have irregular borders or coloration, or are more than one-quarter inch in diameter should be of special concern and be brought to the attention of a medical professional.

A biopsy is necessary to make a definite diagnosis of melanoma. The doctor will try to remove all of the unusual-looking growth or mole. The entire tumor along with a margin of tissue that is not a visible part of the tumor is removed. This type of biopsy is called an *excisional biopsy*. If the doctor cannot remove

all of the growth, then a sample of the tissue will be removed. This is called an *incisional biopsy*. The removed tissue sample is examined under a microscope to determine if cancer cells are present and, if so, which kind. If an excisional biopsy is performed, the physician examining the sample also should be able to determine how deeply the cancer has penetrated the skin. If the sample reveals melanoma cells then further testing is usually carried out to determine the extent of the cancer growth before a specific treatment plan is developed.

Present Problems for Biopsy

Excisional biopsy is the preferred method for removing lesions suspected to be melanoma. The main limitation of excisional biopsy is the problem of sampling error. The assumption that pathological examination of a few samples of tissue is representative of the pathological process involving the entire organ is not always correct. This is particularly true when there is a localized pathological process. Furthermore, when performing incisional biopsy, large volumes of the tissues are required in order to reduce the sampling error. It is not realistic to take such amounts from patients suffering from diseases. A technique that enables visualization of in-situ cellular detail in multiple areas would therefore provide superior information to that obtained by biopsy.

Present Problems for Optical Microscopy

Conventional optical microscopes are often used for observing such data from tissues or cells taken from patients. However, the cells or the tissues need to be chemically stained and/or fixed for optical microscopic observation. The staining and/or fixation usually kill the cells. Therefore, when those techniques are applied, it is difficult to understand the real effects of the treatment or the medicine, as the transformation in the tissue may only be visible in living cells. Further, it takes at least one week to prepare the specimen for pathological diagnosis.

Why SAM?

The contrast mechanism of SAM is different from that of a conventional optical microscopy [1]. Since staining and/or fixation of the specimen are not required for the SAM, living cell activities can be observed directly with the SAM [2] so that the sample preparation process can be effectively reduced. Furthermore, SAM can nondestructively observe not only the surface but also the internal structure of the specimen with sub-micron resolution when the SAM is operated at a frequency at 1.0 GHz or more [3]. The SAM also has the capability of measuring the mechanical properties (*i.e.*, loss factor and modulus) of tissues [4]. Therefore, a high frequency ultrasonic diagnostic apparatus could provide pathological information about multiple areas of skin (*i.e.*, epidermis and dermis) and enable a more accurate assessment of pathology. It sampling error is effectively reduced, the transformation of living cells and the real effects of treatment or medicine within the tissue can be observed more readily.

Objective of the Present Work

There are a number of publications on investigating thinly sectioned tissue with SAM [5-18,29], but few publications have studied thickly sectioned biological tissues including cancer cells or tumors [19-23,28]. Here, we present the first attempt to systematically study thin and thick specimens sectioned from the same melanoma skin tissue with the SAM. In this report, the systematic procedures of the acoustic characterization of the thickly sectioned tissue are described.

(1) High Quality Imaging and Characterization of Thickly Sectioned Biological Tissue

The present study investigates the feasibility of applying *in-vivo* acoustic microscopy to the analysis of cancerous tissue. However, observation of an internal structure of a thickly sectioned biological tissue with ultra-high-frequency SAM is relatively difficult for the following reasons. First, an ultrasonic wave is attenuated in proportion to the square of its frequency. Therefore, when a high frequency ultrasonic wave is emitted

from the acoustic lens to the tissue through the coupling medium (*i.e.*, water), the wave may not penetrate into the appropriate internal focal plane of the tissue. Even if the wave can penetrate into the internal focal plane, the wave may not reflect from the tissue to the acoustic lens with enough amplitude to form the acoustic image. Second, when a low frequency ultrasonic wave is used, the image of the appropriate internal focal plane of the specimen may be formed, but the resolution of the image may not be very useful. Most importantly, if the surface has irregularities or is rough, subsurface imaging is sub-optimal. Thus, surface roughness poses a major limitation to acoustic microscopy. In order to overcome these limitations in the present study, or imaging of thickly sectioned cancer tissues was carried out with acoustic lenses operating at frequencies in the range of 25MHz to 250MHz. This was found to provide useful information without some of the disadvantages of the ultra-high-frequency systems. Lower frequency acoustic lenses provide better tissue penetration and stronger backscattered signals. However, to determine the ideal trade-off between resolution and penetration, it is important to establish the lowest frequency at which cellular imaging for identification of tissue pathology is feasible. The resultant images were then arranged to find out appropriate techniques for improving scanning acoustic microscopy of melanoma cancer tissues.

(2) Mathematical Modeling

Using an angular spectrum approach, we developed a mathematical model to analyze waveforms of the transducer output. The approach was found to be useful to predict contrast in an acoustic image of thickly sectioned tissue.

Note that part of the material included in Chapter III of this thesis has been published [157] during the research process.

CHAPTER II

REVIEW OF THE LITERATURE

2.1 BRIEF HISTORY OF SAM

Basic Concept

In 1949, Sokolov suggested the possibilities of SAM as a concept and indicating the advantages such a technology would have over conventional optical light microscopes. He made a remarkable statement in his article that the microstructure of a material could be microscopically visualized when using ultrasound having a frequency at 1 GHz or more [31]. However, the realization of a practical scanning acoustic microscope was delayed until the development of electronic imaging, high frequency processing, and an acoustic lens.

Hardware Development

In 1973, Lemons *et al.* developed a mechanically scanning acoustic transmission microscope including two acoustic lenses (one for emitting focused ultrasound into a specimen and another for receiving the ultrasound transmitted from the specimen), and an RF generator emitting a high frequency of 1 GHz and above [32]. For this type of microscope, a specimen is located between the lenses so that the thickness of the specimen is limited. To overcome this disadvantage, the reflection mode of a mechanically scanning acoustic microscope having one acoustic lens was developed [1]. This type of SAM has been widely accepted as standard hardware in industry because of its simple system configuration and capability of forming a highly resolved image.

Quantitative Data Acquisition

In 1979, Weglein *et al.* found that a change in voltage of an acoustic lens, which gives the so-called V(z) curve, when defocusing the acoustic lens toward

a specimen, is unique to the elastic properties of the specimen [33]. This phenomenon was modeled by ray tracing by Parmon *et al.* [34], and Fourier optics by Atalar [35]. Also, they found that the velocity of surface acoustic waves traveling within a spot of an ultrasonic beam could be obtained by measuring the distance between the periods of the V(z) curves. By the establishment of these basic theories, the SAM became the accepted apparatus for not only imaging but also quantitative data acquisition. After its development, the SAM was modified or newly designed to improve the resolution, contrast, penetration depth, and capability of quantitative data acquisition of the system, as well as to design the SAM for a specific application.

Improvement of Resolution

Resolution of an image formed by the SAM is determined by the frequency of the wave, the wave velocity in the coupling medium, and the lens geometry. Therefore, three approaches were pursued to increase the resolution.

The first approach was to raise the acoustic frequency. By means of this approach, Hadimiooglu *et al.* achieved a resolution of 0.2 micron by operating at about 4.4 GHz with the specimen in boiling water in order to minimize the attenuation of the coupling medium [36]. The second approach was to use low velocity coupling media. Using the second approach, referred to as cryogenic microscopy, Foster *et al.* were able to obtain a resolution of 20 nano-meters using super-fluid liquid helium as coupling medium at a temperature of 0.2°K [37].

These approaches are excellent for increasing resolution on the surface of a specimen, but not necessarily in its interior. In the first approach, the ultrasonic wave is attenuated in proportion to the square of its frequency; therefore, when a high frequency ultrasonic wave is used as a probe, the wave will not penetrate the inside of the specimen, and the internal information may not be obtained. In the second approach, the acoustic impedance if the coupling medium and the specimen are very different, so that most of the

ultrasonic waves are reflected at the interface between the coupler and the specimen, and it is unlikely that an image from any significant depth may be obtained [38]. Hence, acoustic microscopy's most important and unique feature, namely obtaining subsurface information may not be realized by these two approaches.

The third approach, which was to design a new acoustic lens, has been considered to be the best approach for maintaining the most important feature of the SAM. By means of the third approach, the following new acoustic lenses were proposed. Chubachi *et al.* developed the concave transducer to increase resolution by removing spherical aberration [39]. Davids *et al.*, Atalar *et al.,* Yakub *et al.* and Miyasaka *et al.* proposed new acoustic lenses having restricted apertures using Rayleigh waves [40], a non-spherical aperture using Lamb waves [41], a pin hole aperture for near-field imaging [42], and a center-sealed aperture substantially using shear waves [43], respectively.

Improvement of Contrast

Apart from increase in resolution, contrast enhancement is another way to increase imaging quality. Daft *et al.*, Chou *et al.*, and Atalar *et al.* proposed an acoustic lens having a large transducer for phase contrast imaging [44], a shear polarized transducer for increasing contrast of acoustic images [45], and a slit aperture for pseudo line focusing to image anisotropy of materials [46], respectively.

Penetration Depth

In the field of plastic matrix composites, especially fiber-reinforced plastic (denoted as "FRP") laminates, it is necessary to detect delaminations located at an interface between laminates. In the field of inspecting microelectronic integrated circuits (denoted as "IC"), it is necessary to form a cross-sectional image for displaying the details of defects (*i.e.*, voids, delaminations, micro-cracks or the like) located within an IC package. Materials commonly used for these have highly attenuating properties so that a frequency of 100

MHz or higher may not penetrate into a portion of interest. Therefore, to meet the requirements, a new SAM, which is an improved version of C-scan imaging apparatus, was designed for using the time-of-flight method (pulse-wave mode) with the lower frequency range of 10-100 MHz. [47-50]. This SAM can perform A-scan and B-scan as well as C-scan so that conventional ultrasonic techniques can be directly used. Therefore, this type of SAM is the most widely used in various industries [51-56].

Improvement of Quantitative Data Acquisition Methods

Quantitative data (*i.e.*, velocities of surface acoustic waves) obtained by a spherical lens, which is commonly used for acoustic imaging, may not provide sufficient information on the elastic anisotropy of materials. Kushibiki *et al.* developed a cylindrical lens (or called "line-focus lens") and a measuring method to overcome this issue [57].

Liang *et al.* developed a SAM which can obtain complex V(z) curves based on a non-paraxial formulation of the V(z) integral, and a reflectance function of a liquid-solid interface by inverting the V(z) curves formed at frequencies of 10 MHz or less [58]. Endo *et al.* improved the above SAM in terms of mechanical movement and an increase in frequency range (up to 3.00 GHz) to perform higher precision measurements [59].

Kulik *et al.* developed a SAM for continuous wave operation obtaining V(z) curves having better signal-to-noise ratios [60].

Not adopting the V(z) curve techniques, Tsukahara *et al.* developed a SAM, a so-called ultrasonic microspectometer, for accurately measuring an acoustic reflection coefficient of isotropic and/or anisotropic materials at a frequency at 100 MHz or more [61].

Modifications for Applications

(1) Phase Contrast Imaging

An acoustic image can be formed by using either amplitude or phase of the ultrasonic signals reflected or transmitted from a specimen. The amplitudes were often used to form the image because of the simplicity of designing electric circuits. However, the phase contrast can often provide significant information such as a residual stress distribution.

Nikoonahad developed the tilted transducer to obtain the differential phase contrast [62]. Meeks *et al.* developed a phase-sensitive SAM, which operated at large bandwidth into the GHz regime [63].

(2) Use of Various Coupling Media

Water is commonly used as a coupling medium for the SAM. However, some specimens allow only dry conditions. Attal *et al.* proposed liquid metals (*i.e.*, mercury or gallium) as coupling media [64]. Wickramasinghe *et al.* developed a SAM using gases (*i.e.,* Argon and Xenon) as coupling media under elevated pressure [65]. To increase resolution, Karaki *et al.* developed an acoustic microscope using liquid nitrogen instead of superfluid liquid helium, and obtained images at 1.0 GHz [66]. Yamanaka *et al.* developed a low-temperature microscope to study a 0.5 mm thick epoxy bonding between two 1mm Polymethyl Methacrylate (PMMA) sheets at 40 MHz at –50°C using methyl alcohol as a coupling medium [67]. The above types of SAMs were designed for use strictly in a laboratory because they required environmental chambers for the coupling media.

For industrial use, the air-coupled SAM is desirable although the resolution is limited. The challenge is the transfer of acoustic energy across the solid/air interface. A calculation of the transmission coefficient between a steel-transducer-face-plate and air is equal to only 1.797×10^{-5}. This means that 99.996% of the power is reflected back from the interface. Therefore, an appropriate transducer needed to be developed. Fox *et al.* manufactured transducers using silicone rubber as the front acoustic impedance matching layer, and operating frequencies at 1 MHz and 2 MHz [68]. By using such a transducer operating frequency at 1 MHz, the distance in air could be

measured from 20 mm to 40 mm with an accuracy of 0.5 mm. Further improvements in transmission efficiency were shown by planting an acoustic impedance matching layer that is composed of tiny glass spheres in matrix of silicone rubber on piezoelectric elements [69], and [70]. Reilly *et al.* have reported air-coupling transducers using piezoelectric composites, and operating with tone-burst waves with frequency ranging from 250 kHz to 1.5 MHz. They have been successful in producing transmitted signals (milli-volt level) through a composite laminated honeycomb structure at 500 kHz [71]. Shindel *et al.* developed a micro-machined capacitance air transducer characterized by high bandwidths for evaluating composite materials [72]. The micro-machined capacitance air transducer could be operated with frequency at 11.4 MHz [73]. Bhardwadj *et al.* equipped a transducer for a non-contact SAM (reflection type) [74].

(3) Elevated Temperature

Observation of changes of interior portions of materials due to a temperature increase had been desired with the SAM. Miyasaka *et al.* developed a SAM for operating temperature up to 500°C to observe a specimen located in motor oil [75]. Ihara *et al.* developed a SAM for operating up to 920°C for liquid metals [76]. However, issues such as frequency increase still remain.

(4) Nonlinear Imaging with High Frequency Ultrasound

The sharply convergent acoustic beam used in the SAM can provide sufficient intensity to produce strong nonlinear effects at microwave frequencies. First, nonlinear imaging was performed with a mechanically scanned transmission acoustic microscope. Second, harmonic acoustic radiation generated in the vicinity of the beam focus is readily detected and used to form an image of an object placed in the focal plane [77]. To obtain nonlinear data, the receiving transducer is tuned to either the second or third harmonic. When harmonics are produced, the resultant images have a complex appearance. However, a significant portion of the detected signal is due to the non-linearity not associated with specimen, but for example, with the water serving as a

coupling medium. To minimize these phenomena, Yeack *et al.* used a three-lens scanning acoustic microscope (transmission type) to achieve non-secular oblique incidence. This enables the mixing of two independent inputs to occur only in the specimen, thus eliminating the contribution from, for example, the water coupling medium [78]. Germain *et al.* used high-order harmonic acoustic radiation to form nonlinear images with a mechanically-scanned reflection acoustic microscope [79], and evaluated biological media [80]. Tan *et al.* constructed a micron wavelength acoustic microscope to observe third-order nonlinear products [81]. More recently, nonlinear effects have been studied in pressurized superfluid helium in which resolution was shown improved beyond the diffraction limit [82-85]. Recently several investigators have studied non-linear propagation with application to acoustic tomography [86-89].

2.2 BIOLOGICAL APPLICATIONS FOR SAM

In the biomedical field, many new treatment methods and new medications have been developed. Obviously, their effects and side effects need to be studied qualitatively and quantitatively. Conventional optical microscopes are often used for observing such data from tissues or cells taken from patients as specimens. However, the cells or the tissues need to be chemically stained and/or fixed, in order to emphasize particular tissue features of interest for optical microscopic observation. Such staining and/or fixation can be quite involved and elaborate, many can take several days to implement and they usually kill the cells. Therefore, when these techniques are applied for microscopy, it is virtually impossible to visualize fresh or living tissue, as well as it is difficult to understand the real effects of the treatment or the medicine, because the transformation of interest in the tissue may only be visible in living cells.

On the other hand, the contrast mechanism of a mechanical scanning acoustic reflection microscope is different from that of a conventional optical microscope; it has great inherent sensitivity and requires no staining to bring out the features of interest [90]. Hence, acoustical methods permit us, in principle, to observe living cells in fresh tissues. Furthermore, the SAM can nondestructively observe not only the surface but also the internal structure of the specimen with sub-micron resolution [91]. Although, as will be seen, many similarities do exist between optical and acoustic images, many of the important differences (such as the differences between the optical and elastic properties of tissue) are not well known or fully appreciated. Part of the problem centers on the fact that many of the subtle features noted in the acoustic image are not understood or have not yet been correlated with a particular biological process.

The acoustics have strong correlations to physics. Since a biological tissue is assumed to be a liquid material or soft solid material, the elastic bulk modulus, Young's modulus and Poission's ratio can be applied to assess the elastic properties of biological tissues. Also, the sound speed and density of the

tissue have close relation to elasticity of the tissues. The SAM has the capability of measuring the mechanical properties (*i.e.*, loss factor and modulus) of biological specimens. Even from the beginning of acoustic microscopy in the mid-1970's, biomedical problems were thought to be an important application area for this new technology.

The first attempt to study the microstructure of biological specimens with a mechanical scanning acoustic transmission microscope was undertaken by Lemons and Quate [92]. Maev *et al.* extended this technique, and intensively applied it to various biological objects [93-95]. For their type of a system, a specimen is located between the lenses so that the thickness of the specimen is limited. Therefore, this technique did not receive widespread attention, and over the past two decades wide application of acoustic microscopy to biomedicine never developed as initially predicted. Recently, however, a new generation of scientists has rediscovered acoustic microscopy and is applying this tool to a myriad of applications in both the basic sciences as well as diagnostic medicine. Biologists are beginning to apply acoustic microscopy to the study of living cells, including cellular development and biochemical processes, in a way simply not possible with any other imaging modality. Pathologists are beginning to use acoustic microscopy to develop a new gold standard by which tissue changes and disease processes may be defined. Medical scientists are developing new tools, based on acoustic microscopy technology, for the non-invasive and minimally invasive diagnosis of tissue state.

Cell Visualization

In 1979, R. Johnston *et al.* investigated the possibility of using SAM to analyze subcellular components [96]. By sequential viewing of identified fixed cells with acoustic, light, and electron microscopy, they have established that the acoustic microscope can readily detect such features as nuclei and nucleoli, mitochondria, and actin cables. Under optimal conditions, images can even be obtained of filopodia, slender projections of the cell surface that are approximately 0.1–0.2μm in diameter. It has also been proposed that acoustic microscopy technology might be adopted for *in vivo* applications.

SAM has been applied in medicine and biology by Tohoku University since 1980 [97,98]. There are several objectives for using SAM for medicine because SAM can be applied for intra-operative pathological examination since it does not require a special staining technique.

Biological cells and/ or tissues with acoustic impedances close to that of water and virtually no contrast caused by the difference in reflection coefficient have been displayed in acoustic micrographs. Basically, contrast in the acoustic images of living cells in the tissues was generated from the acoustic properties (*i.e.*, density, stiffness, and the variation in attenuation) of the cells as the acoustic waves propagate within the tissues. Hence, it was necessary for the specimens to be mounted onto substrates composed of highly reflective materials (*i.e.*, glass, fused quartz, or the like) as background for making maximum use of the variation in absorption. Using this technique, Hildebrand *et al.* applied the SAM to acoustically visualize different living cells grown on substrates of different materials [99]. They report preliminary results of the observation by high-frequency acoustic microscopy of living cells *in vitro*. Variation in distance separating the acoustic lens and the viewed cell also has a profound effect on the image. When the substratum is located at the focal plane, thick regions of the cell show a darkening that can be related to cellular acoustic attenuation. When the top of the cell is placed near the focal plane, concentric bright and dark rings appear in the image. The location of the rings can be related to cell topography, and the ring contrast can be correlated to the

stiffness and density of the cell.

Additionally, for investigation of the feasibility of imaging at the cellular level using acoustic microscopy, P. Anthony *et al.* have examined the possible effects of high-frequency ultrasound on cellular integrity of cultured fibroblasts [100]. Their results show that the exposure of fibroblasts to 600MHz ultrasound at intensities sufficient to image cellular detail did not result in observed changes in cell shape, cell swelling, or disruption of the cell or nuclear membrane. Moreover, neither thermal nor non-thermal effects were observed and the acoustic power levels were estimated to be well below those where adverse effects are noted.

Y. Saijo *et al.* evaluated the human umbilical vein endothelial cells (HUVECs) before and after exposure to endotoxin by using SAM with a frequency range of 100-210MHz. The acoustic images were successfully obtained to identify the outer shape of the HUVEC and the location of the nucleus in the cell. The attenuation of the nucleus is higher than that of the cytoplasm. The attenuation of the cytoplasm was increased and became inhomogeneous after endotoxin exposure. Thus, they demonstrated that SAM is useful for assessing cellular viscoelastic properties since it can detect both the morphological and acoustic changes without contacting the cellular surface [101].

Also, acoustic microscopy in principle allows distinguishing between modulation of the signal by the viscous properties of a material and its elastic properties. It is a unique tool for the investigation of mechanical properties of cells. This might bridge the gap between the level of supra-molecular structures and ultrasound signals used in medical diagnosis. In the last decade several efforts have been made to obtain elastic properties of a variety of materials by acoustic microscopy techniques. This is done by analyzing the V(z) curve which is also known as the acoustic material signature (AMS) of the investigated specimen. Investigations of biological cells by acoustic microscopy have been performed by Hildebrand *et al.* [102,103], Hildebrand and Rugar [104], Bereiter-Hahn [105,106], and Litniewski and Bereiter-Hahn [107] among others. Some of these investigations outlined a qualitative

connection between image contrast and cellular elastic properties [102,103,105,106] and some others [104,107] tried to obtain quantitative measurements of elastic properties of cells on a microscopic scale. There are quite a few publications reporting that the elastic properties of living cells with SAM [108-114] were investigated.

V(z) Curve

V(z) curves show the variation of voltage generated by an acoustic microscope as the distance between the microscope lens and the specimen varies. Different researchers used V(z) curves for measuring different properties of materials; Kushibiki *et al.* [115,116] evaluated velocity and attenuation of surface waves analyzing the V(z) curves, Weglein [117,118] measured coating thickness; Kushibiki *et al.* [119] suggested the possibility of using it for material anisotropy investigation, Briggs and his associates [120] used it for crack detection, Yamanaka *et al.* [121] measured rates of surface hardening, Kino and his associates [122] measured residual stress patterns in materials, Hildebrand and Rugar [123], Litniewski and Bereiter-Hahn [124] determined elastic properties of living and dead cells from V(z) analyses. Every investigator computed V(z) curves with different simplifying assumptions which are appropriate for their analysis. Then experimental V(z) curves were properly compared with the corresponding theoretical V(z) curves to obtain parameters of interest.

Tissue Characterization

Similarly, the elastic microstructure and properties of various thinly sliced tissues have also been studied [125-131]. However, few articles have been published for a tissue including cancer cells or tumors [132-138]. They have been conducted with liver, prostate and eye cells, performed with frozen or formalin-fixed slices, and have demonstrated that acoustic images distinctly and precisely reveal abnormal portions in the tissues.

A group of researchers at University of California at Irvine determined that the obtainable resolution of a 600 MHz SAM was sufficient to render a microscopic

diagnosis [139,140]. Their studies began with a detailed comparison between optical and acoustic microscopy. The optical image is of a standard hematoxylin and eosin (hereinafter called simply "H&E") section; (*i.e.*, the tissue has been fixed and stained to bring out those features which could lead to a diagnosis). The acoustic image was made from the adjoining tissue block and was neither fixed nor stained. However, it was frozen to permit accurate slicing. The samples were 6 microns thick. Since the optical images represented the standards used for making a pathological evaluation, the acoustic imaging was attempted to produce similarities to their optical counterpart.

Y. Saijo *et al.* have shown that SAM can also classify the types of cancer in the stomach [141] and kidney [142] by quantitative measurement of ultrasonic attenuation and sound speed at 200MHz.

Ultrasonic data obtained with high-frequency SAM can be used for assessing reflectability or texture in clinical echo-graphic imaging. It has been shown that the calculated reflection and clinical data were matched in the myocardium [143]. Chandraratna *et al.* also assessed the echo-bright area in the myocardium by using 600 MHz SAM [144]. The values of attenuation and sound speed in six types of tissue components in atherosclerosis were measured by 100~200 MHz SAM [145]. As the term arteriosclerosis means hardening of the artery, atherosclerotic tissues have been known to increase in stiffness or hardness in the development of atherosclerosis. Assessment of the mechanical properties of atherosclerotic tissue is important, in addition to determining the chemical components of the tissue. The composition of atherosclerotic tissue is defined as the collagen fibers, with lipid and calcification in the intima, smooth muscle and elastic fiber in the media, and collagen fibers in the adventitia, respectively. Variations in the degree of staining for optical microscopy indicate that the collagen content or the chemical property is not homogeneous in fibrotic lesions in the intima.

The recent introduction of high frequency ultrasound in dermatology has opened new perspectives concerning skin architecture studies and skin

diagnosis in dermatological disease. Up to now, only a few quantitative studies on skin have been reported in the literature. Skin attenuation measurements [146-151] have been done in most cases in the transmission mode for characterization of wounds, aging and burns of the skin. T. Baldeweck *et al.* present the first simulation study on attenuation measurements for the skin with the reflection mode [152]. Since skin is a highly attenuating medium, the measurement of acoustic attenuation in biological tissues has received much interest in the field of ultrasound tissue characterization. For most biological tissues, the frequency-dependent attenuation varies linearly with frequency across a usable frequency bandwidth. With this assumption of a linear-with-frequency attenuation (β in dB/cmMHz) and a Gaussian spectrum (the spectral variance is a constant σ^2 versus depth), the attenuation coefficient β can be calculated with the following relation:

$$\beta = \frac{8.68}{c\sigma^2} \cdot \frac{df_c}{d\tau} \tag{2.1}$$

where c is the speed of sound in the tissue.

For soft tissue characterization in the reflection mode, the spectra can be estimated with the classical Short Time Fourier Analysis using Fast Fourier Transform (hereinafter called simply "FFT") [153]. However, in the case of highly attenuating media, limitations due to the method (stationarity, window size) may prevent the use of Fourier analysis. Normally we find a higher attenuation in cancerous tissue [154].

Thick Biological Tissues

To date, biomedical imaging with ultrasound for observing cellular tissue structure has been limited to very thinly sliced tissue at very high ultrasonic frequencies (*i.e.*, 1GHz). Research has been done mainly concentrated on thinly sectioned biological tissues which are of several micrometer thicknesses. However, only a few publications have been made for thick section biological tissues [155-157]. E. Maeva *et al.* conducted an *ex vivo* imaging and characterization of a fixed but unfrozen human breast cancer tissue that contains breast cancer tumors with thickness about 2-5mm [155]. The appropriate frequency range is 15-50MHz to produce the optimal resolution

and contrast. C-scan images were shown to correlate well with corresponding optical images. Also, the internal structures could be highlighted in C-scan images that were not visible from the surfaces of the slice. Moreover, velocity and attenuation image maps of the sample were also made and used to identify the tumor regions based on quantitative criteria.

Further, a recent study to investigate the feasibility of applying *in-vivo* acoustic microscopy to the analysis of cancerous tissue was investigated by C. Miyasaka and E. Maeva *et al.* [157]. The study implemented ultrasonic imaging for both thinly and thickly sectioned normal/abnormal skins, (abnormal skin tissue contains a large amount of malignant melanoma tumors). Both tissues were ultrasonically visualized with two different modes (*i.e.*, pulse and tone-burst wave modes) to obtain the highest quality ultrasonic images, and in order to select the best mode for the design of a future SAM for *in vivo* examination. In addition, a mathematical modeling technique based on an angular spectrum approach for improving image processing and comparing numerical to experimental results was developed.

CHAPTER III

THICK SECTIONED MELANOMA TISSUE

3.1 DESIGN AND METHODOLOGY

3.1.1 Imaging Principle (Pulse-Wave Mode)

Figure 1 is the schematic diagram of the SAM (pulse-wave mode). The imaging mechanism of the pulse-wave mode is described below.

An electrical signal (*i.e.*, pulse wave) generated by a RF source is transmitted via a circulator to a piezoelectric transducer (*i.e.*, $LiNbO_3$), located on the top of a long buffer rod designed for the time-of-flight method. Input voltage from the source to the transducer is approximately 100 V. The electrical signal is converted into an acoustic signal (*i.e.*, ultrasonic plane wave) by the transducer. The ultrasonic plane wave travels through the buffer rod made of fused quartz to a spherical recess (hereinafter called simply the "lens") located at the bottom of the buffer rod. The lens converts the ultrasonic plane wave to an ultrasonic spherical wave (*i.e.*, ultrasonic beam).

The specimen is located on a c-cut sapphire substrate (thickness: 1.78 mm), and is submerged in de-ionized water. A biological tissue with acoustic impedances close to that of water has virtually no contrast because differences in reflection coefficients are displayed. In other words, the contrast in the acoustic image of the tissue is generated from the variation in attenuation from tissue structure to tissue structure as the acoustic waves propagate within the tissues. Therefore, it was necessary for the specimens to be mounted onto substrates composed of highly reflective materials (*i.e.*, sapphire, fused quartz, or the like) as background for making maximum ultrasound signal reflection.

The ultrasonic beam is focused on the back surface of the specimen via a thin transparent poly-silicon cover, and reflected from the back surface. It comprises a variety of properties such as good electrical insulation, thermal stability, low toxicity, low chemical reactivity, etc., which are suitable for medical preparation and applications. Also, it is stable for months and even years and, in contrast to other materials, insensitive to rough handling. The thickness of the cover is about 0.5 mm. The cover *(i.e.*, Cover Well™ imaging chamber gasket with adhesive) is manufactured by Molecular Probes. The cover was fixed by an aluminum holder. When the specimen does not have noticeable surface roughness, it is not necessary to place the cover for visualization. The reflected ultrasonic beam, which carries acoustic information of the specimen, is again converted into an ultrasonic plane wave by the lens. The ultrasonic plane wave returns to the transducer through the buffer rod. The ultrasonic plane wave is again converted into an electric signal by the transducer.

Suppose that a pulse wave emitted from an acoustic lens via a coupling medium (*i.e.*, de-ionized water) is focused on to the back surface of the specimen. Suppose that the pulse wave is strong enough to travel through the specimen and reflect back to the acoustic lens. The timing of each reflection is different because the traveling distance is different. The waveform includes information such as amplitude, phase, or delay, and can be monitored by the oscilloscope (see Fig. 2). The reflected pulse wave is electronically gated out to visualize the portion of a horizontal cross-sectional image by horizontally scanning the acoustic lens.

The acoustic lens is able to translate axially along the z-direction varying the distance between the specimen and the lens for clearly focused sub-surface focusing to obtain clear visualization. That is, when the acoustic lens is focused on the surface of the specimen, the amplitude of the reflected signal from the surface is optimized (we denote z = 0 μm). Then, we look for a reflected signal from the specimen. When focusing the acoustic signal reflected from the subsurface plane of the specimen, the acoustic lens is mechanically move towards the specimen (we denote z = - x μm, where x is

the distance from the surface to the subsurface of the specimen) until the amplitude of the reflected signal is optimized.

In order to form a two-dimensional acoustic image, an acoustic lens is mechanically scanned across a certain area of the specimen.

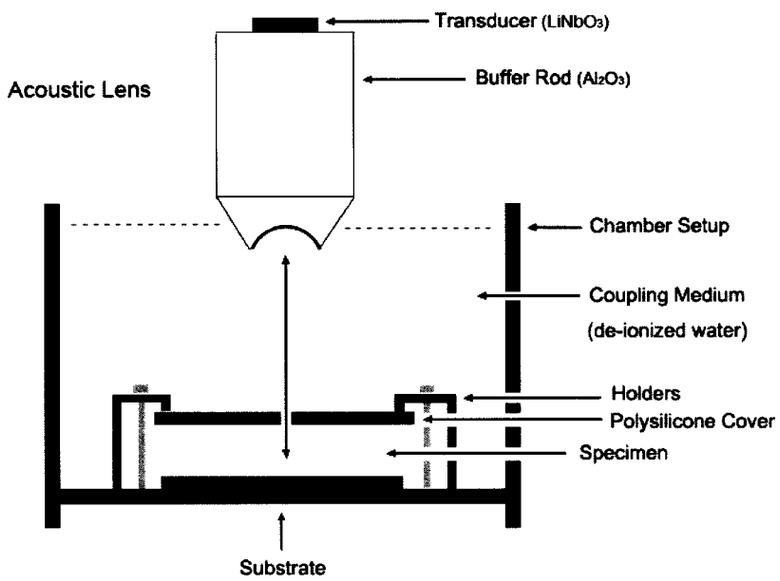

Fig. 1: Schematic diagram of the experimental setup for the SAM (Pulse-Wave Mode). An appropriate acoustic lens must be selected considering its penetration depth in a specimen and resolution in the image obtained from the interior plane of the specimen.

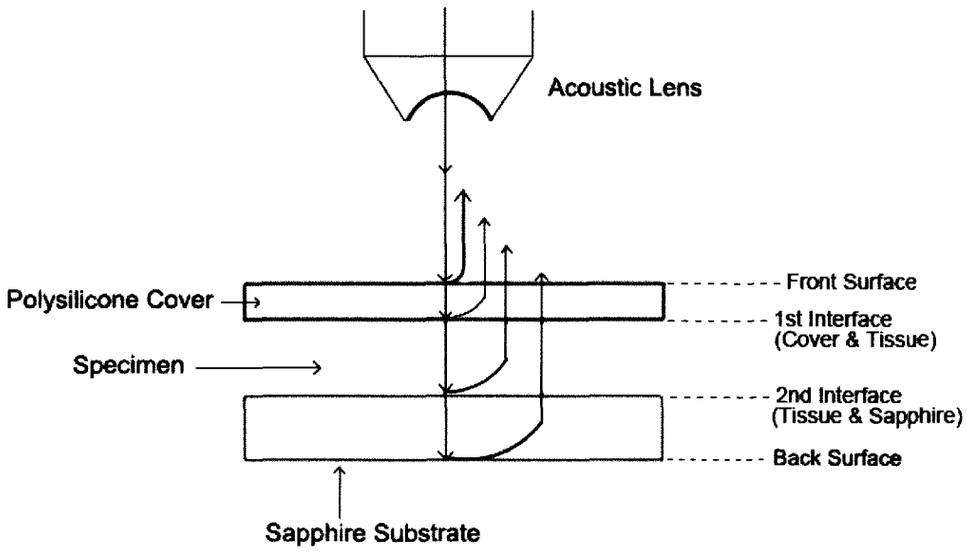

Fig. 2(a): Schematic diagram showing reflected acoustic beams from each interface of a specimen system.

In this setup, a thickly sectioned biological specimen is sandwiched between a thin transparent poly-silicone cover and a sapphire substrate. Four reflections of the acoustic waves are shown. The reflections are from the surface of the cover, interface between the cover and the front surface of the specimen, the interface between the back surface of the specimen and the surface of the substrate and the back surface of the substrate, respectively. Thickness of specimen is measured as substantially 2.1 mm.

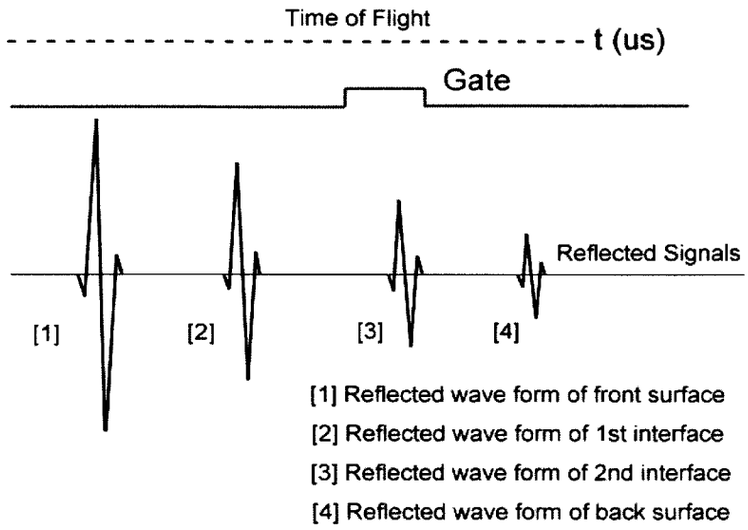

Fig. 2(b): Schematic diagram of acoustic waves from the specimen located on the substrate via a cover. The diagram shows timings of reflected pulse waves reflected from a specimen.

The 1st signal is the reflected wave from the surface of the cover. The 2nd signal is the reflected wave from the 1st interface between the back surface of the cover and the surface of the specimen. The 3rd signal is the reflected wave from the 2nd interface between the back surface of the specimen and the front surface of the substrate. The 4th signal is reflected wave from the back surface of the substrate.

For forming an interior acoustic image, a gate is set on an appropriate reflected signal. Selecting the appropriate reflected signal from the specimen is an important step in the experiment. This step can be implemented by observing the change of signal amplitude when moving the acoustic lens along its z-axis. When the acoustic lens is focused on the interior plane of the specimen, the amplitude of the wave from the interior plane is maximized.

In this study, the 3rd reflected wave is gated to visualize the specimen interior. Since the specimen is acoustically transparent, no image can be formed by gating the reflected signal from the 1st interface. (see appendix A)

3.1.2 Resolution

Two types of resolution must be considered for the SAM. One is a lateral resolution (*i.e.*, Δr), and the other is a vertical resolution (*i.e.* $\Delta\rho$). They are expressed as follows [158]:

$$\Delta r = F\lambda = F\left(\frac{v_w}{f}\right) \tag{3.1}$$

$$\begin{aligned}\Delta\rho = 2F^2\lambda &= \left(2F^2\right)\left(\frac{v_w}{f}\right)\\ &= 2\left(\frac{f_0}{D}\right)^2\left(\frac{v_w}{f}\right)\\ &= 2\left(\frac{1}{2\tan\theta}\right)^2\left(\frac{v_w}{f}\right)\\ &= \frac{1}{2\tan^2\theta}\left(\frac{v_w}{f}\right)\end{aligned} \tag{3.2}$$

where F is a constant related to lens geometry (*i.e.,* F-number), which is given by F=focal length/diameter of entrance pupil, λ is the wavelength in the coupling medium (*i.e.*, de-ionized water), f is the frequency of the wave generated by the transducer, v_w is the longitudinal wave velocity in the coupling medium, f_0 is the focal distance of the lens, D is the diameter of the lens aperture, and θ is one-half of the aperture angle of the lens.

In order to observe cellular details within the tissue, the maximum lateral resolution, Δr, has to be at least the same size of a cell, and is about 10 μm. For example, suppose the acoustic wave velocity in water is 1,500 m/s, and the F-number is 0.7. Then the lowest frequency for pulse-wave mode to visualize the cells is approximately 100 MHz. Therefore, when the frequency of the transducer output signal is less than 100 MHz, the pulse-wave mode apparatus with the conventional c-scan technique is not capable of visualizing the cells.

Referring to Eq. (3.1), we know that the resolution of the image formed by the SAM is determined by the frequency of the ultrasonic wave, the velocity in the

coupling medium, and the lens geometry. Therefore, one approach to increase resolution is to increase the acoustic frequency. However, as can be appreciated, the ultrasonic wave is attenuated in proportion to the square of its frequency; therefore, when a high-frequency ultrasonic wave is applied as a probe, the wave will not penetrate to a significant depth inside the specimen, and the internal information may not be obtained. Therefore, we need to know the upper limitation of the frequency which can be applied to the biomedical imaging of thickly sectioned tissues.

3.1.3 Description of Specimen

Figure 3(b) is a thickly sectioned normal skin tissue. The tissue is consistent in color and softness. The thickness of the tissue is 3.0 mm. Figure 3(a) is a thickly sectioned abnormal skin tissue. The abnormal tissue has a firmer consistency, is substantially flatter, and has less surface roughness. When compared to normal tissue, its thickness is also 3.0 mm. The tissue includes black, white, and yellow colored portions. The black colored portions have been diagnosed as melanoma carcinoma. In addition, the carcinoma area has less surface roughness than the normal sections.

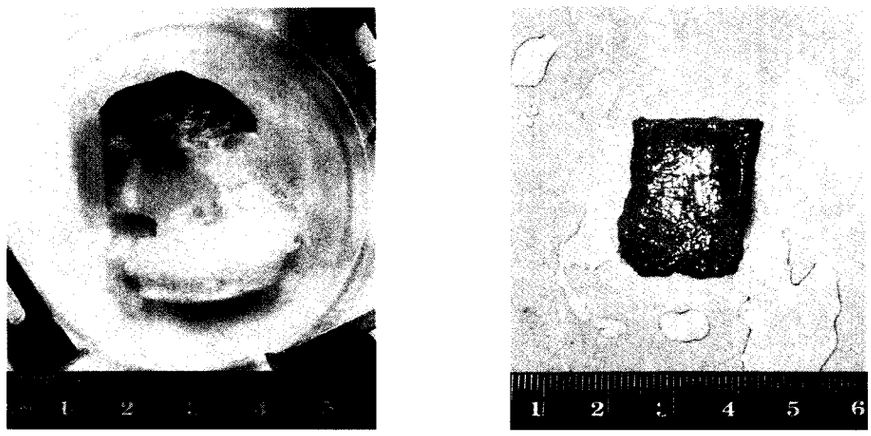

(a) (b)

Fig. 3: Optical images of thickly sectioned abnormal and normal skin tissue.

The images are formed by the digital camera (Olympus); (a) Thickly sectioned melanoma tissue including groups of cancer cells, (b) Thickly sectioned normal skin tissue

3.1.4 Experimental Procedures and Results

3.1.4.1 Experimental Setup

Acoustical Image

Figure 4 shows a thickly sectioned skin tissue as a specimen located on the surface of a substrate made of c-cut sapphire with a thin transparent poly-silicone (thickness: 500 μm) cover pressed onto the tissue by a holder made of aluminum. The cover makes the surface of the specimen flat, thereby reducing effects to the acoustic image caused by surface roughness. The cover also prevents the specimen from floating into the water. The chamber is filled up with a coupling medium (*i.e.*, water). For obtaining better acoustic reflection, the specimen is located on a substrate made of a material having highly reflective property such as a sapphire (see Table 1).

Table 1: Comparison of Acoustic Impedance, Z

Polystyrene	$Z= 2.52\ kg/m^2 \times 10^6$
Silica Glass	$Z= 13.0\ kg/m^2 \times 10^6$
Sapphire	$Z= 44.3\ kg/m^2 \times 10^6$

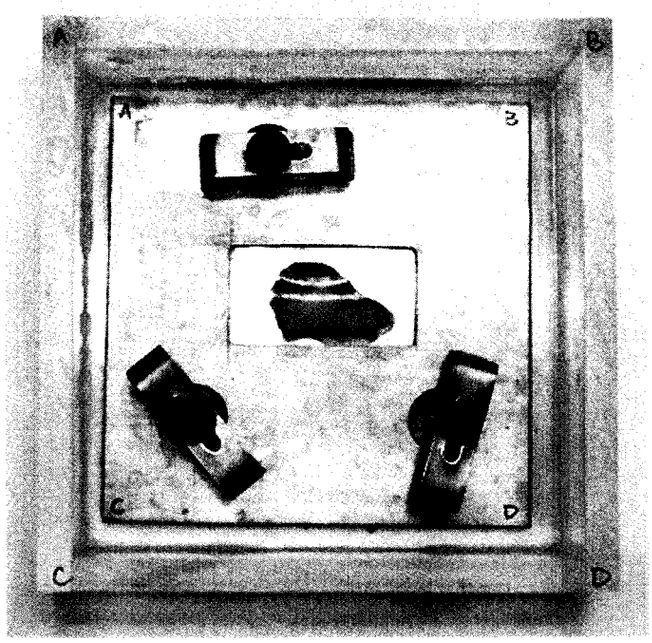

Fig. 4: Setup of the specimen in the chamber.

The thickly sectioned melanoma tissue is placed on the sapphire substrate; is covered by a transparent cover made of poly-silicone, and is pressed by the holder toward the substrate to reduce the effect on the acoustic image caused by surface roughness.

3.1.4.2 Optical Image

Figures 5 (a) and (b) are comparisons of the optical images of horizontal cross-sections of the thickly sectioned melanoma and normal skin tissues. These images are formed by Stereoscopic Microscope (Olympus, Model: SZX16). The optical image shows only the surface information of the thick tissues. The surface of melanoma tissue varies in contrast, which indicates the specimen has difference in electromagnetic properties. However, the normal skin tissue is consistent in contrast, meaning the internal structure of the specimen is continuous.

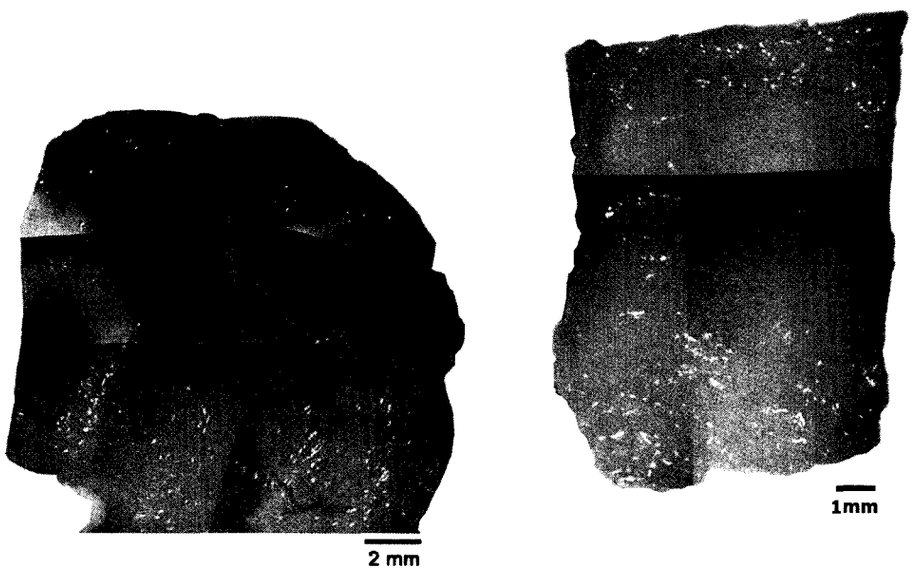

(a) Optical Image of the Melanoma Skin Tissue **(b)** Optical Image of the Normal Skin Tissue

Fig. 5: Optical montage images of both horizontal cross-sections of thickly sectioned melanoma and normal skin tissues (thickness: 3mm).

By comparison with the normal tissues, the appearance of the black coloration in the abnormal tissue is evidently recognized as melanoma. The optical image of the abnormal tissue shows the full extent of the carcinoma tumors spread mostly in the epidermis and the dermis, as well as some that have scattered into the hypodermis and appeared around the cartilage, which is present in the yellow zone that is surrounded by mostly fat. Within this zone, cartilage is merged with adjacent supporting tissue containing adipocytes, capillaries and small nerves.

3.1.4.3 Acoustic Images (C-Scan)

Figures 6 (a) and (b) show acoustic C-Scan images of both thickly sectioned abnormal melanoma and normal skin tissues horizontal cross-sections (thickness: 3mm), respectively, with an acoustic lens (Olympus NDT) which has an operating frequency at 50 MHz. The input frequency was 50 MHz, which was the maximum frequency emitted from the acoustical lens to the specimen. The acoustic beam was focused at the interface between the specimen and the substrate. (*i.e.*, Z=0 μm or V(0)). The resolution of the image is limited due to the frequency of the acoustical lens. At this point we are unable to diagnose the melanoma cancer cells from the acoustic images of the thick tissues. However, they show both the surface and the internal structures of the thickly sectioned tissue. Since the images cannot review cellular details of the thickly sectioned tissue, we need to select an acoustic lens capable of operating at a frequency at 50 MHz or more.

Furthermore, since acoustic properties (*i.e.*, reflection coefficient, attenuation, and velocity of acoustic wave) and the surface condition (*i.e.*, surface roughness and discontinuities) of the specimen are factors in forming acoustic images, it is also significantly important to study the acoustic images in order to obtain the acoustic properties and surface condition. Therefore, waveforms, FFT analysis and B-Scan images need to be performed and carefully reviewed.

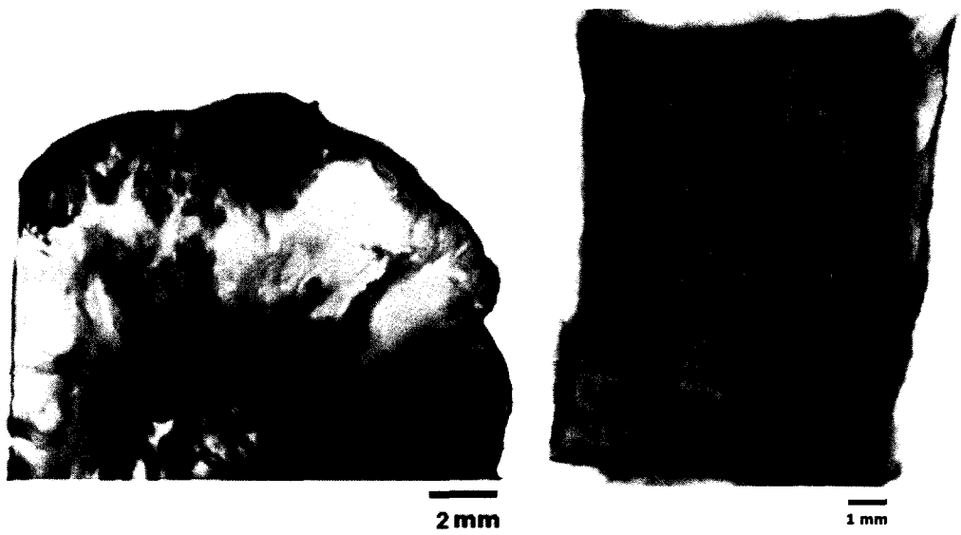

(a) Acoustic Image of the Melanoma Skin Tissue **(b)** Acoustic Image of the Normal Skin Tissue

Fig. 6: (a) An acoustic Image (C-Scan) of a thickly sectioned melanoma skin tissue (Left), and (b) a normal skin tissue (Right). Thickness of the tissues is about 3mm. Operating frequency for pulse wave mode is 50 MHz.

3.1.4.4 Acoustic Images (B-Scan)

A SAM b-scan image can form a vertical cross-sectional 2-D image of a specimen. Figures 7(a) and 7(b) are B-scan images of melanoma and normal skin tissues, respectively, and show the pseudo surface condition of the normal and abnormal tissues. Figure 7(a) clearly illustrates the surface is much rougher. The surface structure of the normal tissue is more uniform, consistent, and homogeneous. The pseudo-surface discontinuities correspond and are seen as the contrast difference in C-scan images, which is caused by attenuation (*i.e.*, absorption of ultrasound) due to surface irregularities. This leads to a significant understanding of the contrast mechanism of ultrasound.

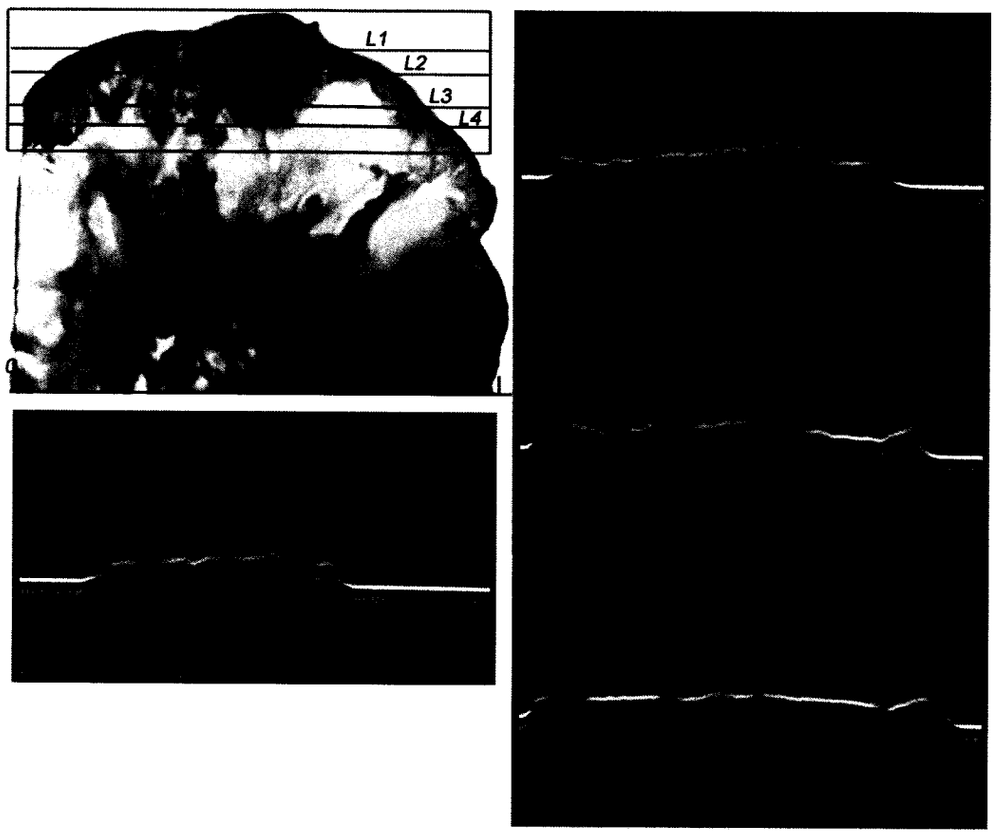

(a) Melanoma Tissue (Frequency: 50 MHz; Mode: Pulse-wave mode)

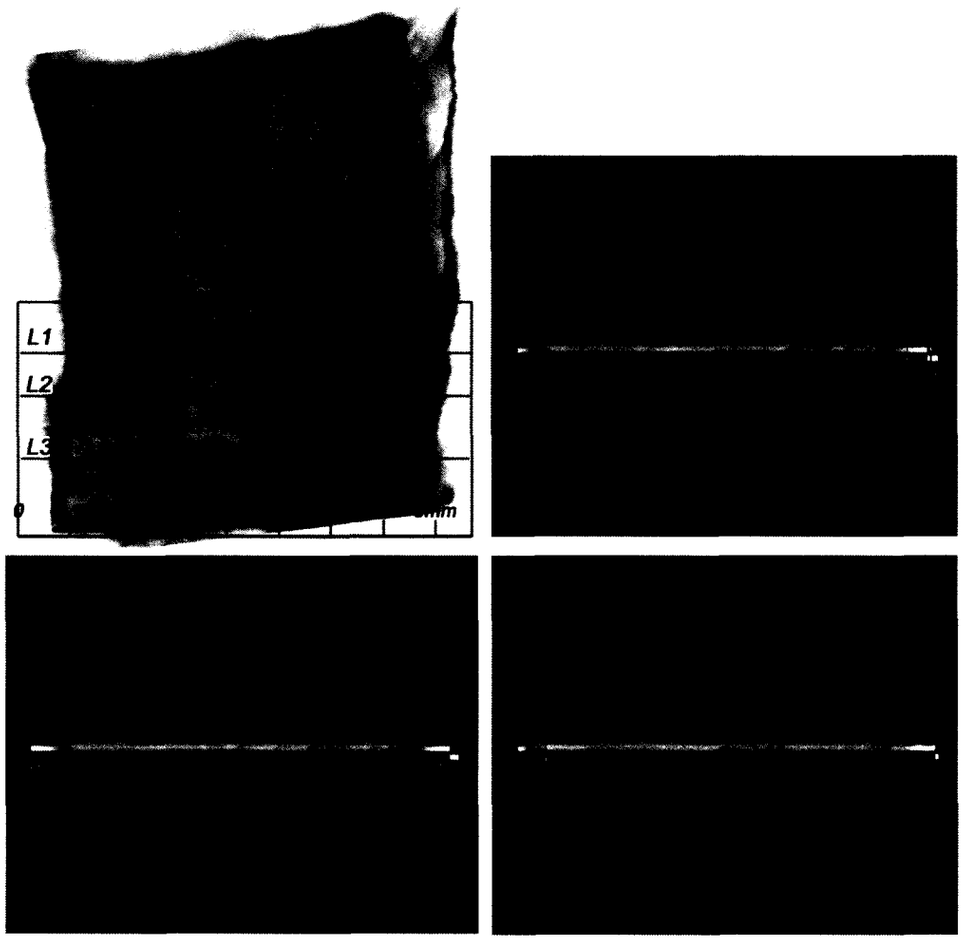

(b) Normal Skin Tissue (Frequency: 50 MHz; Mode: Pulse-wave mode)

Fig. 7: B-scan images of thickly sectioned abnormal and normal skin tissues, wherein scanning positions are selected from the C-scan image of the tissues.

3.1.4.5 Waveform Analysis

Attenuation

The insertion technique [22] is used to measure the acoustic properties of the different materials. This technique is a relative measurement method which employs water as the reference to study the transmission of longitudinal ultrasonic waves through solid media embedded in an aqueous environment (*i.e.*, water). Therefore, the waveform of the wave reflected from the substrate via water was taken as a reference waveform (see Fig. 8). In this case, the acoustic beam is focused on the sapphire substrate, and because of high reflectivity, the reflected signal carries relative high energy and its waveform has an amplitude of 100% Full Screen Height (hereinafter called simply "FSH"). The echo amplitudes represent the product of the local scattering strength and the attenuation loss factor, which takes into account scattering in all directions and absorption. Based on the difference in contrast, three points (*i.e.*, P1, P2 and P3 in Fig. 9) were chosen. The waveforms corresponding to these points are shown in Fig. 9, and their amplitudes are shown in Table 2.

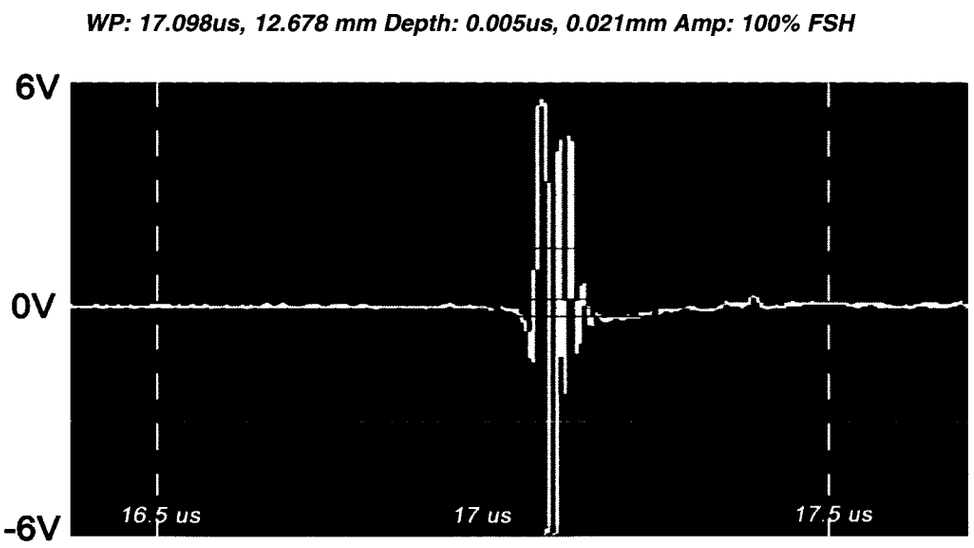

Fig. 8: Reference for waveform analysis. The waveform of the reflected wave from the surface of the sapphire substrate via water shows that its amplitude is 100% FSH (Full Screen Height; 12 V_{pp}).

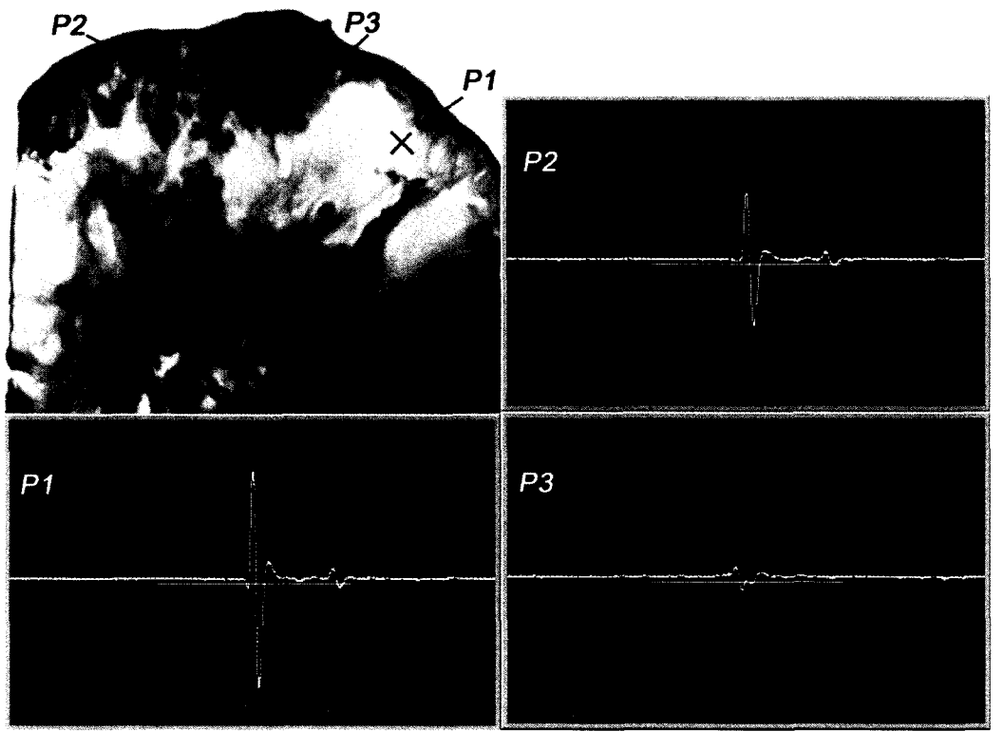

Fig. 9: Waveforms obtained from the thickly sectioned abnormal tissue. The tissue includes melanoma cancer cells that were sandwiched between the poly-silicone cover and the sapphire substrate.

Table 2: Amplitude of waveform (A)

P1	A=86% FSH
P2	A=53% FSH
P3	A=10% FSH

The FFTs of P1, P2 and P3 were obtained (see Fig. 10) as well as their center frequency and signal loss (see Table 3).

Table 3: Center Frequency, f_c, and Acoustic Signal Loss, $\triangle$

P1	f_c = 12.207MHz	$\triangle$ = 14.111 MHz
P2	f_c = 9.766 MHz	$\triangle$ = 16.552 MHz
P3	f_c = 5.371MHz	$\triangle$ = 20.947 MHz

It can be seen that the frequency of the acoustic beam returned from the thickly sectioned abnormal tissue is less than 15 MHz because of high attenuation of the tissue including cancer cells. It could be concluded that emitting a 50 MHz frequency acoustic beam is not an appropriate way to form highly resolved acoustic images in the pulse-wave mode.

The skin tissues are acoustically transparent due to the impedances of skin tissues are close to that of water, therefore, there is no ultrasonic reflection from the interface between water and skin tissue. (The acoustic impedance in human soft tissues ranges from 1.35×10^6 kg $m^{-2} s^{-1}$ for fat, to 1.74×10^6 kg $m^{-2} s^{-1}$ for muscle, the mean being 1.62×10^6 kg $m^{-2} s^{-1}$. The impedance of skin has been reported to range from 1.57×10^6 kg $m^{-2} s^{-1}$ to 1.60×10^6 kg $m^{-2} s^{-1}$ [30], see Table 4 [159].) The contrast of the tissue in acoustic images is primarily generated from difference in attenuation. High attenuation causes significant signal loss. Therefore, by comparing the amplitudes of the waveforms the highest attenuation occurs at P3 and the lowest at P1 (see Table 2).

Table 4: Acoustic Properties of Some Biological Tissue and Water [159]

Material	Density	Speed of Sound	Characteristic Impedance
	g/ml^2	m/s	10^6 kg/m^2 s
Blood	1.06	1528	1.62
Brain	1.03	1505 - 1612	1.55 - 1.66
Fat	0.92	1467	1.35
Kidney	1.04	1558	1.62
Liver	1.06	1547 - 1585	1.64 - 1.68
Muscle	1.07	1542 - 1607	1.65 - 1.74
Spleen	1.06	1557 - 1575	1.65 - 1.67
Tissue, mean value	1.058	1540	1.62
Water	1000	1497	1.48

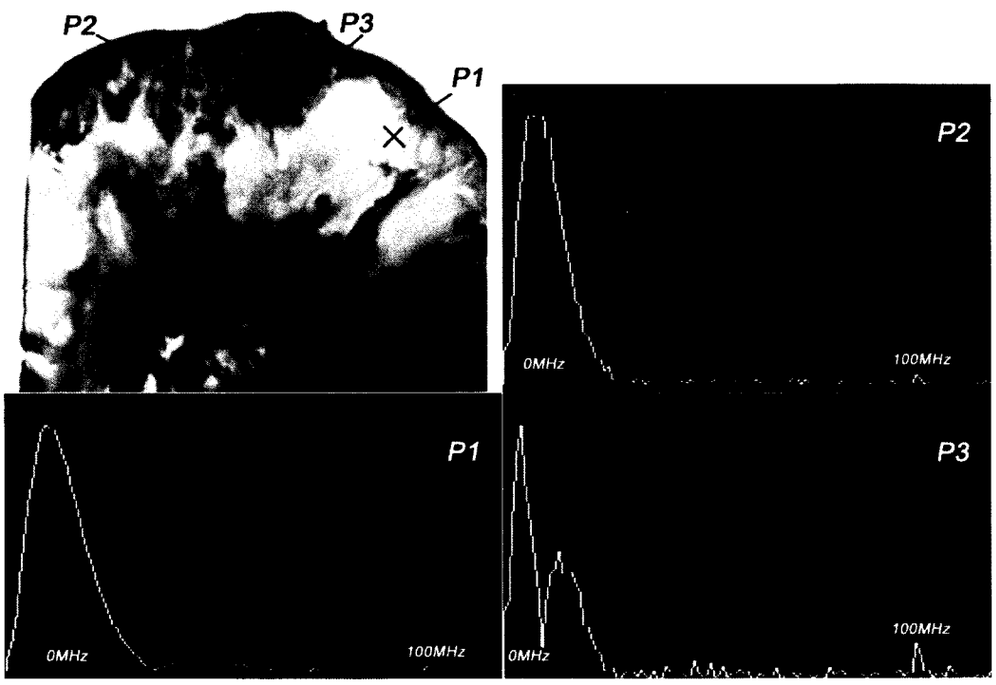

Fig. 10: FFT of thickly sectioned specimen including melanoma cancer cells located between the poly-silicone cover and the sapphire substrate.

Acoustic velocity

Figure 11 shows the reflected waves from the three-layered structure (*i.e.*, the poly-silicone cover, the tissue, and the sapphire substrate) of the specimen system (*i.e.*, A-scan). The longitudinal wave velocity of the tissue (denoted simply as "V_{tissue}") can be calculated by the following equation [28-29]:

$$V_{tissue} = \left(\frac{1}{V_{water}} - \frac{\Delta t}{\Delta x} \right)^{-1} \tag{3.3}$$

where V_{water} is the longitudinal wave velocity in water, Δ t is the time of flight from the 1st interface to the 2nd interface, and Δ x is the thickness of the tissue.

Note that the tissue is compressed during the experiment. Therefore, the real thickness of the tissue is relatively difficult to precisely measure. Further, without the cover, no signal from the surface of the tissue can be seen. The longitudinal wave velocity of the tissue can be more accurately obtained with V(z) analysis and is described in Chapter IV.

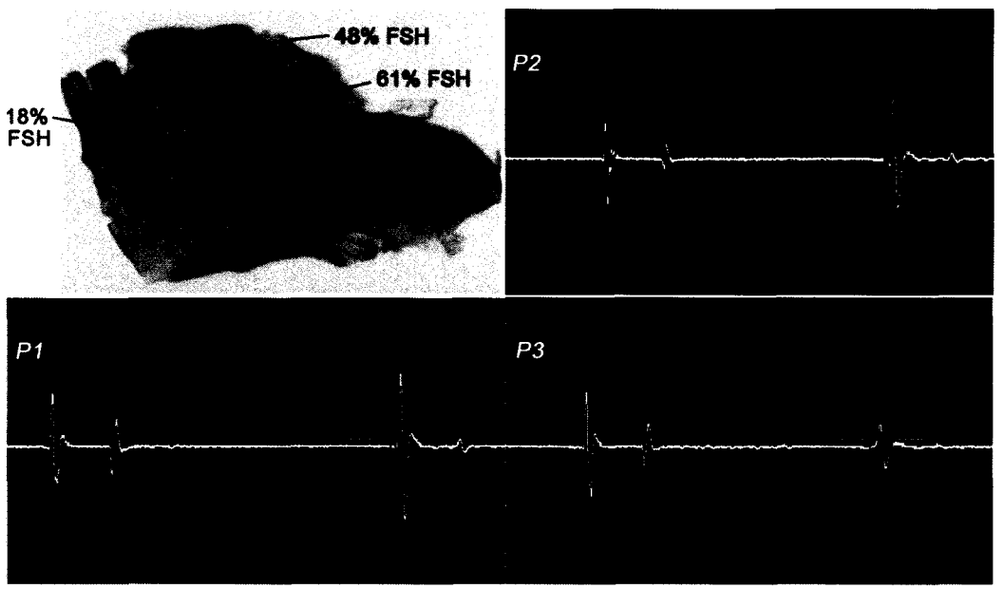

Fig. 11: A-scan images of thickly sectioned specimen including groups of melanoma cancer cells. The time of flight of first layer (poly-silicone) is the distance in μs between the first two reflected signals. The distance between the 2nd and the 3rd signals is the time of flight of acoustic waves traveling within the tissue (Δt), unit in μs.

3.1.4.6 Frequency Analysis

When an acoustic wave travels within a specimen, its amplitude diminishes with distance of travel, and is finally not measurable. There are a few useful methods to obtain the attenuation of the skin tissue with the SAM (pulse-wave mode). The simplest way is to measure the attenuation directly by calculating the signal loss using FFT analysis. This method is effective when the surface roughness of the specimen is not significant compared to the wavelength of the transducer. We briefly describe the procedures of the method below.

In this case, we need to locate the specimen on the substrate without the cover (see Fig. 12). The schematic diagram of the experimental setup is shown in Fig. 13(a).

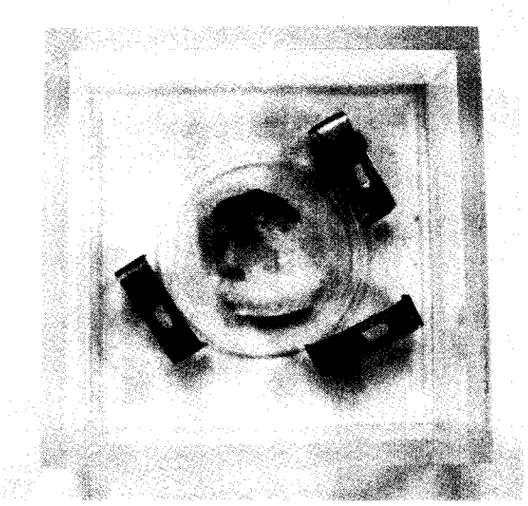

Fig. 12: Experimental setup of the specimen in the chamber desirable for a simple attenuation measurement. A thick melanoma tissue is located on the sapphire substrate (thickness: 1.78mm). There is no transparent poly-silicon cover on the front surface of the specimen.

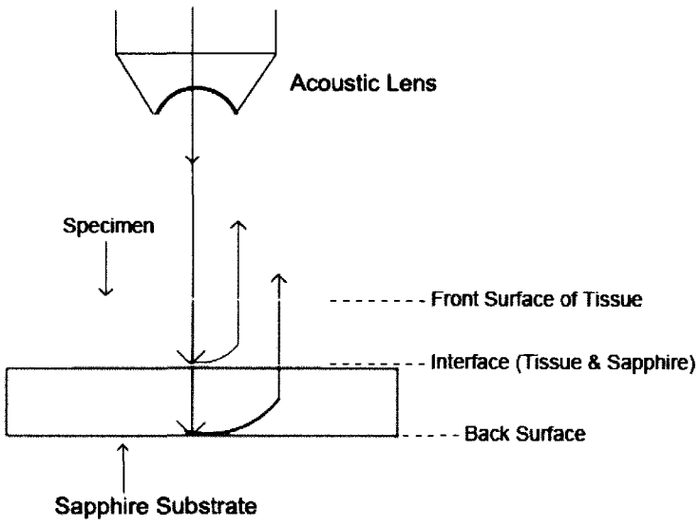

Fig. 13 (a): Schematic diagram shows acoustic beams reflected from the specimen when attenuation is measured. In this setup, a specimen is placed on a sapphire substrate without a transparent poly-silicone cover. No acoustic wave reflected from the front surface of the specimen is seen on the monitor of the oscilloscope because the acoustic impedances of the water and the specimen are similar. In this case, the acoustic wave is primarily focused on the surface of the substrate. Therefore, the image is comprised of the information from the front surface of the specimen relative to the back surface of the specimen.

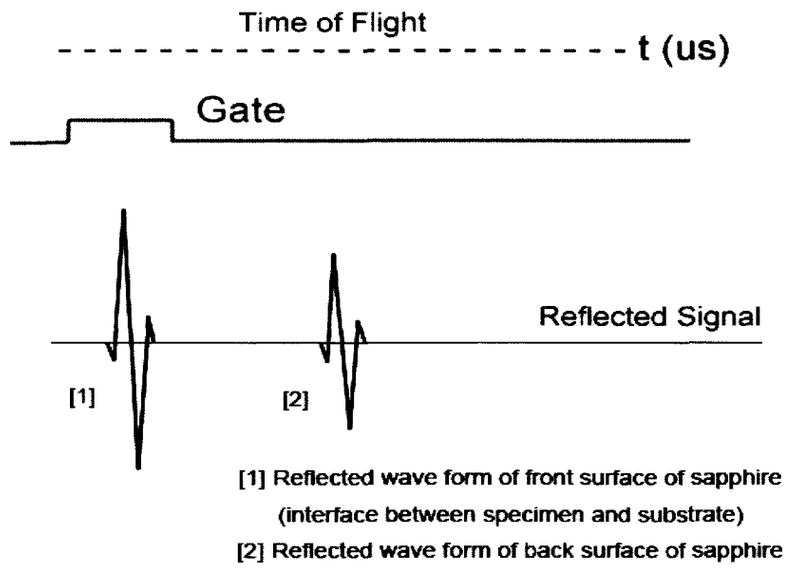

Fig. 13 (b): Schematic diagram shows acoustic waves reflected from the specimen located on the substrate. The acoustic image is formed by gating the interface between the specimen and substrate. The signal loss calculated in this case is caused by the attenuation in the specimen only.

Figure 13(b) shows theoretical waveforms of the longitudinal waves reflected from the 1st interface between the tissue and the front surface of the sapphire substrate, and the back surface of the sapphire substrate, respectively (see Fig. 13(a)). However, in reality, due to the high attenuation property in thick biological tissue specimens, the reflected wave form of the back surface of the sapphire is hardly detectable. To obtain the absolute value of the signal loss for the tissue (denoted simply as "$\triangle_s$"), the attenuation in water (denoted simply as "$\triangle_w$") must be measured.

The attenuation can be obtained simply from a FFT of the reference signal (see Fig. 14). Recall that the acoustic lens emits an acoustic beam having an input frequency of 50 MHz. However, the frequency of the acoustic beam retuned from the substrate in the absence of tissue and any other scattering medium is

23.682 MHz. Thus, any signal loss (*i.e.*, attenuation) in the tissue can be determined by taking the difference of the center frequency obtained from the FFT and the signal loss in water (*i.e.*, 26.318 MHz).

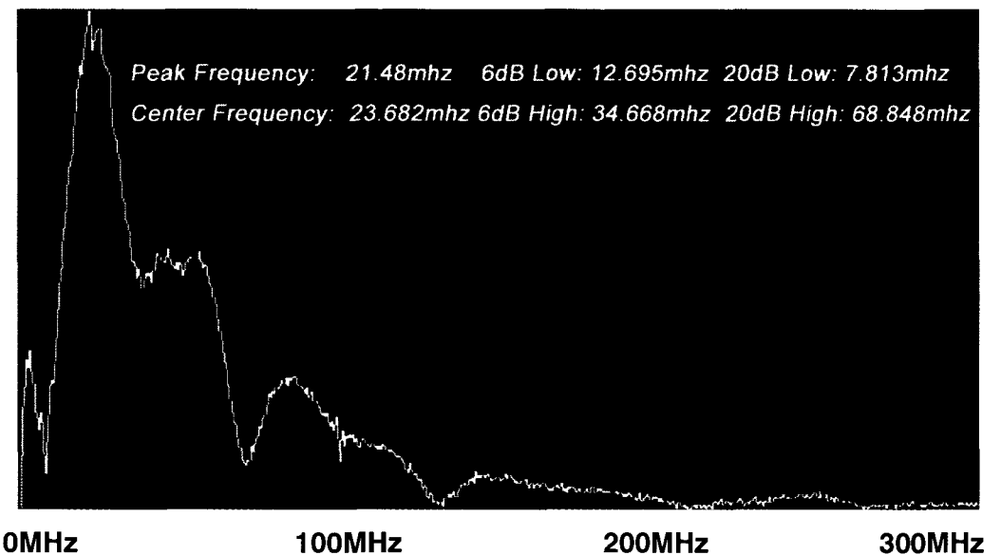

Fig. 14: FFT of Reference Signal (Center Frequency: 23.682 MHz)

By other approaches, the acoustic attenuation coefficients of the specimen (denoted simply as "α_s") can also be calculated according to the following equation:

$$\alpha_s = \alpha_w - \frac{1}{\Delta x}[\log A_s - \log A_w - 2\log(1-R)] \tag{3.4}$$

where A_i is the amplitude of the received ultrasound pulse wave with indices W and S representing water and the specimen, respectively, Δx is the thickness of the specimen, and R is the acoustic reflection coefficient.

Reflection and transmission coefficients are as follows:

$$R = \frac{Z_2 - Z_1}{Z_2 + Z_1} \text{ and,} \tag{3.5}$$

$$T = \frac{2Z_1}{Z_1 + Z_2} \tag{3.6}$$

where $Z_{i\ =\ 1,2}$ are impedances of water and the specimen, respectively. Mathematically, the acoustic impedance is defined as the sound pressure divided by the particle velocity and the surface area, through which an acoustic wave of frequency f propagates:

$$Z = \frac{p}{vS} \tag{3.7}$$

Planar, single-frequency traveling waves have acoustic impedance equal to the characteristic impedance of a medium (*i.e.*, water) divided by the surface area, where the characteristic impedance is the product of longitudinal wave velocity and density of the medium:

$$Z = \rho_s c_s \tag{3.8}$$

where ρ_s is the density of the sample and c_s is the longitudinal wave velocity of the specimen [24].

3.2 PHYSICAL AND MATHEMATICAL MODELING

Angular Spectrum Representation

In this section, the decomposition of a complicated wave front into an angular spectrum of plane waves by the Fourier transformation is briefly described [25-26].

Suppose that a monochromatic wave, propagating along z-axis, is incident at z_1 plane. The complex field of the wave is given by $u_1(x, y)$ with the $e^{-i\omega t}$ time dependence suppressed. Then, the angular spectrum in the plane is given by the following equation:

$$U_1(k_x, k_y) = \mathrm{F}\{u_1(x, y)\} = \int_{-\infty}^{\infty} \int u_1(x, y) e^{-i(k_x x + k_y y)} dx dy \tag{3.9}$$

where F gives a transformation from the spatial domain to the frequency domain. With Eq. (3.9), we can decompose the acoustic field $u_1(x, y)$ into plane wave components of the form $e^{-i(k_x x + k_y y)}$ having an amplitude $U_1(k_x, k_y)$. Here, $e^{-i(k_x x + k_y y)}$ represents a unit amplitude plane wave incident on the z_1 plane with an angle

$$\theta = \sin^{-1}\left(-\frac{\sqrt{k_x^2 + k_2^y}}{k_0}\right) \tag{3.10}$$

$$k_0 = \frac{\omega}{V_0} \tag{3.11}$$

where ω is an angular frequency, and V_0 is a sound velocity.

The angular spectrum at another plane, z_2, can be found by multiplying $U_2(k_x, k_y)$ by $e^{ik_z(z_2-z_1)}$ where $k_z = \sqrt{k_0^2 - k_x^2 - k_y^2}$ to give

$$U_2(k_x, k_y) = U_1(k_x, k_y) e^{-ik_z(z_2-z_1)} \tag{3.12}$$

Note that for $k_0^2 < k_x^2 - k_y^2$, k_z is purely imaginary and the corresponding plane waves are evanescent.

With the spectrum in this form, the complex field at z_2 can be determined by inverse transforming

$$u_2(x, y) = \mathrm{F}^{-1}\{U_2(k_x, k_y)\} = \frac{1}{(2\pi)^2} \int_{-\infty}^{\infty} \int U_2(k_x, k_y) e^{i(k_x x + k_y y)} dk_x dk_y \tag{3.13}$$

Note that $\mathrm{F}^{-1}[\mathrm{F}\{u(x, y)\}] = u(x, y)$, but $\mathrm{F}[\mathrm{F}\{u(x, y)\}] = (2\pi)^2 u(-x, -y)$.

In this space, Eq. (3.12) can be written as

$$u_2(x, y) = \left[u_1 * \mathrm{F}^{-1}\left[e^{ik_z(z_2-z_1)}\right]\right]_{\substack{x \\ y}} \tag{3.14}$$

where "*" signifies the convolution operation.

If the so-called paraxial approximation is used, the expression can be simplified, since we have $k_z = \sqrt{k_0^2 - k_x^2 - k_y^2} \cong k_0^2 - \frac{1}{2}\frac{k_x^2 + k_y^2}{k_0}$ for $\sqrt{k_x^2 + k_y^2} << k_0$. Therefore, we can approximate $e^{ik_z(z_2-z_1)}$ as follows:

$$e^{ik_z(z_2-z_1)} \cong e^{ik_0(z_2-z_1)} e^{-i\frac{k_x^2+k_y^2}{2k_0}(z_2-z_1)} \tag{3.15}$$

The first exponential factor in Eq. (3.15) is an overall phase retardation suffered by any component of the angular spectrum as it propagates from z_1 to z_2. The second exponential factor is phase dispersion with a quadratic frequency dependence on the spatial angle.

Let a second region be introduced separated from the first region by a plane boundary at z_3. If a plane wave of the form $U_3(k_x, k_y)e^{i\{k_x x + k_y y + k_z (z - z_3)\}}$ is incident on this boundary, there will be a reflected plane wave of the form $U_3'(k_x, k_y)e^{i\{k_x x + k_y y - k_z (z - z_3)\}}$. Suppose that the reflectance function $\mathscr{R}(l_x, l_y)$ (see Appendix C) of the boundary is known. The function relates $U_3(k_x, k_y)$ to $U_3'(k_x, k_y)$ as follows [25]:

$$U_3'(k_x, k_y) = \mathscr{R}\left(\frac{k_x}{k_0}, \frac{k_y}{k_0}\right) U_3(k_x, k_y) \tag{3.16}$$

Contrast Theory for SAM (Pulse-Wave Mode)

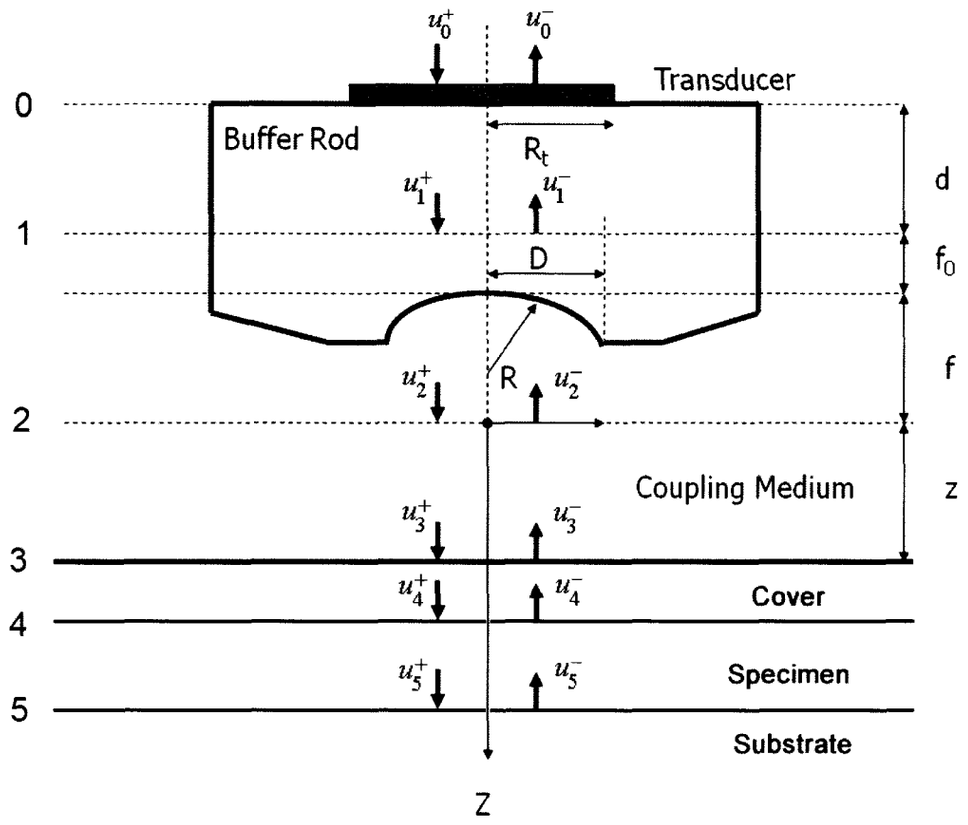

Fig.15: Schematic diagram of the geometry and coordinate system

Figure 15 shows the schematic diagram of the geometry and coordinate system used in mathematical modeling. The planes labeled 1 and 2 represent the back and front focal planes of the acoustic lens. They are not at the same distance from the lens because the different media are involved. Plane 3 is the plane of the surface of the cover. Plane 4 is the 1st interface between the cover and the front surface of the specimen. Plane 5 is the 2nd interface between the back surface of the specimen and the front surface of the substrate.

The transducer excites a uniform field (*i.e.*, $u_0^+(x,y)$) when a unit voltage is applied at its terminals. The transducer output voltage, represented as a

function of z, is the integral of the incident field and reflected field over the transducer area (*i.e.*, plane 0). Then, the contrast of the specimen is expressed as follows [27]:

$$V(z) = \int\int_{-\infty}^{\infty} u_0^+(x,y) u_0^-(x,y) dxdy \tag{3.17}$$

Equation (3.17) is rewritten as follows (see Appendix D):

$$V(z) = \int\int_{-\infty}^{\infty} u_1^+(x,y) u_1^-(x,y) dxdy \tag{3.18}$$

where $u_1^+(x,y)$ is an acoustical field incident at the back focal plane (*i.e.*, Plane 1), $u_1^-(x,y)$ is an acoustical field reflected from the back focal plane. The transducer plane (*i.e.*, Plane 0) is a distance "d" away from the Plane 1. The field $u_1^+(x,y)$ can be determined if properties of the transducer is known (see Appendix E).

Then, we need to calculate an acoustical field on each critical plane.

$$\begin{aligned} u_2^+(x,y) &= \frac{e^{ik_0 f(1+\bar{c}^2)}}{i\lambda_0 f} \int\int_{-\infty}^{\infty} u_1^+(x,y) \mathcal{P}_1(x,y) e^{-i\frac{2\pi}{\lambda_0 f}} dxdy \\ &= \frac{e^{ik_0 f(1+\bar{c}^2)}}{i\lambda_0 f} \mathcal{F}\{u_1^+(x,y)\mathcal{P}_1(x,y)\}\Big|_{\substack{k_x=\frac{k_0 x}{f} \\ k_y=\frac{k_0 y}{f}}} \end{aligned} \tag{3.19}$$

where $k_0 = \frac{2\pi}{\lambda_0}$ is the wave number in the coupling medium *(i.e.*, de-ionized water), λ_0 is the wavelength of the coupling medium, f is the focal length of the lens, $\bar{c}$ is the ratio of the sound velocity in the coupling medium to that in the solid (*i.e.*, material of the buffer rod such as fused quartz), and $\mathcal{P}_1(x,y)$ is the pupil function expressed as the following equation.

$$\mathscr{P}_1(x,y) = circ\left(\frac{\sqrt{x^2+y^2}}{R}\right) \tag{3.20}$$

where R is the radius of the pupil function of the lens.

Propagation of the wave beyond the focal plane is easily calculated if the angular spectrum representation is utilized.

$$\begin{aligned} U_2^+(k_x,k_y) &= \mathscr{F}\{u_2^+(x,y)\} \\ &= \mathscr{F}\left[\frac{e^{ik_0 f(1+\bar{c}^2)}}{i\lambda_0 f}\mathscr{F}\{u_1^+(x,y)\mathscr{P}_f(x,y)\}\Big|_{\substack{k_x=\frac{k_0 x}{f} \\ k_y=\frac{k_0 y}{f}}}\right] \\ &= -i\lambda_0 f e^{ik_0 f(1+\bar{c}^2)} u_1^+\left(-\frac{f}{k_0}k_x,-\frac{f}{k_0}k_y\right)\mathscr{P}_f\left(-\frac{f}{k_0}k_x,-\frac{f}{k_0}k_y\right) \end{aligned} \tag{3.21}$$

$$U_3^+(x,y) = U_2^+(x,y)e^{ik_z Z} \tag{3.22}$$

$$k_z = \sqrt{k_0^2 - k_x^2 - k_y^2} \tag{3.23}$$

The lens is focused at the front surface of the substrate via the cover and the specimen. This means that the amplitude of the reflected signal from the 2nd interface is maximized and gated for acoustical visualization.

$$U_4^+(x,y) = U_3^+(x,y)\mathscr{T}_1^+\left(\frac{k_x}{k_1},\frac{k_y}{k_1}\right)e^{ik_{z1}L_1} \tag{3.24}$$

$$k_{z1} = \sqrt{k_1^2 - k_x^2 - k_y^2} \tag{3.25}$$

where $k_1 = \frac{2\pi}{\lambda_1}$ is the wave number in the cover, and λ_1 is the wavelength in the cover.

$$U_5^+(x,y) = U_4^+(x,y)\mathcal{T}_2^+\left(\frac{k_x}{k_2},\frac{k_y}{k_2}\right)e^{ik_{z2}L_2} \tag{3.26}$$

$$k_{z2} = \sqrt{k_2^2 - k_x^2 - k_y^2} \tag{3.27}$$

where $k_2 = \frac{2\pi}{\lambda_2}$ is the wave number in the specimen, and λ_2 is the wavelength in the tissue.

$$U_5^-(x,y) = U_5^+(x,y)\mathcal{R}\left(\frac{k_x}{k_2},\frac{k_y}{k_2}\right) \tag{3.28}$$

$$U_4^-(x,y) = U_5^-(x,y)\mathcal{T}_2^-\left(\frac{k_x}{k_2},\frac{k_y}{k_2}\right)e^{ik_{z2}L_2} \tag{3.29}$$

$$U_3^-(x,y) = U_4^-(x,y)\mathcal{T}_1^-\left(\frac{k_x}{k_1},\frac{k_y}{k_1}\right)e^{ik_{z1}L_1} \tag{3.30}$$

$$U_2^-(x,y) = U_3^-(x,y)e^{ik_z Z} \tag{3.31}$$

$$u_2^-(x,y) = \mathcal{F}^{-1}\{U_2^-(k_x,k_y)\} \tag{3.32}$$

$$
\begin{aligned}
u_1^-(x,y) &= \frac{e^{ik_0 f\left(1+\bar{c}^2\right)}}{i\lambda_0 f}\int\int_{-\infty}^{\infty} u_2^-(x,y)\mathscr{P}_2(x,y)e^{-i\frac{2\pi}{\lambda_0 f}(x,y)}dxdy \\
&= \frac{e^{ik_0 f\left(1+\bar{c}^2\right)}}{i\lambda_0 f}\mathscr{P}_2(x,y)\mathscr{F}\left\{u_1^+(x,y)\right\}\Bigg|_{\substack{k_x=\frac{k_0 x}{f} \\ k_y=\frac{k_0 y}{f}}} \\
&= \frac{e^{ik_0 f\left(1+\bar{c}^2\right)}}{i\lambda_0 f}\mathscr{P}_2(x,y)U_2^-\left(\frac{k_0}{f}x,\frac{k_0}{f}y\right)
\end{aligned}
\tag{3.33}
$$

Therefore, the output voltage V(z) can be rewritten as an integration of the incident acoustic field (*i.e.*, $u_1^+(x,y)$) and the computed reflected acoustic field at the back focal plane (3.33) in the angular spectrum presentation.

CHAPTER IV

THIN SECTIONED MELANOMA TISSUE

4.1 DESIGN AND METHODOLOGY

The Present problem of Ultrasonic Imaging with Pulse-Wave Mode

The objective of the present study is to visualize the cellular structure acoustically within a thickly sliced biological specimen. Conventionally, the pulse-wave mode of the SAM is applied to the acoustical visualization of the thick specimen. However, the use of the pulse-wave mode does not reveal the cellular structure in the acoustic image very well.

In order to improve the resolution, our primarily choice is to increase the frequency up to more than 100MHz. Note that, although surface waves extend beneath the surface of specimen and are sensitive to variations under the surface of the material, their penetration ability is limited by the wavelength of the surface wave. A higher frequency of operation results in a lower penetration but higher resolution. Therefore, thinly sectioned specimen needs to be prepared for high frequency ultrasonic imaging. Figure 16 is an optical image of a thinly sectioned melanoma tissue. The tissue was embedded into paraffin, and was sectioned with a thickness of 10 μm by a microtome and affixed onto an optical glass substrate. After paraffin was removed from the tissue, the tissue was stained with H&E. Figure 17 is an acoustic image of a thinly sectioned melanoma tissue. The tissue was not stained. The SAM (pulse-wave mode; Sonix) was used with operating frequency at 250 MHz to form the acoustic image. As can be seen, the SAM did not form the image showing any cellular structures. Further, comparing the acoustic and optical images, the acoustical image did not provide much extra information.

The reasons were the same as those for a thickly sectioned tissue described in chapter III.

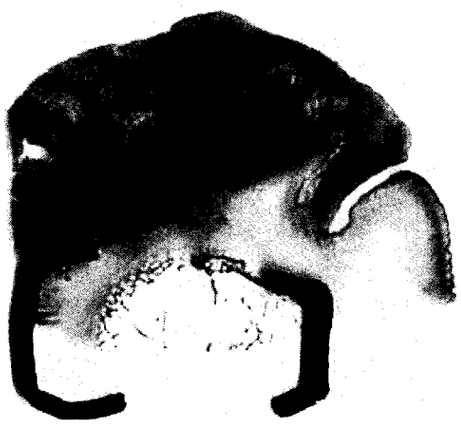

Fig. 16: Optical image of thinly sectioned melanoma tissue

The stereoscopic microscope (Olympus, Model: SZ-PT) was used to form the image.

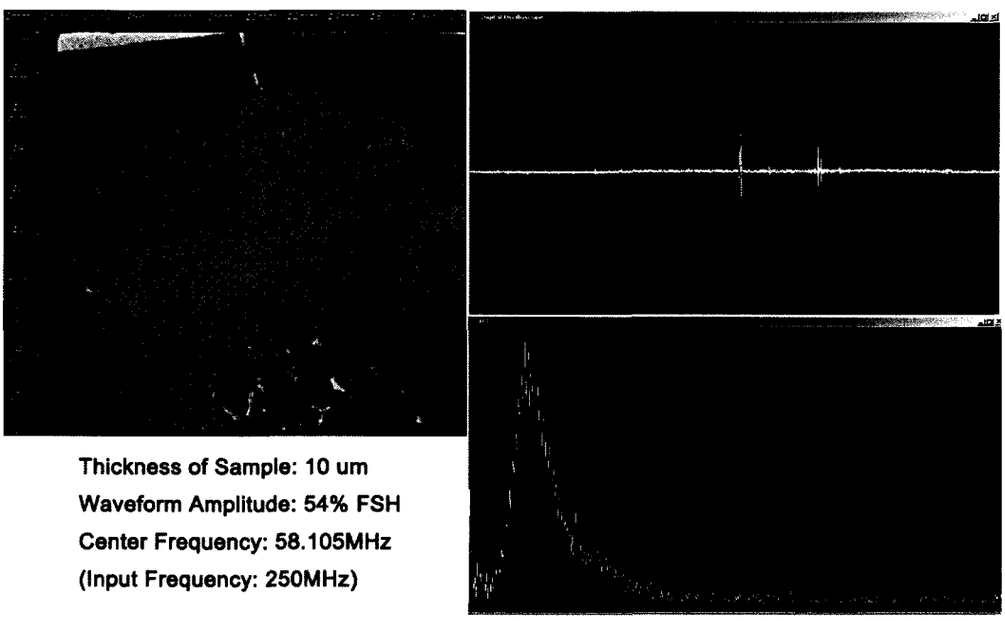

Fig. 17: An acoustic image of a thinly sectioned melanoma tissue (Left). Waveforms of reflected waves observed on a monitor of an oscilloscope at a point X (Upper Right). A result of FFT for 1st reflected signal (Lower Right). The image was formed by the SAM (pulse-wave mode). The amplitude of 1st reflected signal is 54% Full Screen Height (FSH). The result of the FFT analysis shows that the center frequency of the reflected signal is 58.1MHz.

Approach to the Solution

The images shown in Fig. 18 were obtained with the tone-burst-wave mode.

The comparison of resolution in the acoustic images is made of a mole specimen shown in Fig. 18. Resolutions in the acoustic images are formed at scanning frequencies of 200MHz, 400MHz, 600MHz, and 1GHz. Each acoustic lens was focused onto the interface between the specimen and the substrate. As expected when the frequency is increased, resolution in the acoustic image is improved, and shows remarkable details within the tissue. This is an indication of the superiority of the tone-burst mode of operation.

The contrast difference observed in these acoustic images can be related to the elastic properties at the surface and/or sub-surface of the specimen. Interpretation of the contrast is not a simple matter. One cannot simply say that a brighter area corresponds to a higher (or lower) density, or to a greater (or smaller) elastic modulus. The contrast of the biological tissue in the acoustic image is primarily generated from the difference in attenuation. The contrast also varies very sensitively with the distance between the lens and the surface of the specimen. This behavior can be explained with the V(z) analysis. Such analysis leads to quantitative data acquisition from the image.

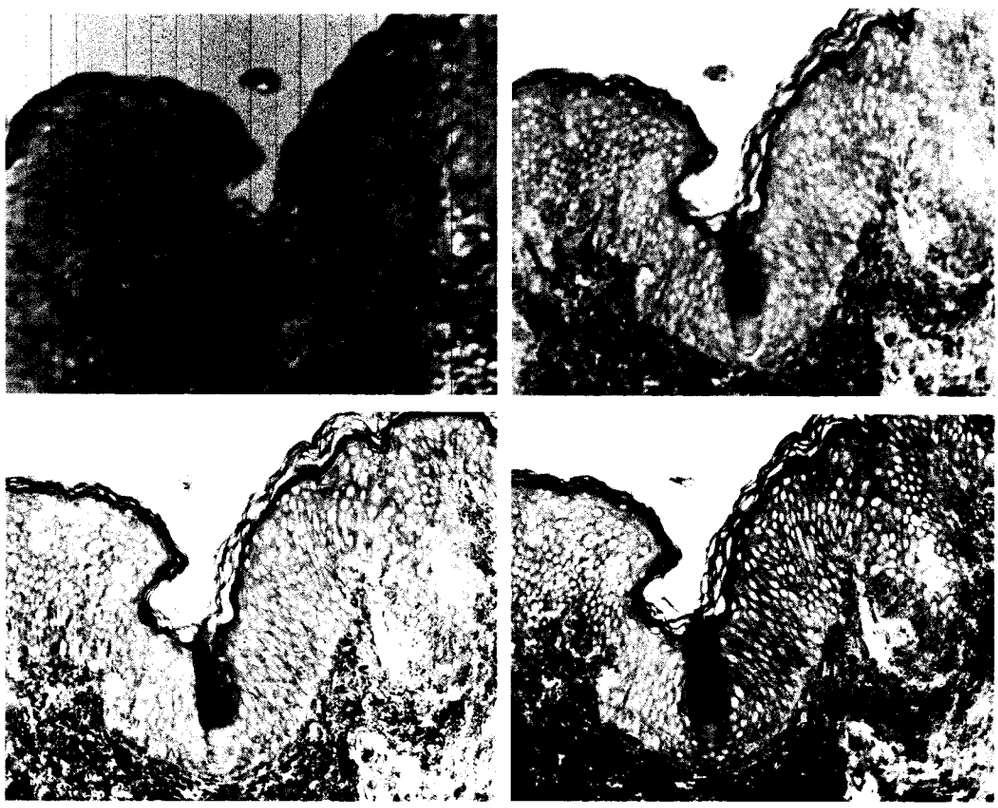

Fig. 18: Resolution Comparison (Tone-Burst-Wave Mode)

Upper Left: Frequency; 200MHz, Upper Right: Frequency; 400MHz, Lower Left: Frequency; 600MHz, Lower Right: Frequency;1GHz, Scanning Width: x=0.5mm, Specimen: Mole

4.1.1 Imaging Principle (Tone-Burst-Wave Mode)

Figure 19 is the schematic diagram of the SAM (Olympus).

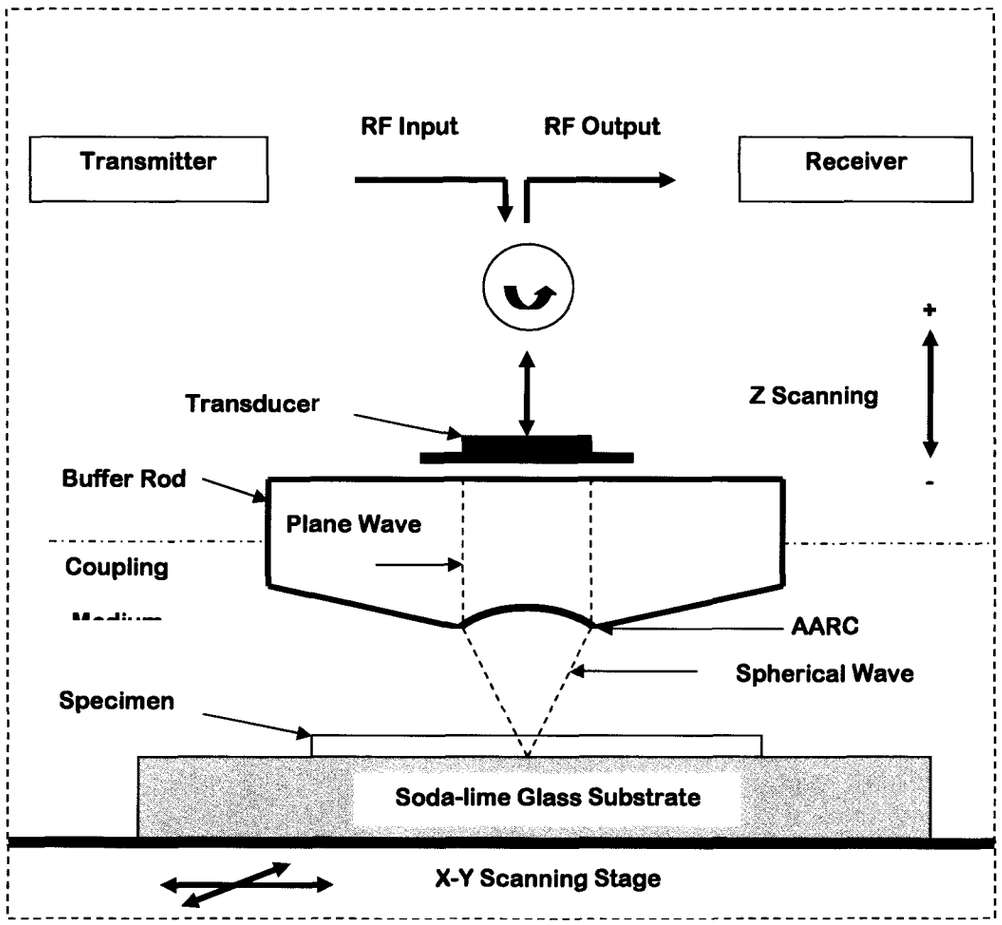

Fig. 19: Schematic diagram of SAM (Tone-Burst-Wave Mode)

Referring to Fig. 19, the mechanism of the V(z) curve is described as follows. An electrical signal (*i.e.*, tone-burst wave) generated by a transmitter inputs to a piezoelectric transducer (*i.e.*, zinc oxide), located on the top of a buffer rod through a circulator. Input voltage from the transmitter to the transducer is approximately 5 V. The electrical signal is converted into an acoustic signal (*i.e.*, ultrasonic plane wave) by the transducer. The ultrasonic plane wave travels through the buffer rod made of sapphire to the lens located at the bottom of the buffer rod, wherein the lens is coated by an acoustic

impedance-matching layer which is a so-called "acoustic anti-reflection coating" made of silicon oxide (hereinafter called simply "AARC"). The lens converts the ultrasonic plane wave to an ultrasonic spherical wave (*i.e.*, ultrasonic beam).

The ultrasonic beam is focused within the specimen, and reflected from the specimen. The reflected ultrasonic beam, which carries acoustic information of the specimen, is again converted into an ultrasonic plane wave by the lens. The ultrasonic plane wave returns to the transducer through the buffer rod. The ultrasonic plane wave is again converted into an electrical signal by the transducer. The voltage of the electric signal ranges from 300 mV to 1 V. When the operating frequencies range from 100 MHz to 1 GHz, the corresponding insertion loss is approximately 30 dB to 80 dB. Therefore, the electric signal must be amplified by 30 to 80 dB at a receiver. Furthermore, the electric signal comprises transmission leaks, internal reflections from the interface between the lens and the AARC, and reflections from the specimen. Therefore, the reflections must be selected by a rectangular wave from a double balanced mixer (hereinafter called simply "DMB") which is the so-called the first gate. Then, the peak of the amplitude of the electric signal is detected by a circuit, which includes a diode and a capacitor (*i.e.*, the peak detection technique). The gate noise is removed by using the second gate existing within the first gate (the blanking technique). The peak-detected signal is stored into memory through an analog-to-digital signal (hereinafter called simply "A/D") converter. The stored signal is again converted into an analog signal by a digital-to-analog signal (hereinafter called simply "D/A") converter. This flow of processes allows the information that is collected at a single spot on the specimen to be displayed as intensity at a certain point on the CRT monitor. In order to form a two-dimensional acoustic image, an acoustic lens and an X-Y stage are mechanically scanned across a certain area of the specimen.

The acoustic lens is able to translate axially along the z direction to vary the distance between the specimen and the lens for sub-surface visualization. That is, when visualizing the surface of the specimen, the acoustic lens is

focused on the specimen (we denote $z = 0\ \mu m$), and when visualizing a subsurface of the specimen, the acoustic lens is mechanically defocused toward the specimen (we denote $z = -x\ \mu m$, where x is the defocused distance) (see Fig 20).

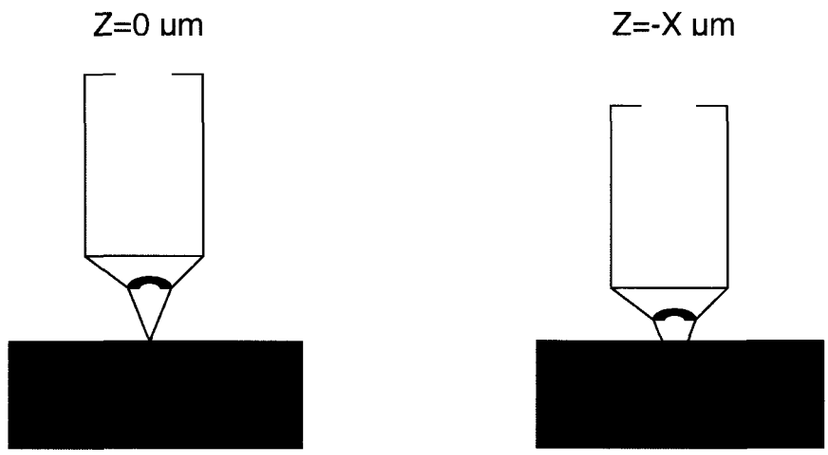

Fig. 20: Interior observation with lens defocusing (tone-burst-wave mode). **(Left)** Focusing the Acoustic Lens onto the Surface of the Specimen to visualize the surface of the specimen; **(Right)** Defocusing the Acoustic Lens into the Interior plane of the Specimen for subsurface visualization.

4.1.2 Description of Specimen

Tissue studied: normal and diseased human skin samples were used in this study. The tissue was obtained from a biopsy of an invasive malignant melanoma of the big toe.

Tissue process: the tissue measuring 3x5mm in size was fixed in 10% buffered formalin and transferred to 70% ethanol. The tissue blocks were then dehydrated with a series of graded ethanol solutions and embedded in paraffin. The paraffin blocks were thin-sectioned with a microtome (Finese) at 5μm thickness and the sections were mounted onto glass slides. For optical microscopic study, the sections were stained with H&E whereas consecutive sections from the same blocks were collected, dewaxed, and examined directly with an acoustic microscope.

Microscopic images of the thinly sectioned normal/abnormal specimens of skin-tissue are shown in Figs. 21(a) and 21(b). These images were obtained with a dissecting microscope (Olympus, Model: SZ-PT). The specimens were embedded in paraffin, thin sectioned with a microtome and mounted on glass slides, and stained with H&E. The thickness of both sections is 5μm. The normal control skin Fig. 21(a) contains fibrous stromal dermal collagen fibres that are pink in the H&E stain. In diseased tissue shown in Fig. 21(b), the upper left red region is an area of hemorrhage and ulceration. The rest of the abnormal specimen shows many mitotically active malignant melanomatous cancer cells infiltrating the dermis and subcutaneous tissue.

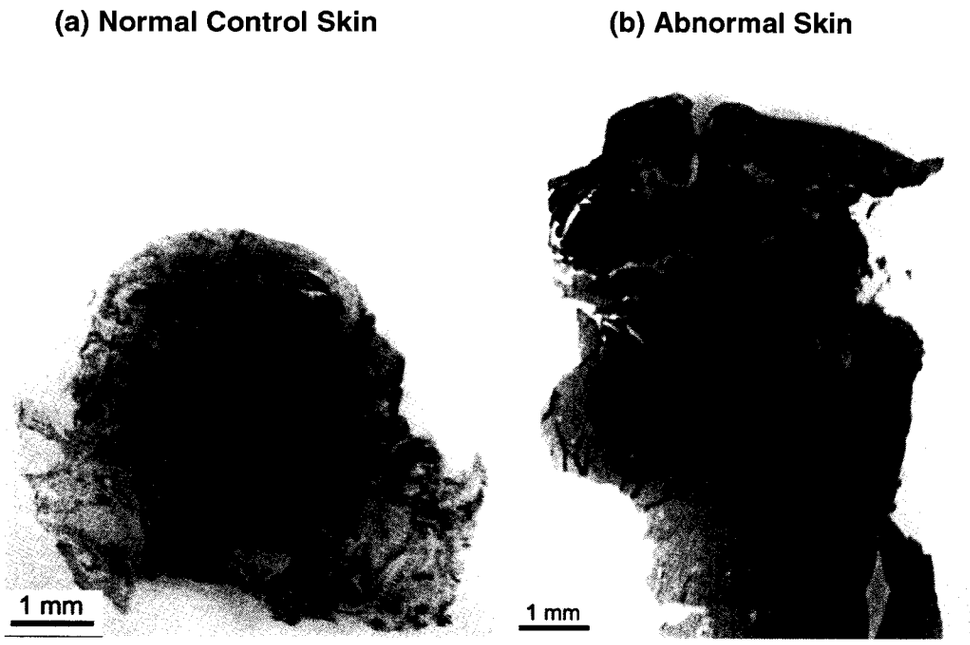

Fig. 21: Optical images at low magnification showing thinly sectioned (a) normal control and (b) abnormal skin tissues (thickness: 5μm) Model: SZ-PT, Olympus.

4.1.3 Experimental Procedures and Results

4.1.3.1 Optical Image

The interconnection between biomedical and mechanical properties inside melanoma cancer cells is of primary interest. Thus, the appropriate magnification for melanoma diagnosis in the optical images has to be found as the first step.

Normal Skin Tissue Control

Optical microscopy (hereinafter simply called "OM") images with high resolution obtained at 4X, 10X, 20X and 40X objective lenses are shown in Figs. 22(a), 22(b), 22(c) and 22(d). These OM images are obtained from a thinly sliced normal control skin tissue. Little information about cellular details can be gathered from Figs. 22(a) and 22(b), which are formed with 4X and 10X objective lenses that have 40X and 100X original magnifications, respectively. By increasing magnification to 200X and 400X original magnification, we begin to observe clearer cellular structures including smooth muscle fibres around blood vessels, fibroblasts in the stroma and focus of calcification and ossification (purple dense spots in Fig. 22(c) and Fig. 22(d)).

Normal Control Skin

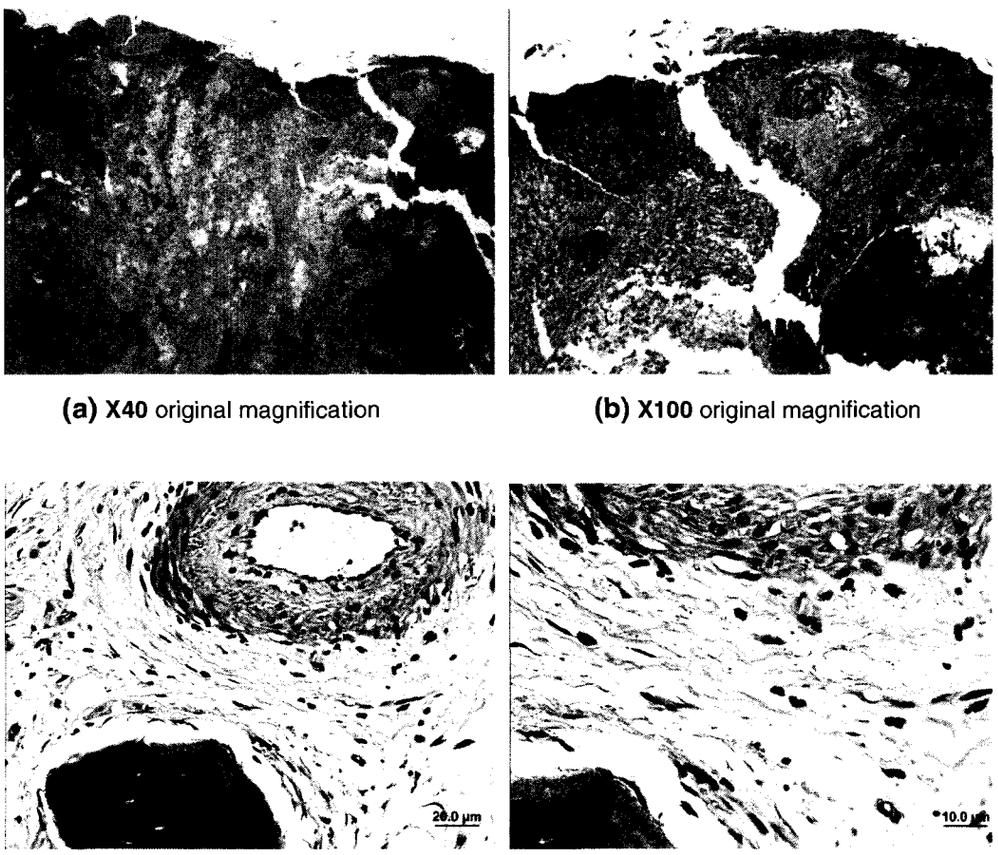

(a) X40 original magnification

(b) X100 original magnification

(c) X200 original magnification

(d) X400 original magnification

Fig. 22: Optical images of a thinly sliced normal skin tissue.

Eyepieces for 10X, and objective lenses for 4X, 10X, 20X and 40X were used for the images (a), (b), (c), and (d). Thickness of the specimen was 5um. The model of optical microscope was Olympus BX61.

Abnormal Skin Tissue

Once the appropriate magnification to observe cellular information has been determined, the same procedure can be applied to examine thinly sectioned melanoma skin tissue. Figure 23 is a montage optical image, which is used to locate an area of interest within the tissue. The entire abnormal skin tissue has a distance spread of neoplastic cells that form subpopulations of neoplastic cells in the sub-epithelial tissues. Malignant neoplasms of surface epithelia usually grow in the form of warty, papillary or nodular outgrowths from the surface and also infiltrate across the epithelial basement membrane to spread into the sub-epithelial connective tissue and further. Therefore, it is easier for us to locate a primitive tumor in between the epidermis and dermis, where it contains a large amount of connective tissues.

By convention, the optical images of a melanoma carcinoma residing underneath the epidermis are obtained at 4X, 10X and 40X objective lenses, shown in Figs. 24(a), 24(b) and 24(c), respectively. As we keep zooming in on the detected area, the cellular details are observed clearly in Fig. 24(c). The malignant tumor under test has an expansile and invasive growth of cells. Those tumor cells are small with blue-staining nuclei and very little cytoplasm; they are also disorganized, crowded together and are less differentiated. Other tumors in the sub-epithelial tissues are composed of sheets of very small cells (see Figs. 24(a) and 24(b)). Within the detecting region, numerous mitoses are seen, which appear as dark dense spots with no clear cell boundary. Many mitoses usually have poorly regulated cell division.

Abnormal Skin

Fig. 23: Montage optical image of abnormal skin tissue that contains a large compact of tumors, which is composed of a neoplastic mass of cells.

Abnormal Skin

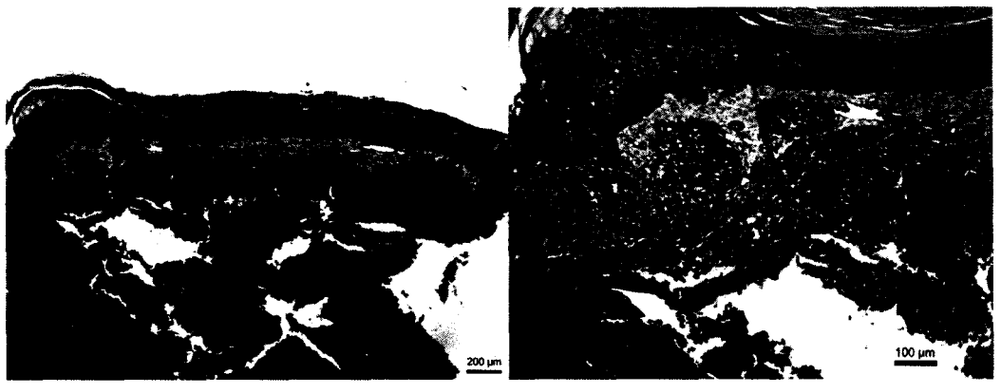

(a) 4X objective lens **(b) 10X** objective lens

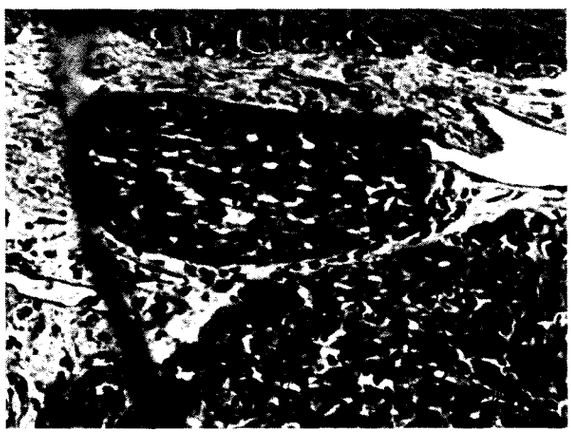

(c) 40X objective lens

Fig. 24: Optical images of a melanoma tumor in the dermis formed by objective lenses with (a) 4X, (b) 10X, and (c) 40X. Thicknesses of the tissues were 5µm. Model of optical microscope used was Olympus BX51.

4.1.3.2 Acoustic Image

For acoustic imaging, thinly sliced normal/abnormal tissues have been placed on to glass substrates. The paraffin was removed from the tissues, but they were not stained. For forming acoustic images, de-ionized water was used as a coupling medium. The acoustic lens was focused onto the interface between the specimen and the soda-lime glass. Each specimen was visualized at frequencies ranging from 200MHz to 1GHz.

Normal Control Skin Tissue

The acoustic image was formed by the acoustic lens (Olympus, Model: AL4M631, Frequency: 400MHz, Transducer: ZnO, Buffer Rod: Sapphire, Aperture Angle: 120°, W.D. 310μm), which was focused onto the surface of a soda-lime glass substrate. Therefore, the acoustic image includes information stemming from the region ranging from the front surface to the back surface.

Two of the main layers of human skin are the epidermis (*i.e.*, an outer keratinising stratified squamous epithelium) and the dermis *(i.e.*, an underlying touch supporting and nourishing layer of fibroelastic tissue). As can be seen in Fig. 25, both layers are clearly identifiable. The top layer which presented in the light grey color is the thin epidermis with an overlying layer of loose keratin. The external surface of the epidermis is fairly smooth and flat, but the junction between epidermis and thick dermis is marked by downward folds of epidermis. The thick dermis, which lies just beneath the epidermis, contains large compact of fine collagen and elastic fibres and small blood vessels. Melanocytes as seen in the optical micrograph are responsible for the synthesis and release of the brown pigment melanin which is largely responsible for skin coloration. They are located in the basal layer of the epidermis and scattered infrequently inside the dermis, appearing as dark blue round cells with pale-staining cytoplasm. The skin appendages such as sweat glands and hair follicles reside within the dermis. The hair follicles are essentially cylindrical downgrowths of the surface epithelium ensheathed by collagenous tissue; and sweat glands are simple, coiled tubular glands which

secrete a watery fluid onto the skin surface by the process of merocrine secretion. Both of them are easily discernable from the acoustic images by comparing to the optical image as a reference (indicated as a landmark). However, the melanocytes (*i.e.*, nevus cells) and other cellular details in all skin layers of the acoustic image are poorly reviewed.

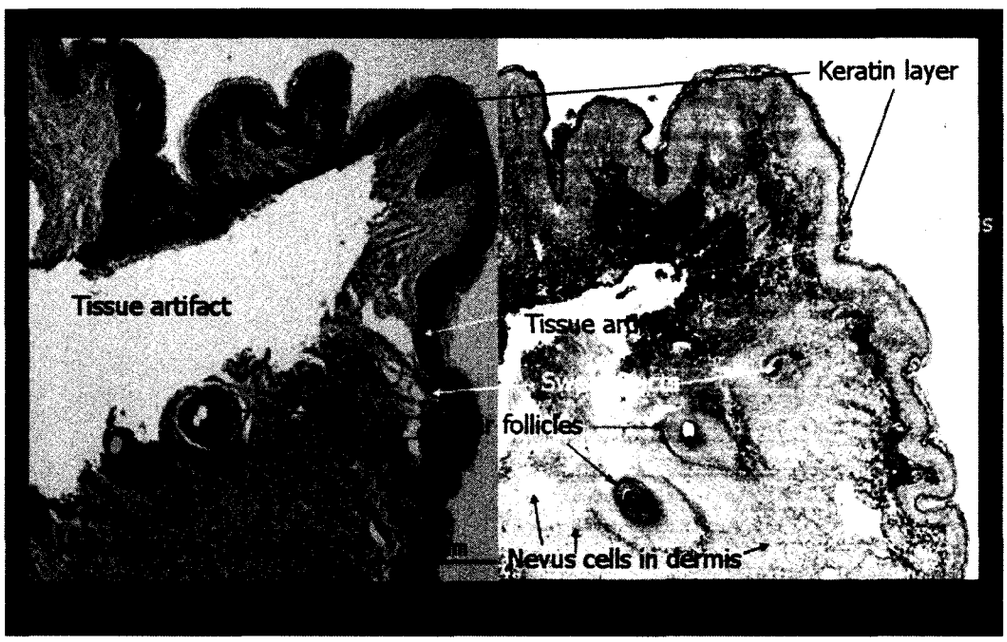

Fig. 25: Comparison of optical and acoustic images of thinly sliced normal skin specimen. (Left) Optical image formed at 4X objective lens; (Right) Acoustic image scanned at 400MHz.

Abnormal Skin Tissue

For abnormal skin tissue, the series of micrographs in Fig. 26 show the comparisons between the optical and acoustic images. The melanocytes and other cellular details were not fully observed in acoustic images.

Figure 26(a) reviews the general structure of the thin skin tissue; all skin layers can be identified easily because of the contrast differences for both optical and acoustic images. The cornified layer (**C**) that appears in the darkest outer layer in the acoustic image, also called the keratin layer, is mainly composed of fibrous protein and loose keratin. The external surface of the underlying layer, which is the epidermis (**E/ED**), is seen to be fairly smooth and flat. The dermis (**D**) comprises two layers: the papillary dermis (**PD**) just beneath the epidermis which contains fine collagen and elastic fibres and small blood vessels; and the thicker reticular dermis (**RD**) which contains large compact collagen fibres and thick elastin fibres. The carcinoma tumors are readily distinguishable at a higher magnification in Fig. 26(b). The stratum basale (or the basal layer) (**B**) in the epidermis can also be discerned in the acoustic image at this level, where the cells are small uniform and darkly stained in the basal epidermis shown in the optical image. Figure 26(c) that shows the carcinoma tumor resides underneath the epidermis which is surrounded by loose connective tissues. The melanocytes that are located in the basal layer and appear as round cells with cytoplasm scattered infrequently between the low columnar basal cells are seen in both images.

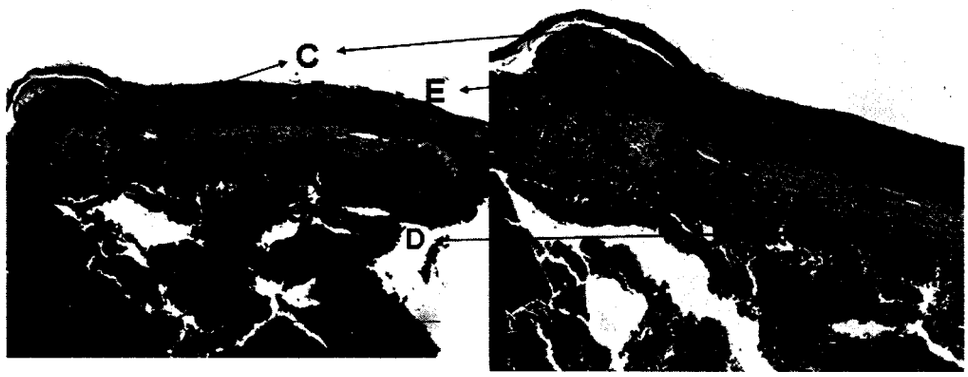

(a) Optical: **4X** objective lens; Acoustic: scanning area x=2.00mm

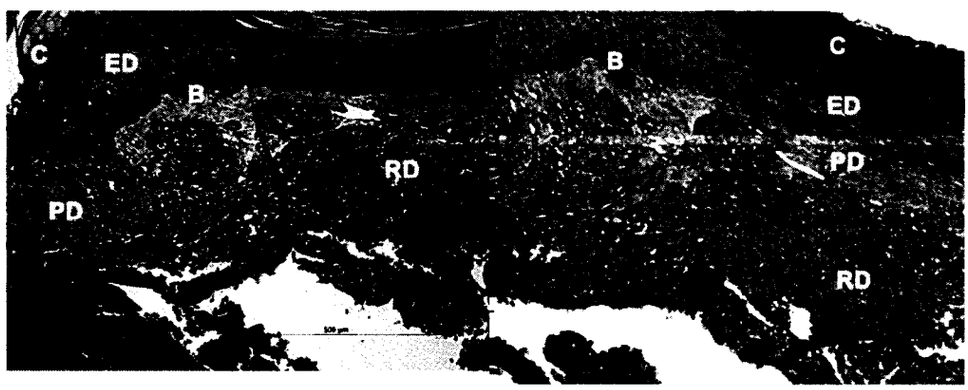

(b) Optical: **10X** objective lens; Acoustic: scanning area x=1.00mm

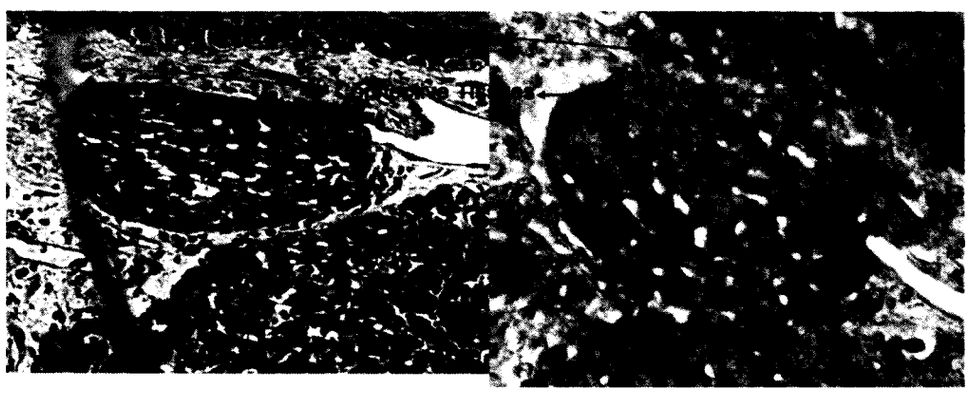

(c) Optical: **40X** objective lens; Acoustic: scanning area x=0.25mm

Fig. 26: Comparison of optical and acoustic images of thinly sliced abnormal specimen. Operating Frequency: 600MHz; Defocusing Distance: z = -3.5 um; Temperature: 21.5°.

4.1.3.3 TEM Images

Melanocyte cytoplasm contains specialized membrane-bound oval granule called premelanosomes and melanosomes which synthesise the pigment melanin. Since Transmission Electron Microscopy (hereinafter called "TEM") is the only methodology to identify intracellular melanosomes at ultrastructural level, TEM was used to examine the tissues, which were originally processed for optical microscopy, to verify that what we observed above is definite melanoma carcinoma. The premelanosome which synthesizes melanin is oval to boat-shaped, membrane-bound and contains characteristic transverse striations. After a period of melanin synthesis this striated pattern is obscured by the melanin (melanosomes). The example in Fig. 27 illustrates the maturational stages of melanosomes [182]. The premelanosome stage I (upper left) is characterized by its spherical form. It contains dense spots and occasionally filaments. In premelanosome stage II (upper left), there is an ellipsoidal organelle containing filaments, clearly exhibiting a periodicity perpendicular to the long axis of the organelle. At stage III (lower left) the matrix is partly melanized, whereafter the melanization is completed at stage IV (lower right).

The TEM images (see Fig. 28) were photographed at 20,000X and 40,000X original magnifications in Figs. 28(a) and 28(b), respectively. Referring to our TEM results, most of the cellular content has been washed off during the chemical process which left the indistinct shapeless form of dark dense spots (arrows indicated) which are too poorly defined to be called melanosomes. In this case, ideally a fresh melanoma skin tissue without staining and fixing is preferred in advance.

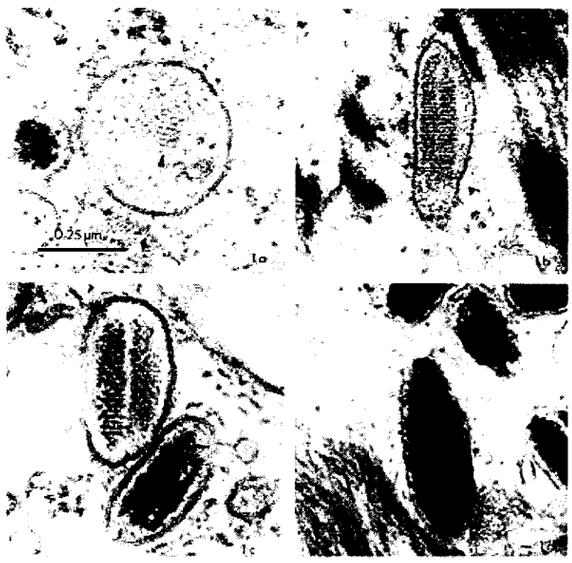

Fig. 27: Maturational stages of melanosomes (magn. ±100.000x). (Upper Left) Stage I; (Upper Right) Stage II; (Lower Left) Stage III and (Lower Right) Stage IV. Source: MUTAVI Research & Advice Group [182]

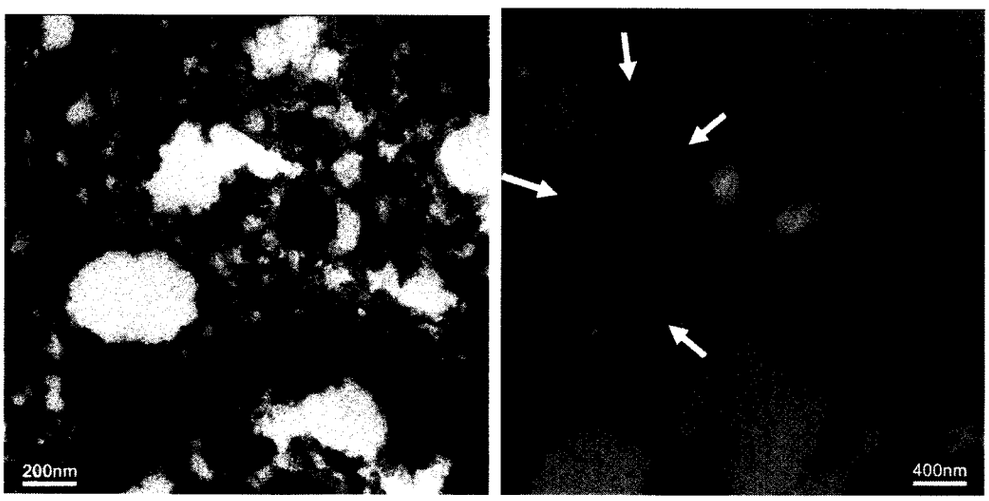

Fig. 28: Experimental TEM images of thinly sectioned melanoma skin tissue. (a) Mag x 20,000; (b) Mag x 40,000

4.1.3.4 Method for Visualizing Anisotropy

We used a shear polarized transducer-lens system (see Fig. 29) to determine whether or not the thinly sectioned melanoma skin tissue is isotropic [160-161]. The advantage of using the shear wave transducer-lens system is that the transmitted signal into the water is directional along one axis, and there is no specular reflection from normal incidence on the specimen. The acoustic beam that is excited in the water with the shear wave transducer has a directionality that allows for visualization and/or measurement of anisotropy. The tissue was visualized with the transducer-lens system with frequency at 75MHz. The tissue was rotated with angles of 0°, 45° and 90° (see Fig. 30).

In the thin specimen prepared for this study, anisotropy was not observed. Since virtually no contrast difference was observed in the acoustic images when formed at different angles, we concluded that there is no or weak anisotropy. This implies that conventional V(z) analysis can be applied when developing the mathematical model to predict contrast in an acoustic image.

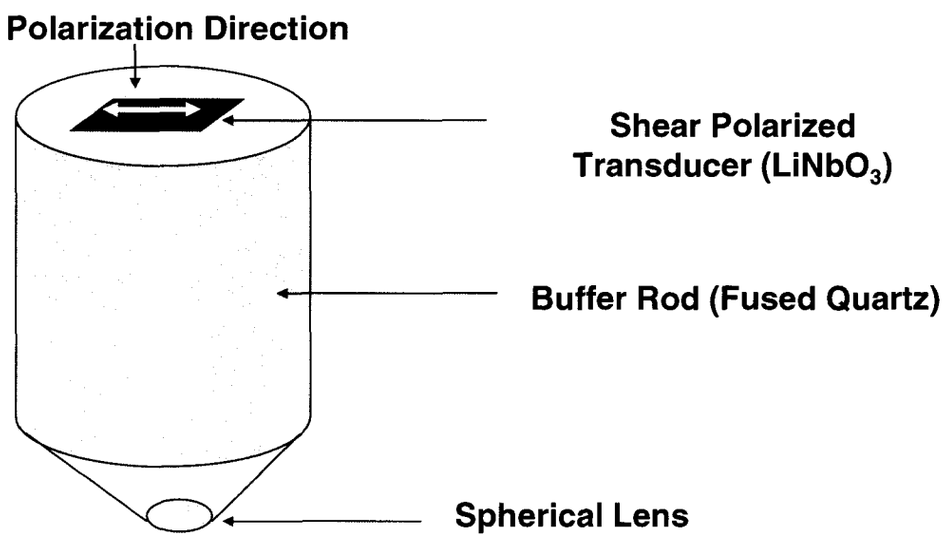

Fig. 29: Schematic diagram of shear wave-buffer rod lens system.
(Operating Frequency: 75MHz)

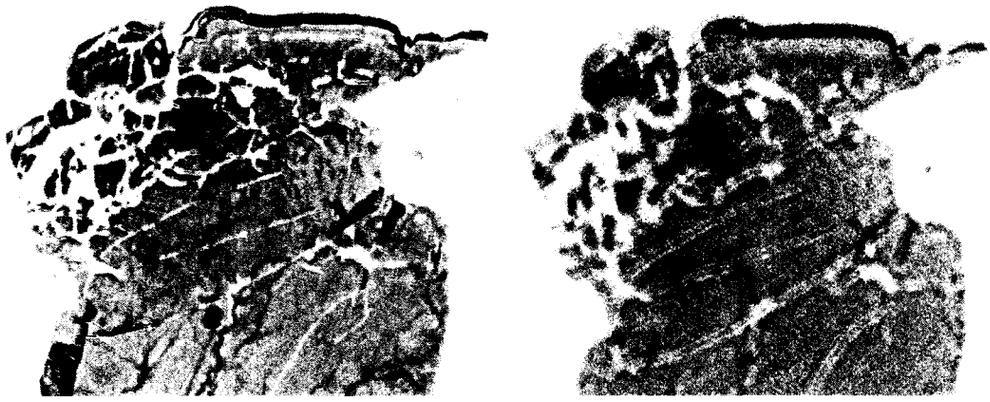

(a) θ = 0°

(b) θ = 45°

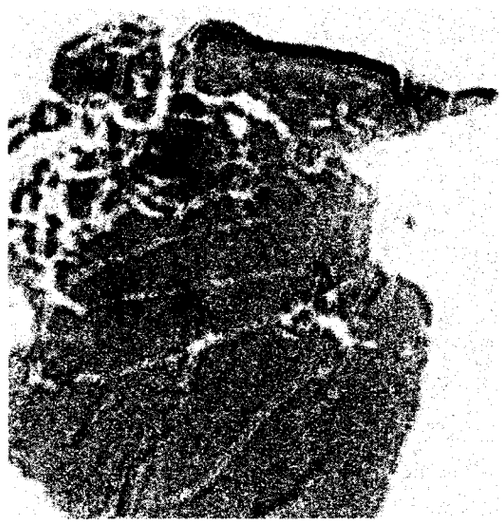

(c) θ = 90°

Fig. 30: Acoustical Images of Skin Tissues (Thickness: 15μm)

Acoustical images were visualized with a polarized shear wave transducer-lens system (Frequency: 75MHz) with pulse-wave mode. A lens was focused at the interface between the tissue and the substrate to form the image. The images show no anisotropy. The specimens were rotated with angles of (a) θ = 0°; (b) θ = 45° and (c) θ = 90°.

4.2 PHYSICAL AND MATHEMATICAL MODELING

The V(z) effect is a "source of contrast" and is used to record the quantitative information on the elastic properties of a specimen with microscopic precision [162-169]. The understanding of the V(z) curve effect in the SAM is of great significance. The transducer output voltage may be periodic with axial motion as the acoustic lens advances from the focal plane toward the specimen. The period of this variation is characteristic of the specimen's elastic material properties involved and results from the interface between the two component rays, shown in Fig. 31, that radiate into the liquid from the solid-liquid interface. First, there is the strong central maximum, centered on the focal plane (z=0). Second, the curve for positive z attenuates rapidly with increasing distance z because in this region the sample surface is farther away than the focal plane; much of the energy is reflected outside the lens. Third, on the negative z side, there are strong oscillations, where there are a series of periodic maxima and minima occurs, characterized by a period Δz. This region is characteristic of sample's acoustic properties: the patterns vary with material, as do the depths of the minima and the relative magnitudes of the maxima.

V(z) is an interference effect between surface acoustic waves (hereinafter called simply "SAW"), which are excited in the specimen and often referred to as Rayleigh waves, and specularly reflected waves, which are often referred to as longitudinal waves.

The theory of V(z) has been derived in two different ways: those involving Fourier angular spectrum analysis and those based on a ray optical model. Both models are of importance for explaining the V(z) effect.

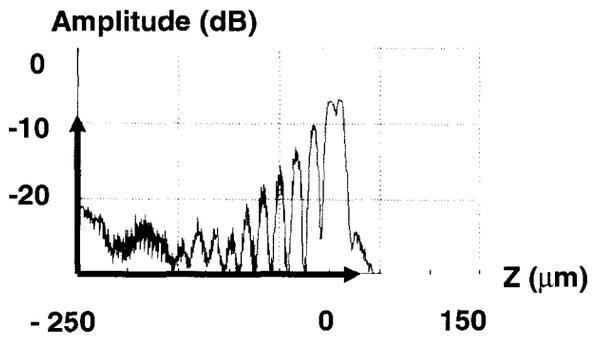

Fig. 31: The V(z) curve (experimental result) for fused quartz.

The acoustic lens having an aperture angle of 120° and a working distance of 310 μm was used at an operating frequency at 400MHz. The specimen was located in the water tank. The temperature of 20.0°C in the coupling medium (*i.e.*, distilled water) was measured by a thermocouple. The temperature was stabilized (change less than $\pm$0.1°C).

Contrast Mechanism

The schematic diagram of the contrast mechanism for expressing V(z) using a Fourier angular approach is shown in Fig. 32 below.

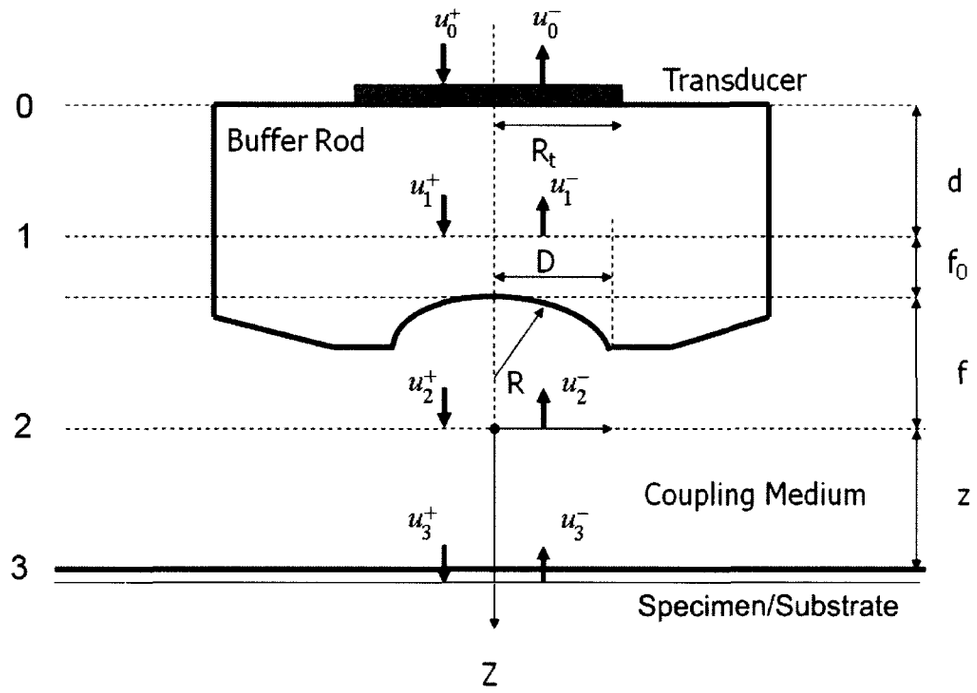

Fig. 32: Schematic diagram of the contrast mechanism in the spatial distribution.

'Plane 0' is the transducer plane, 'Plane 1' is the back focal plane, 'Plane 2' is the front focal plane, 'Plane 3' is the surface of the specimen, and $u_i^{\pm}$ is the acoustic field at each critical plane, where i = 0, 1, 2, and 3; "+" or "–" indicates the direction the field travels.

The output signal at the transducer plane (*i.e.*, V(z)) is expressed as follows [170]:

$$V(z)=C^{-1}\int_0^{\infty}u^2(r)P^2(r)R\left(\frac{r}{f}\right)\exp\left\{i2kz\sqrt{1-\left(\frac{r}{f}\right)^2}\right\}rdr \tag{4.1}$$

where u is an acoustic field, P is a pupil function, R is a reflectance function, k is a wavelength in the coupling medium, f is a focal length and C is expressed as the following equation:

$$C=\int_0^{\infty}u^2(r)P^2(r)rdr \tag{4.2}$$

Equations (4.1) and (4.2) are expressed by using $r=f\sin\theta$ as follows:

$$V(z)=C^{-1}\int_0^{\infty}u^2(\theta)P(\theta)R(\theta)\exp(i2kz\cos\theta)\sin\theta\cos\theta d\theta \tag{4.3}$$

$$C=\int_0^{\theta_0}u^2(\theta)P^2(\theta)\sin\theta\cos\theta d\theta \tag{4.4}$$

where θ is half the aperture angle of a lens.

When using $k_z=k\cos\theta$, Eqns. (4.3), (4.4) are expressed as follows:

$$V(z)=C^{-1}\int_k^{k\cos\theta_0}Q^2(k_z)R(k_z)\exp(i2k_z z)dk_z \tag{4.5}$$

$$C=\int_k^{k\cos\theta_0}Q^2(k_z)dk_z \tag{4.6}$$

$$Q^2(k_2)=u^2(k_z)P^2(k_z)k_z \tag{4.7}$$

From Eq. (4.5), the following equation is obtained.

$$F^{-1}\{V(z)\} = C^{-1}Q^{2}(k_z)R(k_z) \tag{4.8}$$

where $F^{-1}\{\ \}$ is the inverse Fourier transform.

Reflectance Function

Figure 33 shows the specimen and its periphery conditions. In the present case, the coupling medium and the specimen were water and biological tissue. Using the method described Tittmann *et al.* [171], the reflectance function must be appropriately determined.

When an acoustic beam is emitted from the acoustic lens onto the biological tissue mounted on the substrate in the culture medium, the reflectance function is determined by the layered media comprise the culture medium, the biological tissue, and the substrate. Suppose the surface of the tissue is very smooth, and the ultrasonic waves traveling within the tissues are as well behaved as those in water. Hence, the boundary condition for this case (*i.e.*, coupling medium-specimen-substrate) is considered the same as that of a liquid-liquid-solid.

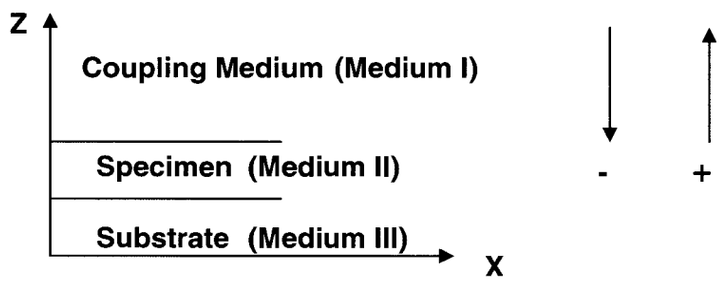

Fig. 33: The structure of the specimen and their periphery conditions

When a longitudinal wave is incident from water to the specimen, waves in water, the biological tissue, and the substrate can be expressed by using potentials as follows:

Water (Medium I)

$$\phi^{I-} = \Phi^{I-} \exp(i\alpha^{I} z)\exp\{-i(sx-\omega t)\} \tag{4.9}$$

$$\phi^{I+} = \Phi^{I-} \exp(-i\alpha^{I} z)\exp\{-i(sx-\omega t)\} \tag{4.10}$$

Biological Specimen (Medium II)

$$\phi^{II-} = \Phi^{II-} \exp\{i\alpha^{II}(z-d)\}\exp\{-i(sx-\omega t)\} \tag{4.11}$$

$$\phi^{II+} = \Phi^{II-} \exp\{-i\alpha^{II}(z-d)\}\exp\{-i(sx-\omega t)\} \tag{4.12}$$

Substrate (Medium III)

$$\phi^{III+} = \Phi^{III+} \exp\{-i\alpha^{III}(z-d)\}\exp\{-i(sx-\omega t)\} \tag{4.13}$$

$$\psi^{III+} = \Psi^{III+} \exp\{-i\beta^{III}(z-d)\}\exp\{-i(sx-\omega t)\} \tag{4.14}$$

where ϕ is the potential of the longitudinal wave, ψ is the potential of the shear wave, Φ is the amplitude of the potential of the longitudinal wave, Ψ is the amplitude of the potential of the shear wave, the superscript "+" shows waves propagating in the positive direction of Z axis, the superscript "-" shows waves propagating in the negative direction of Z axis, and Roman numerals I, II, III indicate media for wave propagation.

By Snell's law, we obtain the following equation:

$$k_L^I \sin\theta_L^I = k_L^{II} \sin\theta_L^{II} = k_L^{III} \sin\theta_L^{III} = k_S^{III} \sin\theta_S^{III} = s \tag{4.15}$$

$$\alpha = k_L \cos\theta_L, \text{ and } \beta = k_S \cos\theta_S \tag{4.16}$$

where θ is an incident angle or a reflected angle, a subscript L indicates a longitudinal wave, and a subscript S indicates a shear wave.

The boundary conditions of the present case are a particle velocity in direction of Z-axis and a continuity of stress. Those are expressed as follows:

$$\sigma_z^I = \sigma_z^{II}, \text{ and } v_z^I = v_z^{II} \text{ at } z = 0 \tag{4.17}$$

$$\sigma_z^{II} = \sigma_z^{III}, \ \tau_{xz}^{II} = \tau_{xz}^{III}, \text{ and } v_z^{II} = v_z^{III} \text{ at } z = 0 \tag{4.18}$$

From Eqs. (4.17) and (4.18), we obtain the sets of the first order of simultaneous equations relating to the potentials.

$$\begin{bmatrix} -\sigma_z \\ v_z/\omega \end{bmatrix}_{z=d} = \begin{bmatrix} \lambda^I k_L^{I^2} & 0 \\ 0 & \alpha^I \end{bmatrix} \begin{bmatrix} \Phi^{I^+} + \Phi^{I^-} \\ \Phi^{I^+} - \Phi^{I^-} \end{bmatrix} = \begin{bmatrix} \lambda^{II} k_L^{II^2} & 0 \\ 0 & \alpha^{II} \end{bmatrix} \begin{bmatrix} \Phi^{II^+} + \Phi^{II^-} \\ \Phi^{II^+} - \Phi^{II^-} \end{bmatrix} \tag{4.19}$$

$$\begin{aligned} \begin{bmatrix} -\sigma_z \\ v_z/\omega \end{bmatrix}_{z=d} &= \begin{bmatrix} \lambda^{II} k_L^{II^2} \cos\alpha^{II} d & i\lambda^{II} k_L^{II^2} \sin\alpha^{II} d \\ i\alpha^{II} \sin\alpha^{II} d & \alpha^{II} \cos\alpha^{II} d \end{bmatrix} \begin{bmatrix} \Phi^{II^+} + \Phi^{II^-} \\ \Phi^{II^+} - \Phi^{II^-} \end{bmatrix} \\ &= \begin{bmatrix} \mu^{III}\left(\beta^{III^2} - s^2\right) & 2\mu^{III} s\beta^{III} \\ \alpha^{III} & s \end{bmatrix} \begin{bmatrix} \Phi^{III^+} \\ \Phi^{III^+} \end{bmatrix} \end{aligned} \tag{4.20}$$

$$2s\alpha^{III}\Phi^{III^+} + \left(s^2 - \beta^{III^2}\right)\Psi^{III^+} = 0 \tag{4.21}$$

From Eqs. (4.19), (4.20), (4.21), the reflectance function of the amplitude is expressed as follows:

$$\frac{\Phi^{I^-}}{\Phi^{I^+}} = \frac{(B_1 - \gamma B_2)\cos\alpha^{II} d + i(\gamma B_1 - B_2)\sin\alpha^{II} d}{(B_1 + \gamma B_2)\cos\alpha^{II} d - i(\gamma B_1 + B_2)\sin\alpha^{II} d} \tag{4.22}$$

$$\gamma = \frac{\rho^{I}\alpha^{II}}{\rho^{II}\alpha^{I}} \tag{4.23}$$

$$B_1 = \left(k_s^{III^2} - 2s^2\right)^2 + 4s^2\alpha^{III}\beta^{III}, \text{ and } B_2 = \frac{\rho^{II}\alpha^{III}}{\rho^{III}\alpha^{II}} k_s^{III^4} \tag{4.24}$$

The output of the transducer can be simulated after determining the reflectance function by Eqs. (4.22), (4.23), and (4.24).

Velocity Measurement

Ever since the advent of the Mechanical Scanning Acoustic Reflection Microscope [171], a key objective has been quantitative data acquisition besides the enhancement of the resolution in the acoustic images. For quantitative data acquisition with the SAM, the V(z) curve techniques have been developed and applied to various materials with fruitful results [172-178]. However, it is not easy to characterize soft materials by the V(z) curve technique. First, the critical angle of the Rayleigh wave generation of soft materials is generally high. Therefore, the Rayleigh wave is often not generated within a specimen, even though an acoustic lens having a high numerical aperture (*i.e.*, 120°) is used. This means that no V(z) curve is formed. Second, attenuation in soft materials is high. Therefore, the V(z) curve may not have enough oscillations for the FFT analysis to measure the Rayleigh wave velocities accurately, even though the Rayleigh wave is generated. When an acoustic lens, having a high numerical aperture and a long working distance, with a low frequency (*i.e.*, 10 MHz or less) is used for the soft materials, the V(z) curve might be formed. However, in this case, an advantage of the V(z) curve technique for characterizing a small area of the materials is lost.

There may be a simple solution for applying V(z) curve techniques to soft materials when the soft material is treated as a thin film coated on an isotropic substrate (*i.e.*, sapphire, fused quartz, silica glass, or the like). Then, the reflectance function can be obtained by using the theory of ultrasonic propagation in layered media [179]. Using the reflectance function, the V(z)

curve for the thin soft material mounted on the substrate can be simulated. In the simulation, only velocity of the longitudinal wave of the soft material is set by estimation. The actual velocity of the longitudinal wave of the soft material can be obtained by matching the V(z) curve obtained from the experiment in an iterative procedure. This report presents analyses and laboratory results for the above case.

4.3 COMPUTER SIMULATION

Experimental V(z) Curve

The main procedures for characterizing the SAW velocity of the specimen by the V(z) curve method are illustrated in Fig. 34. Figs 34(a) and 34(b) show the major components contributing to the V(z) curve in Fig. 34(c) conceptually. We now assume that the entire transducer output V(z) can be approximately represented by combining ray theory for the leaky SAW component and field theory for the directly reflected component in the negative z region. Once the V(z) curve has been smoothed, we window the smoothed curve by selecting its first 3 to 5 oscillations. The SAW velocity is obtained from the power FFT result by transforming V(z) curve into a frequency domain.

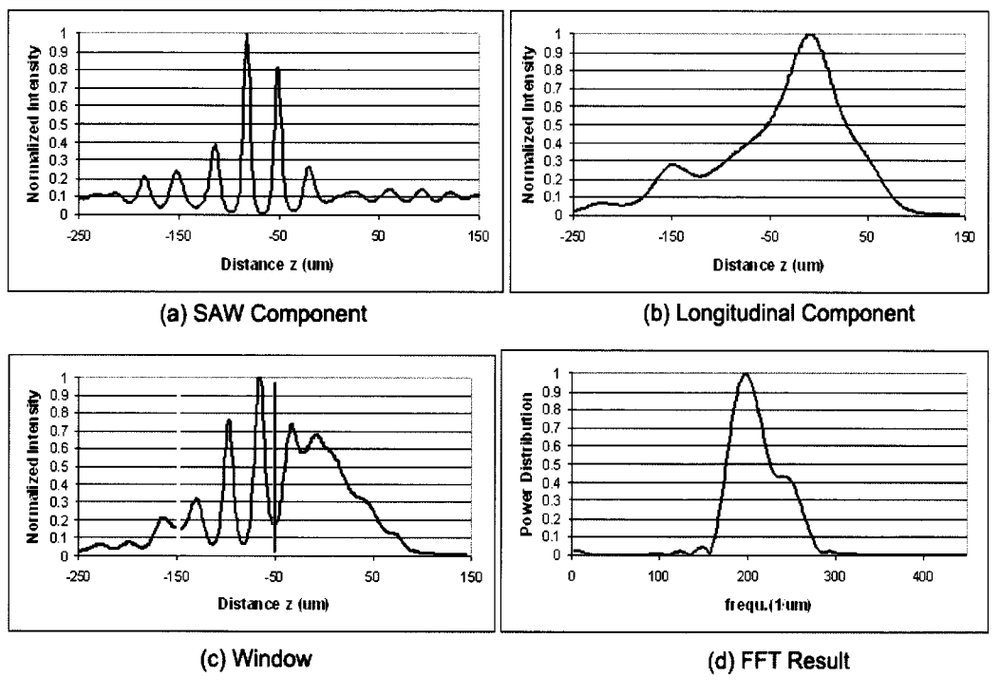

Fig. 34: SAW Velocity Acquisition with FFT

Figure 35 shows the original V(z) curves obtained at both normal and abnormal points of the thin melanoma tissue mounted on the soda-lime glass substrate, while the corresponding FFT analyses are shown in Fig. 36.

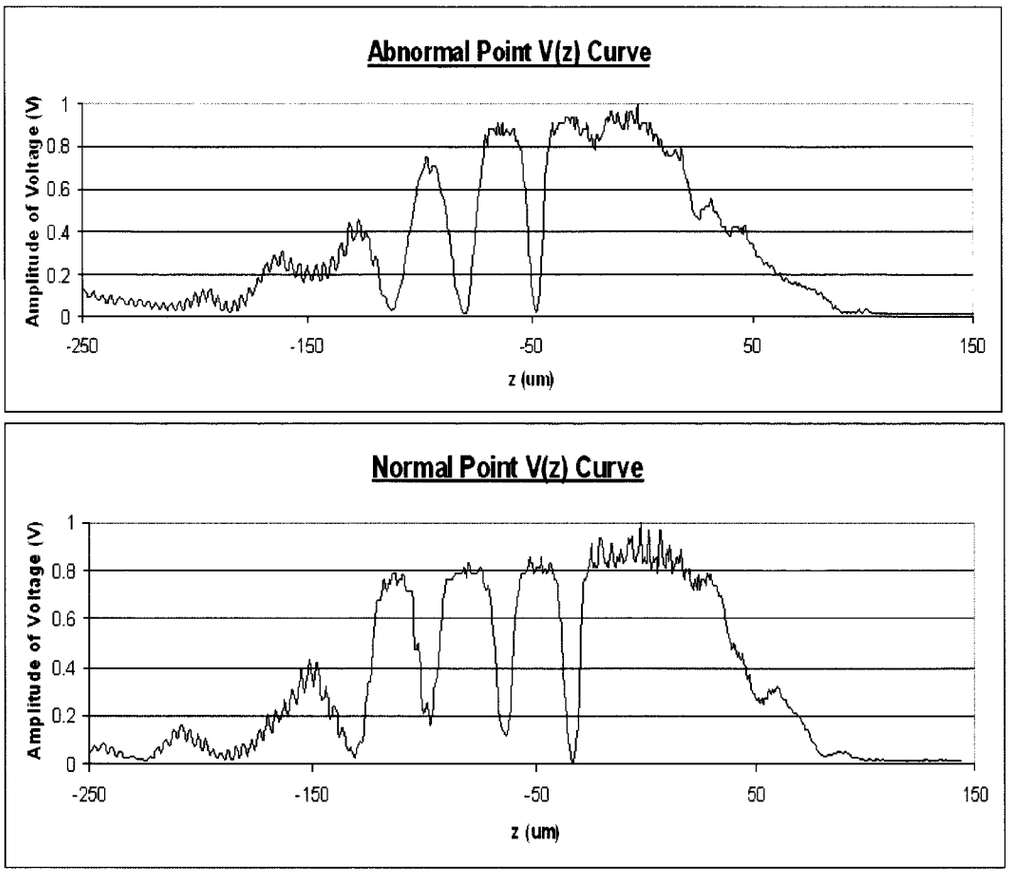

Fig. 35: V(z) curves obtained at (Upper) abnormal and (Lower) normal points of the melanoma thin tissue on soda-lime glass substrate. (Input frequency: 200MHz; thickness of the specimen: 5μm; temperature: 21.5°C)

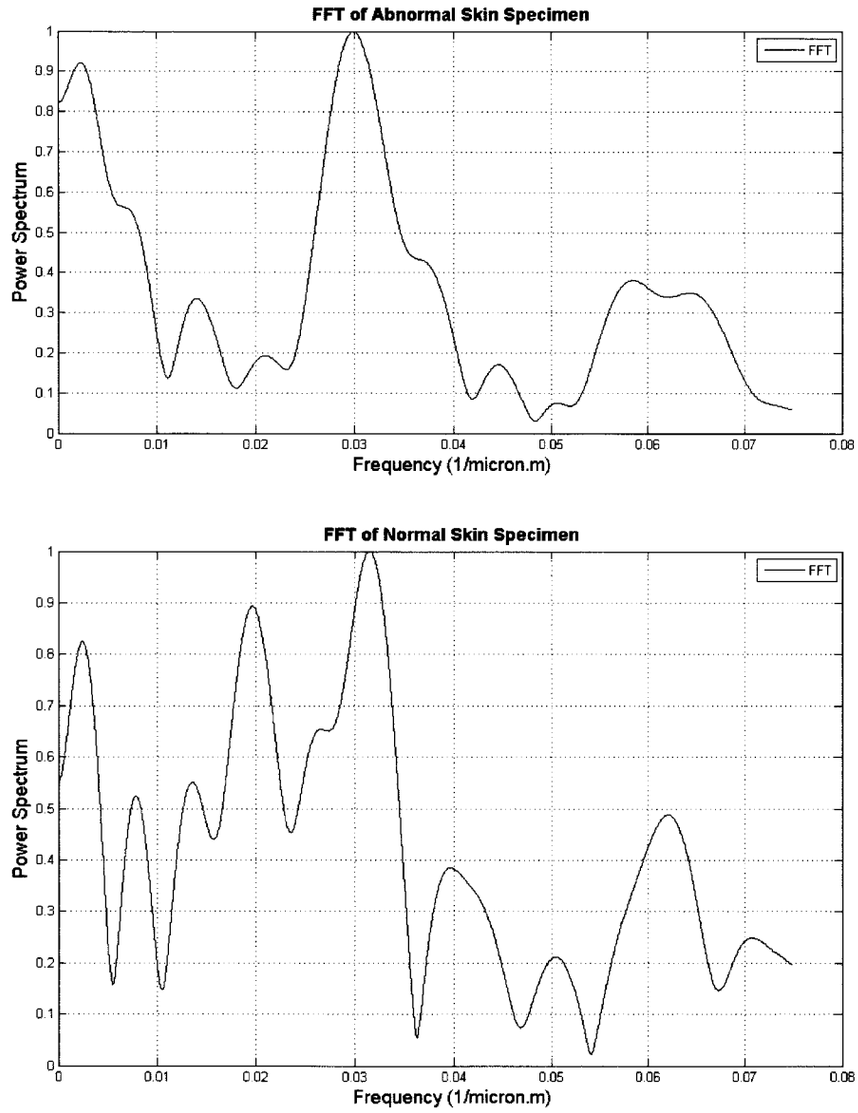

Fig. 36: FFT analysis obtained at (Upper) abnormal and (Lower) normal points of the melanoma thin tissue on soda-lime glass substrate. (Input frequency: 200MHz; thickness of the specimen: 5μm; temperature: 21.5°C)

Theoretical V(z) Curve (Simulation of V(z) Curve)

As shown above, the SAW velocity is computed by FFT analysis, in contrast, the longitudinal wave velocity is obtained by implementing a computer parameter-fitting technique. The algorithm of the V(z) curve simulation is described in the following steps. First, initialize the parameters of the acoustic lens, specimen (thinly sectioned biological tissue), and soda-lime substrate. Second, calculate the parameters of the acoustic field at the back focal plane, pupil function of the lens, and the reflectance function. Third, calculate and draw the V(z) curve. In the simulation, parameters of the acoustic lens are shown in Table 5.

The velocity of the longitudinal wave of water was set as 1,487 m/s. Based on the previous research study [180], the speed of sound in most normal tissues of the human body is quite constant and close to that in water, and the ultrasound velocities in malignant melanoma tissues varied between 1,553 m/s and 1,588 m/s with a mean of 1,564 m/s. Therefore the longitudinal velocity of the normal/abnormal skin tissue (thickness: 5μm) was set to range from 1,540 m/s to 1,590 m/s. Moreover, the human skin density is set within a range of 1.11 – 1.19 (10^3 kg m^{-3}) [181]. Soda-lime glass was chosen as the substrate; its velocities of longitudinal and shear waves are 6,000 m/s and 3,200 m/s respectively. The summarized physical parameters of biological tissue for computer simulation are shown in Table 6.

Figure 37 shows the matched up result of the V(z) curve simulation with the experimental data for normal/abnormal skin tissue.

By applying the power FFT shown in Fig. 36, the surface acoustic wave velocities of the specimen system for abnormal and normal skin tissues/soda-lime glass were obtained as 3248.02 m/s and 3,162.90 m/s, respectively. Changing the values of the longitudinal wave velocity and the density, the simulations were continued until the surface acoustic velocities were substantially coincided with the experimental values. The longitudinal wave velocities were obtained as 1,560 m/s and 1,540 at a density 1.15 (10^3 kg

m^{-3}) for abnormal and normal specimens, respectively. Those values are in accordance with the longitudinal wave velocity and density obtained from the literature.

Table 5: Parameter of Acoustic Lens

Name	Acoustic Lens Olympus
Model	AL2M631
Transducer	ZnO
Buffer Rod	Al2O3
Radius of Transducer	383.000 um
Longitudinal Wave Velocity in Buffer Rod	11175.00 m/s
Shear Wave Velocity in Buffer Rod	6950 m/s
Density in Buffer Rod	3.980 g/cm^3
Frequency	200.00 MHz
Focal Length	577.52 um
Half Aperture Angle	60.00 degree
Acoustic ZL	6122.00 um

Table 6: Physical Parameters of Biological Tissue

Lens	AL2M631
Liquid	De-ionized Water
Temperature of Water	22°C
Substrate	soda-lime glass
Radius of Lens	500.6207 micro.m
Wave Length in Water	7.4400 micro.m
Longitudinal Wave Velocity of Tissue	1540.00 – 1590.00 m/s
Density of Tissue	1.11 to 1.19 g / cm^3
Thickness of Tissue	5.0000 micro.m

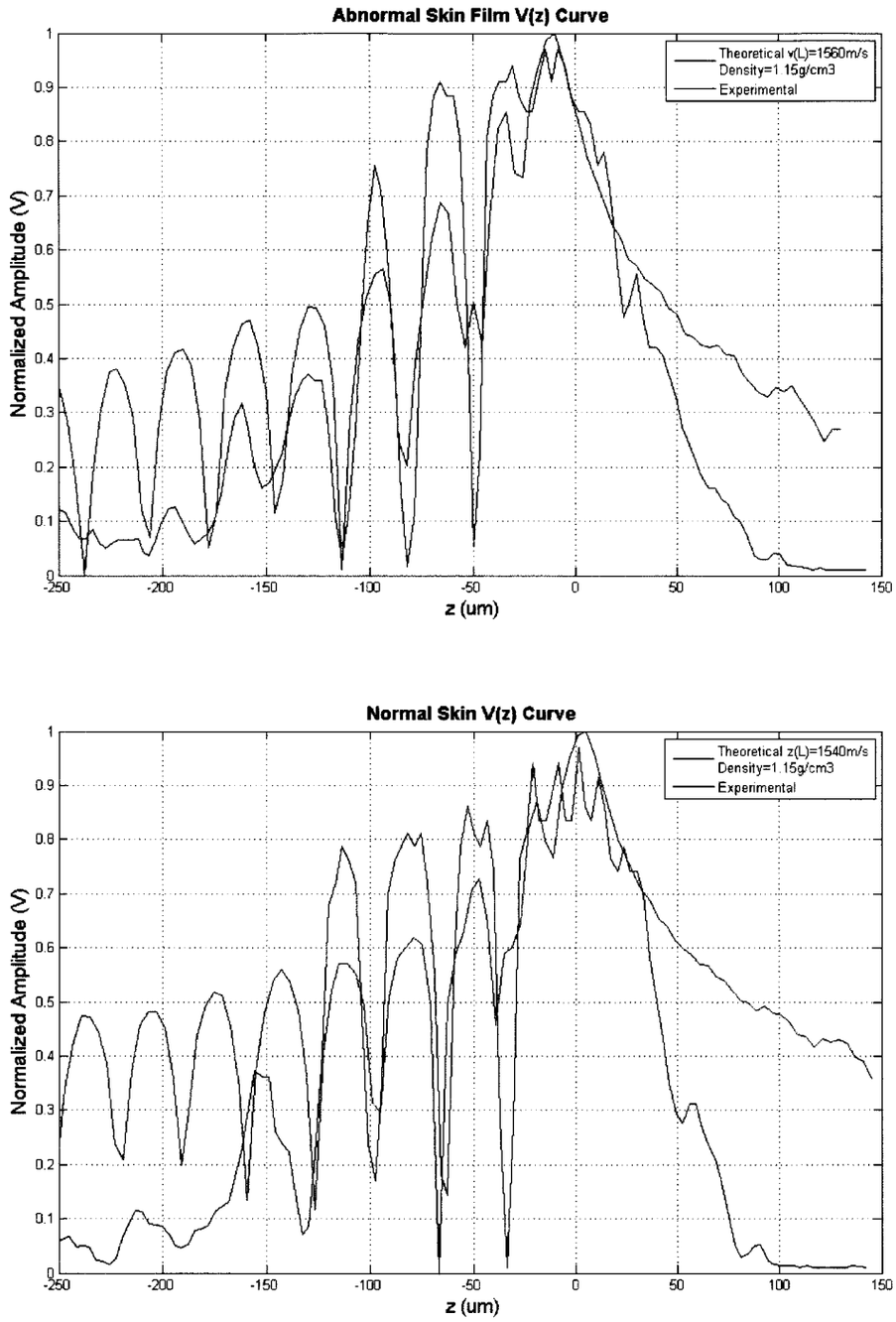

Fig. 37: Simulation of V(z) curve of (Upper) abnormal and (Lower) normal skin tissue mounted on the soda-lime glass substrate.

CHAPTER V

CONCLUSIONS AND RECOMMENDATIONS

Acoustic images of thickly sectioned skin tissues (normal and abnormal) were formed by the pulse-wave mode using the SAM with optimized frequency. These images were compared to optical images, and were systematically characterized. Moreover, by using the angular spectrum approach, a mathematical model to predict contrast in the image with acoustic microscopy for thickly sectioned skin tissues was developed.

For thinly sectioned skin tissues, we have also proved that the tone-burst wave mode can visualize cells in the tissue for medical diagnosis. Quantitative data acquisition to characterize the tissue is achieved in the following three steps:

1. The V(z) curve for the melanoma/soda-lime glass specimen was simulated by developing a software program.
2. The procedure of obtaining longitudinal wave velocity of biological tissue was developed by using the V(z) curve technique.
3. Longitudinal wave velocities of abnormal and normal tissues were obtained by the above simulations.

In the future, we need to observe fresh tissue with the high frequency tone-burst-wave mode for medical diagnosis. In addition, the accuracy of acoustic parameters needs to be refined.

APPENDIX A – RAY TRACING

The difference in attenuation primarily generates the contrast of the tissue in an acoustic image. Therefore, it is necessary to place a highly reflective substrate at the bottom of the specimen to ensure that most incident waves are reflected at the surface of the substrate rather than from other materials underneath. In this work, the substrate was sapphire. The acoustic impedance of the tissue is similar to that of water (the coupling medium), therefore the image has virtually no contrast difference caused by the reflections, illustrated in Figs. A1(a) and A1(b).

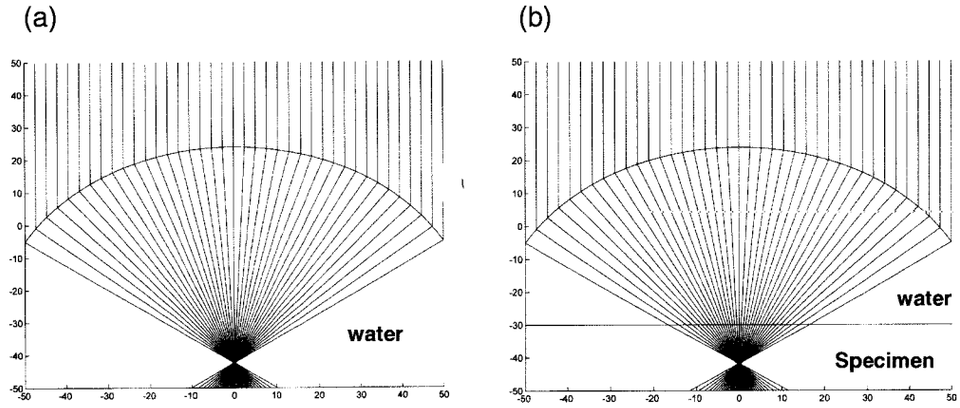

Fig. A1. Ray Tracing. (a) Acoustic lens is focused on the substrate when there is no specimen in water; (b) Acoustic lens is focused within the biological specimen.

APPENDIX B- ACOUSTIC WAVES IN ISOTROPIC MEDIA

Hooke's Law

Using Hooke's law, the relation between stress and strain of the elastic wave is shown as follows:

$$\sigma_{ij} = C_{ijkl}\varepsilon_{kl} \tag{B1}$$

$$\text{where } \sigma_{ij} = \begin{bmatrix} \sigma_1 & \sigma_6 & \sigma_5 \\ \sigma_6 & \sigma_2 & \sigma_4 \\ \sigma_5 & \sigma_4 & \sigma_1 \end{bmatrix} \qquad \varepsilon_{ij} = \begin{bmatrix} \varepsilon_1 & \frac{1}{2}\varepsilon_6 & \frac{1}{2}\varepsilon_5 \\ \frac{1}{2}\varepsilon_6 & \varepsilon_2 & \frac{1}{2}\varepsilon_4 \\ \frac{1}{2}\varepsilon_5 & \frac{1}{2}\sigma_4 & \varepsilon_1 \end{bmatrix} \tag{B2}$$

The Eq. (B2) is rewritten as follows:

$$\sigma_I = C_{IJ}\varepsilon_J \tag{B3}$$

$$C_{IJ} = \begin{bmatrix} C_{11} & C_{12} & C_{12} & 0 & 0 & 0 \\ C_{12} & C_{11} & C_{12} & 0 & 0 & 0 \\ C_{12} & C_{12} & C_{11} & 0 & 0 & 0 \\ 0 & 0 & 0 & C_{44} & 0 & 0 \\ 0 & 0 & 0 & 0 & C_{44} & 0 \\ 0 & 0 & 0 & 0 & 0 & C_{44} \end{bmatrix} \tag{B4}$$

$$C_{12} = C_{11} - 2C_{44} \tag{B5}$$

$$\text{where} \qquad C_{12} = \lambda \qquad C_{44} = \mu \tag{B6}$$

Note that λ and μ are Lamē's constant.

Put Eq. (B4) to Eq. (B1), we obtain Eq. (B7) as follows:

$$\sigma_{ij} = \begin{cases} C_{11}\varepsilon_{ij} + C_{12}\varepsilon_{kl} & (i = j \neq k = l) \\ 2C_{44}\varepsilon_{ij} & (i \neq j) \end{cases} \tag{B7}$$

Put (B5) to Eq. (B7), we organize the Eq. (B7) as follows:

$$\sigma_{ij} = 2C_{44}\varepsilon_{ij} + (C_{11} - 2C_{44}) div\vec{u}\,\delta_{ij} \tag{B8}$$

where $\vec{u}$ is a position vector.

Wave Equation

Equation of motion is expressed as follows:

$$\rho \frac{\partial^2 u_i}{\partial t^2} = \frac{\partial \sigma_{ij}}{\partial x_j} \tag{B9}$$

Put Eq. (B8) to Eq. (B9), we rewrite Eq. (B9) as follows:

$$\begin{aligned} \rho \frac{\partial^2 \vec{u}}{\partial t^2} &= C_{44}\left\{\nabla^2 \vec{u} + grad(div\vec{u})\right\} + (C_{11} - 2C_{44}) grad(div\vec{u}) \\ &= C_{44}\nabla^2 \vec{u} + (C_{11} - C_{44})\nabla(\nabla \cdot \vec{u}) \end{aligned} \tag{B10}$$

Then, Eq. (B10) is expressed as follows:

$$\rho \frac{\partial^2 \vec{u}}{\partial t^2} = C_{11}\nabla(\nabla \cdot \vec{u}) - C_{44}\nabla \times (\nabla \times \vec{u}) \tag{B11}$$

$$\because \quad \nabla \times (\nabla \times \vec{u}) = \nabla(\nabla \cdot \vec{u}) - \nabla^2 \vec{u}$$

The position vector $\vec{u}$ is expressed by the following equation.

$$\vec{u} = \nabla\phi + \nabla \times \vec{H} \tag{B12}$$

where ϕ is a scalar potential, and $\vec{H}$ is a vector potential.

Put Eq. (B12) to Eq. (B11), we obtain

$$\rho\frac{\partial^2\nabla\phi}{\partial t^2}+\rho\frac{\partial^2\nabla\left(\nabla\times\vec{H}\right)}{\partial t^2}=C_{11}\nabla\cdot\left(\nabla\phi\right)-C_{44}\nabla\times\left(\nabla\vec{H}\right) \tag{B13}$$

$$\because \qquad \nabla\times\left(\nabla\phi\right)=0 \qquad\qquad \nabla\cdot\left(\nabla\times\vec{H}\right)=0$$

Eq. (B13) must be satisfied with Eqs. (B14), (B15) expressed as follows:

$$\frac{\partial^2\phi}{\partial t^2}=\frac{C_{11}}{\rho}\nabla^2\phi \tag{B14}$$

$$\frac{\partial^2\vec{H}}{\partial t^2}=\frac{C_{44}}{\rho}\nabla^2\vec{H} \tag{B15}$$

Eqs. (B14), (B15) describe that ϕ and $\vec{H}$ are the elastic waves propagating within the isotropic medium with the following equations, respectively.

$$v_l=\sqrt{\frac{\lambda+2\mu}{\rho}} \tag{B16}$$

$$v_t=\sqrt{\frac{\mu}{\rho}} \tag{B17}$$

The position vector $\vec{u}_l$ relating ϕ is expressed as follows:

$$\vec{u}_l=\nabla\phi=i\vec{k}\phi_0e^{i\left(\vec{k}\vec{x}-\omega t\right)} \tag{B18}$$

Eq. (B18) shows that $\vec{u}_l$ is the longitudinal wave.

$$\vec{u}_t=\nabla\times\vec{H}=\vec{u}_{0t}e^{i\left(\vec{k}\vec{x}-\omega t\right)}=0 \tag{B19}$$

$$\nabla \cdot \vec{u}_t = i\vec{k} \cdot \vec{u}_{0t} e^{i\left(\vec{k}\vec{x}-\omega t\right)} = 0 \tag{B20}$$

$$\because \qquad \nabla \cdot \left(\nabla \times \vec{H}\right) = 0$$

$$\vec{k} \cdot \vec{u}_{ot} = 0 \tag{B21}$$

Eq. (B21) shows that $\vec{u}$ is the shear wave.

APPENDIX C – REFLECTANCE FUNCTION

Suppose an ultrasonic wave is incident onto an interface between a liquid and a solid (see Fig. C1). In this case, the reflectance function is determined as the ratio between the amplitude of the wave incident from the liquid onto the interface and that of the wave reflected from the interface toward the liquid.

Referring to Fig. C1, with Snell's law, we obtain the following equation.

$$\frac{\sin\theta}{c} = \frac{\sin\theta_1}{c_1} = \frac{\sin\gamma_1}{b_1} \tag{C1}$$

where c is the longitudinal wave in the liquid, c_1 is the longitudinal wave propagating in the solid, b_1 is the shear wave propagating in the solid, θ is the angle of the longitudinal wave that is incident into the interface. It is the same as the angle of the longitudinal wave reflected from the interface, θ_1 is the angle of the longitudinal wave propagating from the interface when the longitudinal wave is incident from the liquid into the interface with θ, and γ_1 is the angle of the shear wave propagating from the interface when the longitudinal wave is incident from the liquid into the interface with θ.

Multiply angular frequency ω to Eq. (C1), we rewrite Eq. (C1) as follows:

$$k\sin\theta = k_1\theta_1 = \kappa_1\sin\gamma_1 = \xi \tag{C2}$$

where k is the wave number of the longitudinal wave in the liquid, and κ_1 is the wave number of the shear wave in the solid.

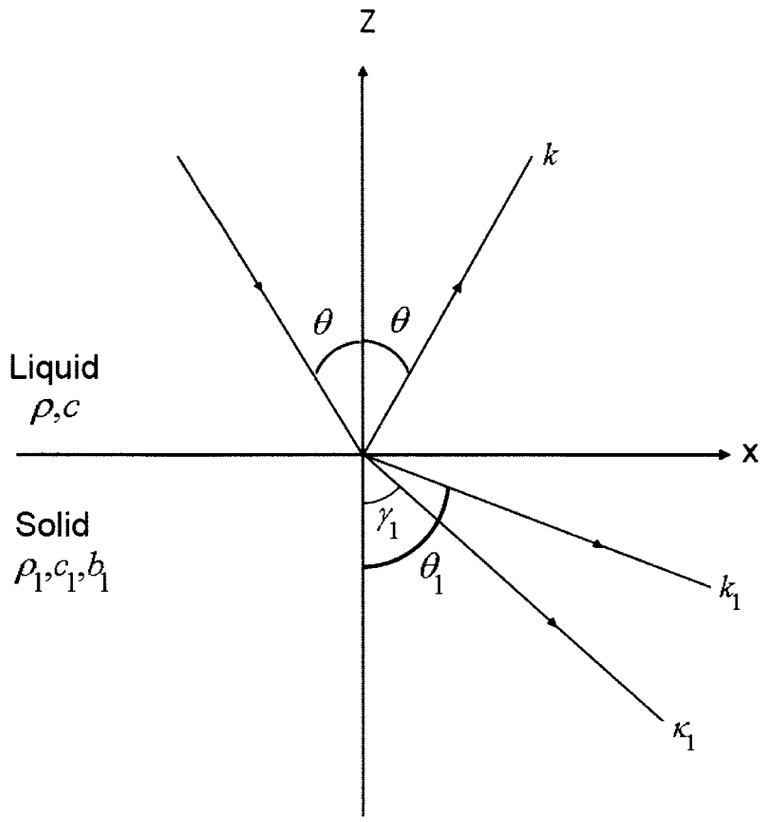

Fig. C1. The reflected and transmitted rays at a liquid-solid interface.

Not considering the potential in the direction of y-axis, we obtain

$$\phi = \phi_{(x,z,t)}, \quad \overline{H} = \left(0, \psi_{(x,z,t)}, 0\right) \tag{C3}$$

No shear wave propagates in liquid. Therefore, we obtain

$$\phi_{(x,z,t)} = \left(\phi' e^{i\alpha z} - \phi'' e^{-i\alpha z}\right) \cdot e^{i\xi x} e^{-i\omega t} \tag{C4}$$

$$\alpha = \left(k^2 - \xi^2\right)^{1/2} = k\cos\theta \tag{C5}$$

where ϕ' is wave reflected from the interface, and ϕ'' is the wave incident into the interface.

For solid, we obtain the following equations.

$$\phi_{1(x,z,t)} = \phi_1'' e^{-i\alpha_1 z} \cdot e^{i\xi x} e^{-i\omega t} \tag{C6}$$

$$\alpha_1 = \left(k_1^2 - \xi^2\right)^{1/2} = k_1 \cos\theta_1 \tag{C7}$$

$$\psi_{1(x,z,t)} = \psi_1'' e^{-i\beta_1 z} \cdot e^{i\xi x} e^{-i\omega t} \tag{C8}$$

$$\beta_1 = \left(\kappa_1^2 - \xi^2\right)^{1/2} = \kappa_1 \cos\gamma_1 \tag{C9}$$

From Eqs. (C4), (C6), and (C8), we obtain the following position vectors.

$$\begin{aligned} u_x &= \frac{\partial \phi}{\partial x}, u_z = \frac{\partial \phi}{\partial z} \\ u_{1x} &= \frac{\partial \phi_1}{\partial x} - \frac{\partial \psi_1}{\partial z}, u_{1z} = \frac{\partial \phi_1}{\partial z} + \frac{\partial \psi_1}{\partial x} \end{aligned} \tag{C10}$$

Next, we consider the boundary condition. At the interface, stresses in the direction of z-axis are equal. Therefore, we obtain the following equation.

$$\sigma_{zz} = \sigma_{1zz} \quad \text{on} \quad z = 0 \tag{C11}$$

No shear stress is generated along the liquid interface, therefore, we obtain the following equation.

$$\sigma_{1xz} = 0 \quad \text{on} \quad z = 0 \tag{C12}$$

Displacements at the interface in the direction of z-axis are equal, therefore, we obtain the following equation.

$$u_z = u_{1z} \quad \text{on} \quad z = 0 \tag{C13}$$

In liquid, $\mu = 0$ in Eq. (C11),

$$\sigma_{zz} = \lambda\left(\frac{\partial u_x}{\partial x} + \frac{\partial u_z}{\partial z}\right) = \lambda\nabla^2\phi = -\lambda\frac{\omega^2}{c^2}\phi = -\rho\omega^2\phi \tag{C14}$$

$$\begin{aligned}\sigma_{1zz} &= \lambda\frac{\partial u_{1x}}{\partial x} + (\lambda + 2\mu)\frac{\partial u_{1z}}{\partial z} = (\lambda + 2\mu)\nabla^2\phi + 2\mu\left(\frac{\partial^2\psi_1}{\partial x\partial z} - \frac{\partial^2\phi}{\partial z^2}\right) \\ &= -\rho_1\omega^2\phi_1 + 2\rho_1 b_1^{\,2}\xi^2\phi_1 + 2\rho_1 b_1^{\,2}\cdot i\xi\frac{\partial\psi_1}{\partial z}\end{aligned} \tag{C15}$$

With Eqs. (C14) and (C15), we obtain the following equations from (C14).

$$\rho\phi = -2\xi\rho_1\kappa_1^{-2}\left(p_1\phi_1 + i\frac{\partial\psi_1}{\partial z}\right) \tag{C16}$$

$$p_1 = \left(\xi^2 - \kappa_1^{\,2}/2\right)\xi^{-1} \tag{C17}$$

From Eq. (C12), we obtain

$$\sigma_{1xz} = \frac{\partial u_{1x}}{\partial z} + \frac{\partial u_{1z}}{\partial x} = 2i\xi\frac{\partial\phi_1}{\partial z} + \left(\kappa_1^{\,2} - 2\xi^2\right)\psi_1 = 0 \tag{C18}$$

Multiply $-\frac{i}{2\xi}$ to Eq. (C18), we obtain

$$\frac{\partial \phi_1}{\partial z} + ip_1\psi_1 = 0 \tag{C19}$$

With Eq. (C13), we obtain

$$\frac{\partial \phi}{\partial z} = \frac{\partial \phi_1}{\partial z} + i\xi\psi_1 \tag{C20}$$

Put Eqs. (C4), (C6), (C8) into Eqs. (C16), (C19), (C20), and let $m = \rho_1/\rho$, we obtain

$$\frac{\kappa_1^2}{2\xi m}(\phi' + \phi'') + p_1\phi_1'' + \beta_1\psi_1'' = 0 \tag{C21}$$

$$-\alpha_1\phi_1'' + p_1\psi_1'' = 0 \tag{C22}$$

$$\alpha(\phi' - \phi'') - \frac{\kappa_1^2}{2\xi}\psi_1'' = 0 \tag{C23}$$

Let $R = \phi'/\phi'', W_l = \phi_1''/\phi'', W_t = \psi_1''/\phi''$, the above equations are rewritten as follows:

$$\frac{\kappa_1^2}{2\xi m}(1 + R) + p_1 W_l + \beta_1 W_t \tag{C24}$$

$$-\alpha_1 W_l + p_1 W_t \tag{C25}$$

$$\alpha(R - 1) - \frac{\kappa_1^2}{2\xi} W_t \tag{C26}$$

By solving the above equations, we obtain

$$R = \frac{\left\{4m\alpha\xi^2\left(\alpha_1\beta_1 + p_1^{\,2}\right) - \alpha_1\kappa_1^4\right\}}{\left\{4m\alpha\xi^2\left(\alpha_1\beta_1 + p_1^{\,2}\right) + \alpha_1\kappa_1^4\right\}} \tag{C27}$$

Impedances of liquid and solid in accordance with the longitudinal wave and the shear wave are as follows:

$$Z = \frac{\rho c}{\cos\theta}, Z_l = \frac{\rho_1 c_1}{\cos\theta_1}, Z_t = \frac{\rho_1 b_1}{\cos\gamma_1} \tag{C28}$$

Then, we obtain a reflectance function as follows:

$$R = \frac{Z_l \cos^2 2\gamma_1 + Z_t \sin^2\gamma_1 - Z}{Z_l \cos^2 2\gamma_1 + Z_t \sin^2\gamma_1 + Z} \tag{C29}$$

APPENDIX D – TRANSDUCER OUTPUT

The acoustic field at Plane 1 (*i.e.*, $u_1^+(x,y)$) is expressed as follows:

$$u_1^+(x,y) = \left\{ u_0^+ * \mathcal{F}^{-1}\left(e^{ik_z' d}\right) \right\}_{\substack{x \\ y}} \tag{D1}$$

Similarly, the reflected acoustic field (i.e., $u_0^-(x,y)$) can be expressed as follows:

$$u_0^-(x,y) = \left\{ u_1^- * \mathcal{F}^{-1}\left(e^{ik_z' d}\right) \right\}_{\substack{x \\ y}} \tag{D2}$$

$$\begin{aligned} V(z) &= \int\int_{-\infty}^{\infty} u_0^+(x',y') u_0^-(x',y') dx'dy' \\ &= \int\int_{-\infty}^{\infty} u_0^+(x',y') \left\{ u_1^- * \mathcal{F}^{-1}\left(e^{ik_z' d}\right) \right\}_{\substack{x' \\ y'}} dx'dy' \\ &= \int\int_{-\infty}^{\infty} u_0^+(x',y') \left\{ \int\int_{-\infty}^{\infty} u_1^-(\xi,\eta) \mathcal{F}^{-1}\left(e^{ik_z' d}\right)\Big|_{\substack{x=x'-\xi \\ y=y'-\eta}} d\xi d\eta \right\} dx'dy' \\ &= \int\int_{-\infty}^{\infty} u_1^-(\xi,\eta) \left\{ \int\int_{-\infty}^{\infty} u_0^+(x',y') \mathcal{F}^{-1}\left(e^{ik_z' d}\right)\Big|_{\substack{x=x'-\xi \\ y=y'-\eta}} d\xi d\eta \right\} dx'dy' \end{aligned} \tag{D3}$$

Since $k_z' = \sqrt{k_1^2 - k_x^2 - k_y^2}$ is even function of k_x and k_y, we can write

$$\mathcal{F}^{-1}\left(e^{ik_z' d}\right)\Big|_{\substack{x=x'-\xi \\ y=y'-\eta}} = \mathcal{F}^{-1}\left(e^{ik_z' d}\right)\Big|_{\substack{x=x'\xi-x' \\ y=\eta-y'}} \tag{D4}$$

Then, we can rewrite Eq. (D3) as follows:

$$
\begin{aligned}
V(z) &= \int\int_{-\infty}^{\infty} u_0^+(x',y')u_0^-(x',y')dx'dy' \\
&= \int\int_{-\infty}^{\infty} u_1^+(\xi,\eta)\left\{u_0^+ * \mathcal{F}^{-1}\left(e^{ik_z' d}\right)\right\}\Big|_{\substack{\xi \\ \eta}} d\xi d\eta \qquad \text{(D5)} \\
&= \int\int_{-\infty}^{\infty} u_1^-(\xi,\eta)u_1^+(\xi,\eta)d\xi d\eta
\end{aligned}
$$

Equation (D5) can tells that the transducer at Plane 0 can be replaced by an equivalent transducer at Plane 1. This equivalent transducer is infinite in extent and has the acoustical field given by $u_1^+(x,y)$.

APPENDIX E – DETERMINATION OF $u_1^+(x, y)$

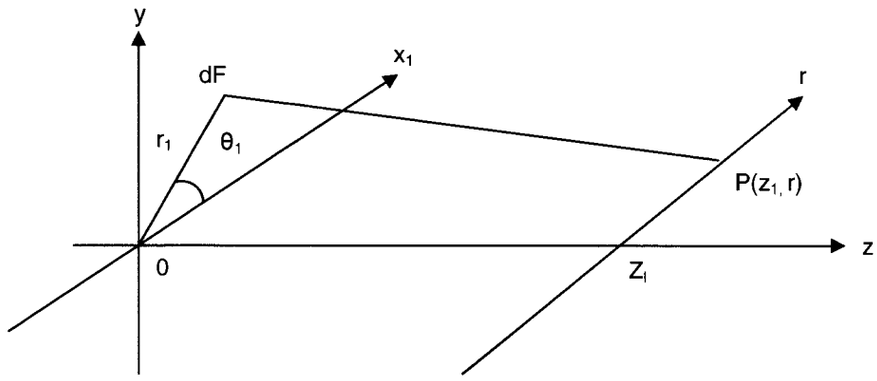

Fig. E1. Schematic diagram for showing the geometry of acoustic field from Plane 0 to Plane 1.

$$p(P) = p(z_l, r) = \frac{i\rho ck\omega_0}{2\pi} \int_F \frac{e^{ik\rho'}}{\rho'} dF \cdot e^{-i\omega t} \tag{E1}$$

$$\rho' \cong z_l + \frac{r^2}{2z_l} - \frac{r_1 r}{z_l}\cos\theta_1 + \frac{r^2}{2z_l} \tag{E2}$$

$$\frac{1}{\rho'} \cong \frac{1}{z_l} \tag{E3}$$

Input Eq. (E3) into (E1), we obtain

$$
\begin{aligned}
p(z_l,r) &= \frac{i\rho ck\omega_0}{2\pi}\frac{e^{-i\omega t}}{z_l}\int_0^{a_t}\int_0^{2\pi} e^{-ik\left(z_l+\frac{r^2}{2z_l}-\frac{r_1 r}{z_l}\cos\theta_1+\frac{r_1^2}{2z_l}\right)} r_1\cdot dr_1\cdot d\theta_1 \\
&= \frac{i\rho ck\omega_0}{2\pi z_l} e^{-i\left\{\omega t-k\left(z_l+\frac{r^2}{2z_l}\right)\right\}}\int_0^{a_t} e^{ik\frac{r^2}{2z_l}}\int_0^{2\pi} e^{-ik\frac{r_1 r}{z_l}\cos\theta_1} d\theta_1\cdot r_1 dr_1 \\
&= \frac{i\rho ck\omega_0}{2\pi z_l} e^{-i\left\{\omega t-k\left(z_l+\frac{r^2}{2z_l}\right)\right\}}\int_0^{a_t} e^{ik\frac{r^2}{2z_l}} J_0\left(\frac{kr_1 r}{z_l}\right) r_1 dr_1 \\
&= i\rho ck\omega_0 e^{-i\left\{\omega t-k\left(z_l+\frac{r^2}{2z_l}\right)\right\}} I(z_l,r)
\end{aligned}
\qquad \text{(E4)}
$$

where

$$
I(z_l,r) = \frac{e^{ik\frac{r^2}{2z_l}}}{z_l}\int_0^{a_t} e^{ik\frac{\xi^2}{2z_l}} J_0\left(\frac{k\xi r}{z_l}\right)\xi d\xi \qquad \text{(E5)}
$$

Finally,

$$
u_1^+(z_l,r) = \frac{I(z_l,r)}{I(z_l,0)} \qquad \text{(E6)}
$$

APPENDIX F – SAW VELOCITY MEASUREMENT

From the analogy of V(z) curves to effects in physical optics, it is natural to consider the V(z) as a result of acoustic ray interference. Consequently, a physical model of the V(z) effect has been proposed, which essentially regards V(z) as an interference between two families of acoustic rays (see Fig. F1).

One component, A, is a family of specularly reflected acoustic rays at almost normal incidence from the surface of the specimen. The second component, B, is a family of laterally displaced leaky Rayleigh waves (non-specular reflection), symmetrical to the incident beam. These two beams, A and B, arrive at the transducer and produce an output signal.

The interference of rays with differing paths gives the period Δz of the resulting oscillations in V(z) as follows. The phase difference between the two rays is given as follows:

$$\begin{aligned}\Delta\phi &= \left(2z - 2z\sec\theta_R + 2z\tan\theta_R \sin\theta_R\right)k_w + \pi \\ &= 2z\left[1 - \sec\theta_R\left(1-\sin^2\theta_R\right)\right]k_w + \pi \\ &= 2k_w z\left(1-\cos\theta_R\right) + \pi\end{aligned} \qquad \text{(F1)}$$

where $k_w = 2\pi/\lambda_w$ is the wave number of sound in liquid and λ_w is the wavelength of sound in the liquid.

Based on the interference principle of double rays in physical optics, an interference pattern occurs in the V(z) response of the transducer. A phase change of 2π in the relative phase difference corresponds to a dip interval Δz in the V(z) curve. Using Eq. (F1) and ignoring the constant phase term π, we get oscillations of periodicity

$$\Delta z = \frac{2\pi}{2k_w\left(1-\cos\theta_R\right)} = \frac{\lambda_w}{2\left(1-\cos\theta_R\right)} \qquad \text{(F2)}$$

Finally the Rayleigh wave velocity v_R is yield to be

$$v_R = \frac{v_w}{\sqrt{1-\left(1-v_w/\left(2f\Delta z\right)\right)^2}} \qquad \text{(F3)}$$

This simple ray optics theory allows quantitative measurement of the phase velocity of a leak Rayleigh wave from the V(z) curve, and characterization of the acoustic properties of materials.

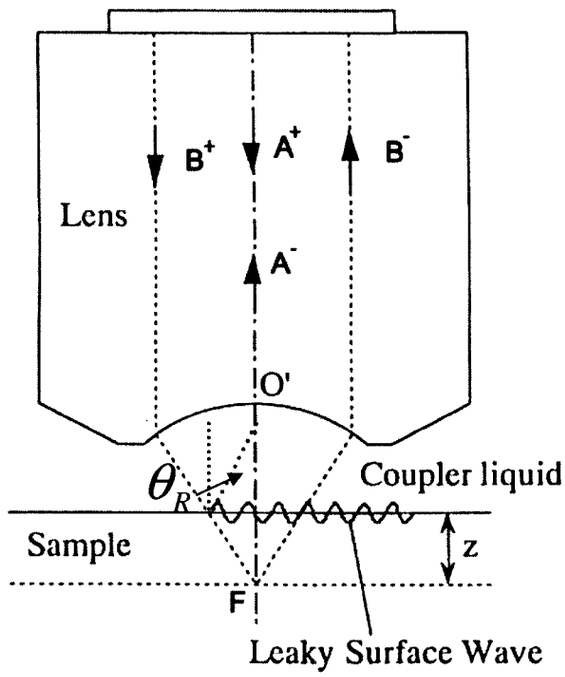

Fig. F1. Cross-sectional geometry of acoustic line-focus beam, explaining the mechanism of the V(z) curves.

REFERENCES

[1] Atalar, C. F Quate, and H. K. Wickramasinge, "Phase imaging in reflection with acoustic microscope", Appl. Phys. Lett., 31, 1977, p. 791.

[2] R. N. Johnston, A. Atalar, J. Heiserman, V. Jipson, and C. F. Quate, "acoustic microscopy: Resolution of subcellular detail",Proc. Natl Acad.. Sci. USA., 76(7), 1979, pp. 3325-3329.

[3] R. A. Lemons and C. F. Quate, "Acoustic microscope-scanning version", Appl Phys. Lett., 24(4), 1974, pp. 163-165

[4] J. L. Lamarque, A. Djoukhadar, M. J. Rodiere, J. Attal and E. Boubals, "Acoustic microscopy in the study of breast tissue" Proc. 1981 Ultrasonic Symposium, pp 565-567

[5] S. D. Bennett, and E. A. Ash, "Differential Imaging with the Acoustic Microscope", IEEE Trans. Sonic.and Ultras. SU-28(2), 1981, pp-59-64

[6] R. Gr. Maev, O. V. Lolosov, V. M. Levin, O. I. Lobkis, "Transmission acoustic microscopy investigation", Acoust Imaging 19, 1992, pp. 679-683

[7] J. A. Hildebrand, D. Rugar, R. N. Johnston, and C. F. Quate, "Acoustic microscopy of living cells," Proceedings of the National Academy of Sciences USA, 78(3), 1981, pp. 1656-1660

[8] R. Gr. Maev, "Acoustic microscopy of biological objects," Proc. Of the VII Intern. Symposium "UBIOMED-VII" WB 1986/73, Eisenach, DDR, 1986, pp. 55-58

[9] N. Chubachi, J. Kushibiki, T. Sannomiya, N. Akashi, M. Tanaka, H. Okawaki, and F. Dunn, "Scanning acoustic microscope for quantitative characterization of biological tissues," Acoust. Imaging 16, 1987, pp. 1-9

[10] V. Kolosov, V. M. Levin, R. Gr. Maev, T. A. Senjushkina, "The use of acoustic microscopy for biological tissue characterization," Ultrasound in Medicine & Biology, 13(8), 1987, pp. 477-483

[11] R. Gr. Maev, "Scanning acoustic microscopy of polymeric and biological substances," Tutorial Archives of Acoustics, 13 (1-2), 1988, pp. 13-43.

[12] P. A. N. Chandraratna, M. I. Awaad, P. Chandrasoma, and M. Khan, "High frequency ultrasound: determination of the lowest frequency required for cellular imaging and detection of myocardial pathology," Am Heart J, 129, 1995, pp. 15-9.

[13] C. M. W. Daft and G. A. D. Briggs, "The elastic microstructure of various tissues," J. Acoust. Soc. Am. 85, 1989, p. 416.

[14] K. Itoh, G. Gosung, E. Jeno, K. Kasashara, and L. Zhao, "Studies of the relationship between acoustic patterns produced by liver carcinoma in ultrasonography and in scanning acoustic microscopy," Asian Medical J., 26(9), 1983, pp. 585-597.

[15] M. Marmor, H. Wickramasinghe, and R. Lemons, Acoustic microscopy of the human retina and pigment epithelium, Invest. Opth. Vis. Sci., 16(7), 1977, pp. 660-666.

[16] F. D'Astous and F. Foster, "Frequency dependence of ultrasound attenuation and backscatter in breast tissue", Ultrasound in Medicine and Biology, 12(10) 1986, pp. 795-808.

[17] J. P. Jones, "Applications of acoustical microscopy in diagnostic medicine", Int J Imaging Syst Technol, 8, 1997, pp. 61–68.

[18] B. R. Tittmann, C. Miyasaka, A. M. Maestro, and R. R. Mercer, "Study of cellular adhesion with scanning acoustic microscopy. Special issue on high resolution ultrasonic imaging in industrial, material and biomaterial applications," IEEE Trans. Ultrason. Ferroelectr. Freq. Control, vol. 54, no. 8, pp. 1502-1513, 2007.

[19] B. R. Tittmann and C. Miyasaka, "Imaging and quantitative data acquisition of biological cells and soft tissues with scanning acoustic microscopy," in Science, Technology and Education of Microscopy: An Overview, A. Mendez-Vilas, Ed. Badajoz, Spain: Formatex, 2003, pp. 325-344

[20] F. S. Foster, C. J. Pavlin, K. A. Harasiewicz, D. A. Christopher, and D. H. Turnbull, "Advances in ultrasound biomicroscopy". Ultrasound Med Biol; 26 2000, pp. 1–27.

[21] E. Maeva, I. Bruno, and M. Docker, "Method of acoustic microscopy for sex determination of sea lamprey, petromyzon marinus, larvae". J. Fish Biol, 65, 2004, pp. 148–156.

[22] R. E. Kumon, I. Bruno, Heartwell, and E. Maeva, "Breast tissue characterization with high-frequency scanning acoustic microscopy". J. Acoust Soc Am; 115, 2004, p. 2376(A).

[23] E. Maeva, F. Severin, C. Miyasaka, B. R. Tittmann, and R. Gr. Maev, "Acoustic Imaging of Thick Biological Tissue". IEEE Trans. Ultrason, and Freq. Control, vol. 56, no. 7, July 2009

[24] Bamber J C 1997 "Acoustical characterization of Biological Media Encyclopedia of Acoustics 4th edn" (New York Wiley)

[25] J. W. Goodman, "Introduction to Fourier Optics" (McGraw Hill, New York, 1968), p. 48.

[26] D. C. Champeney, "Fourier Transformations and Their Physical Applications (Academic Press, London, 1973), p. 142

[27] Atalar, "An angular-spectrum Approach to Contrast in Reflection Acoustic Microscopy"", J. Appl Phys. 49(10) 1978, pp. 5130 – 5139

[28] M. Weichenthal, P. Mohr, and E.W. Breitbart, "The velocity of ultrasound in human primary melanoma tissue – implications for the clinical use of high resolution sonography," BMC Dermatology 1:1 (2001)

[29] C.M.W. Daft, and G.A.D. Briggs, "Wideband acoustic microscopy of tissue", IEEE Transactions on Ultrasonics. Ferroelectrics and Frequency Control, vol. 36, no. 2, (1999)

[30] Ogura, T. Kidokoro, K. Iinuma, Y. Takehara, K. Tanaka, and A. Matsuda, "Measurements of acoustic impedance of skin", Ultrasound in Medicine, Denis White and E.A. Lyons, des., vol. 4, pp. 535-543 (Plenum Press, New York, 1978)
[31] Sokolov, S. Y., "The ultrasonic microscope", *Academia Nauk SSSR Doklady* **64**, 333-5, (1949).
[32] Lemons, R. A. and Quate, C. F., "Acoustic microscope-scanning version", *Appl. Phys. Lett.* **24**, 163-5, (1974).
[33] Weglein, R. D., "A model for predicting acoustic materials signatures", *Appl. Phys. Lett.* **34**, 179-81, (1979).
[34] Parmon, W. and Bertoni, H. L., "Ray interpretation of the material signature in the acoustic microscope", Electron. *Lett.* **15**, 684-6, (1979).
[35] Atalar, A., "An angular spectrum approach to contrast in reflection acoustic microscopy", *J. Appl. Phys.* **49**, 5130-9, (1978).
[36] Hadimioglu, B. and Quate, C. F., "Water acoustic microscopy at sub-optical wavelengths", *Appl. Phys. Lett.* **43**, 1006-7, (1983).
[37] Foster and D. Rugar, "High resolution acoustic microscopy in superfluid helium", *Appl. Phys. Lett.*, **42**, 869 – 871, (1983).
[38] Muha, M. S., Moulthrop, A. A., Kozlowski, G. C., and Hadimioglu, B. "Acoustic microscopy at 15.3 GHz in pressurized superfluid helium", *Appl. Phys. Lett.* **56**, 1019-21, (1990).
[39] Chubachi, N., Kushibiki, J., Sannomia, T., and Iyama, Y. "Performance of scanning acoustic microscope employing concave transducer", *Proc. Ultraso. Symp.*, IEEE, 415-18, (1979).
[40] Davids, D. A. and We, P. Y. and Chizhik, D., "Restricted aperture acoustic microscope lens for Rayleigh wave imaging", *Appl. Phys., Lett.*, **54(17)**, 1639 – 1641, (1989).
[41] Atalar, A., Koymen, H., and Degertekin, L., "Characterization of layered materials by the Lamb wave lens", *Proc. IEEE Ultraso Symp.*, 359 – 362, (1990).
[42] Khuri-Yakub, B. T., Cinbis, C., and Reinholdtsen, P. A., "Near-field scanning acoustic microscope", *Proc. IEEE Ultraso. Symp*, 805-7, (1989).
[43] Miyasaka, C., Tittmann, B. R., and Ohno M., "Practical shear wave lens design for improved resolution with acoustic microscope", *Res Nondestr Eval* **11**: 97-116, (1999).
[44] Daft, C. W. W., Weaver J. M. R., Briggs, G. A. D., "Phase contrast imaging of tissue in the scanning acoustic microscope", *Journal of Microscopy*, **139(3)**, RP3-RP4, (1985).
[45] Kuri-Yakub, B. T., and Chou, C-H. "Acoustic microscope lenses with shear wave transducers", *Proc. IEEE Ultraso. Symp.*, 741-4, (1986).
[46] Atalar, A., Ishikawa, I., Ogura, Y. and Tomita, K., "Anisotropy sensitivity of an acoustic lens with slit aperture", *Proc. IEEE Ultrason. Symp.,* 613–6, (1993).
[47] Ujihashi, S., Skanoue, K., Adachi, T., and Matsumoto, H., "Experimental measurement of the mechanical properties of fiber-reinforced plastics under impact loading", *Proceedings of the mechanical engineering forth international conference FRC'90*, 157-162, (1990).
[48] Matsumoto, H., Adachi, T., and Ujihashi, S., "Static and impact induced damage of CFRP laminates", *Proc. Oji International Seminar on Dynamic Fracture*, 174-182, Chou Technical Drawing Co., Ltd., (1990).
[49] Kasano, K., Bea, T. S., and Miyasaka, C., "Transverse impact of CFRP laminates under static load of axial compression", *Proc., Japan-U.S. CCM-VII*, 601-8.
[50] Howard, A. M. "Evaluation of large die attach using acoustic microscopy", *IEE Colloquium on 'NDT Evaluation of Electronic Components and Assemblies'*, 3, (1990).
[51] Revay, L., Lindblad, G., and Lind, L. "IC package defects revealed by scanning acoustic microscopy (SAM)", *CERT'90; Component engineering, Reliability and Test Conference (Electron Components Inst.)*, 115-22, (1990).
[52] Bauer, R., Luniak, M., and Rebenklau L., "Realization of LTCC-Multilayer with Special Cavity Applications", *Proc. International Symposium on Microelectronics (IMAPS)*, 659-64, (1997).
[53] Adams, T. "Acoustic micro imaging in failure analysis environments", *Electronic Bulletin*, **16(6)**, 51-5, (1998).
[54] Bernier, J. C., and Teems, L., "ESD protection using active area bonding", *Proc. International Symposium for Testing and Failure Analysis (ISFTA)*, 393-8, (1998).
[55] Smith, B., "High-Throughput acoustic microimaging", *American Laboratory*, **31(22)**, 18-21, (1999).
[56] R.Gr. Maev, "New generation of high resolution ultrasonic imaging technique for advanced material characterization", *Acoustical Imaging*, vol. 29, pp. 163-172 (2008)
[57] Kushibiki, J., Horii, K., and Chubachi, N., "Velocity measurement of multiple leaky waves on germanium by line-focus-beam acoustic microscope using FFT", *Electron. Lett.* **19**, 404-5, (1983).
[58] Liang, K., Kino, G. S., and Khuri-Yakub, B. T., "Material characterization by the inversion of V(z)", *IEEE Trans.* **SU-32**, 213-24, (1985).
[59] Endo, T., Sasaki Y., Yamagishi, T., and Sakai, M., "Determination of sound velocities by high frequency complex V(z) measurement in acoustic microscopy", *Jpn. Appl. Phys.*, **31**, 160-2, (1992).
[60] Kulik, A., Gremaud, G., and Sathish, S., "Continuous wave reflection scanning acoustic microscope", *In Acoustic Imaging*, **17**, 71-8, Plenum Press, New York, (1989).
[61] Tsukahara, Y., Takeuchi, E., Hayashi, E., and Tani., Y., "A new method of measuring surface layer-thickness using dip in angular dependence of reflection coefficient", *Proc. IEEE 1984 Ultrason. Symp.*, 992-6, (1984).

[62] Nikoonahad, M., "Differential phase contrast acoustic microscopy using tilted transducers", *Electr. Lett.*, **32(10)**, 489-90, (1987).
[63] Meeks, S.W., Peter, D., Horne, D., Young, K., Novotny, V., "Microscopic imaging of residual stress using a scanning phase-measuring acoustic microscope", *Appl. Pysic, Lett.*, **55(18)**, 1835-7, (1989).
[64] Attal, J., "Acoustic microscopy with liquid metals", In Scanned image microscopy (ed. E. A. Ash), 97-118. Academic Press, London, (1980),
[65] Wickramasinghe, H. K., and Petts, C. R., "Gas medium acoustic microscopy", In *Scanned Image microscopy* (ed. E. A. Ash), 57-70. Academic Press, London, (1980).
[66] Karaki, K., and Sakai, M., "Acoustic microscope using liquid nitrogen", Ultrasonic Technology 1987, *Toyohashi International Conference on Ultrasonic Technology*, Toyohashi, Japan. (ed. K. Toda), 25-30. MYU Research, Tokyo, (1987).
[67] Yamanaka, K., Nagata, Y., and Koda T., "Low temperture acoustic microscopy with continuous temperature control", *Ultrasonics. Int. 89*, 744-9, (1989).
[68] Fox, J. D., Khuri-Yakub, B. T., and Kino, G. S., "High frequency wave measurement in air", *Proc. IEEE 1983 Ultrason. Symp.*, 581-592, (1983).
[69] Yano, T., Tone, M., and Fukumoto, A., "Range finding and surface characterization using high frequency air transducer", *IEEE Trans. Ultraso.*, Ferroelect. Frequ. Contr., **34(2)**, 222-36, (1987).
[70] Haller, M. I., and Khuri-Yakub, B. T., "1-3 composites for ultrasonic air transducer", *Proc. IEEE 1992 Ultraso. Sympo*, 937–9, (1992).
[71] Reilly, D. and Hayward, G., "Through air transmission for ultrasonic non-destructive testing", *Proc. IEEE 1991 Ultraso. Sympo*, 763–6, (1991).
[72] Schindel, D. W., Hutchins, D. A., Zou, L., and Sayer, M., "The design and characterization of micromachined air-coupled capacitance transducer", *IEEE Trans. Ultraso.*, Ferroelect. Frequ. Contr., **42**, 42-51, (1995).
[73] Ladabaum, I., Khuri-Yakub, B. T., and Spoliansky, D., "Michromachined ultrasonic transducers (MUTS): 11.4 MHz transmission in air and more", *Appl. Phys. Lett.*, 68, 7-9, (1996).
[74] Bhardwaj, M. C., Neeson, I., Langron, ME, and Vandervalk, L., "Contact-free ultrasound: The final frontier in non-destructive materials characterization", *Proc. 24th Conference: An International Conference on Engineering Ceramics & Structures, American Ceramic*, Materials, and Structures: A, 163-172, (2000).
[75] Miyasaka, C., and Tittmann, B. R., "Intermediate temperature scanning acoustic microscopy", *Proc. IEEE 1998 Ultraso. Symp.*, 1265–8, (1998).
[76] Ihara, I., Jen, C.-K., and Franca, D. R., "Material evaluation using long clad buffer rods", *Proc. IEEE 1998 Ultraso. Sympo*, 803–7, (1998).
[77] Kompfner, R., and Lemons, R. A., "Nonlinear acoustic microscopy", *Appl. Phys. Lett.*, **28(6)**, 295, (1976).
[78] Yeack, C. E., Chodorow, M., and Cuttler, C. C., "Nonlinear acoustic off-axis imaging", *Appl. Phys.*, **51(9)**, 4631, (1977).
[79] Germain, L., and Cheek, J. D. N., "Generation and detection of high-order harmonics in liquids using a scanning acoustic microscope", *J. Acoust. Soc. Am.* **83 (3)**, 942-9, (1988).
[80] Germain, L., Jacques R., and Cheek, J. D. N., "Acoustic microscopy applied to nonlinear characterization of biological media", *J. Acoust. Soc. Am.* **86 (4)**, 1560-5, (1989).
[81] Tan, M. R. T., Ransom Jr., H. L., Cutler, C. C., and Chodorow M., "Oblique, off-specular, linear, and nonlinear observations with a scanning micron wavelength acoustic microscope", *Appl. Phys.*, **57**, 4931-4935, (1985).
[82] Wickramasinghe, H. K., and Yeack, C. E., "Nonlinear imaging of an edge in the scanning acoustic microscope", *Appl. Phys.*, **48(12)**, 4951, (1977).
[83] Rugar, D., "Resolution beyond the diffraction limit in the acoustic microscope: A nonlinear effect", *Appl. Phys.*, **56**, 1338-1346, (1984).
[84] Kraki, K., Saito, T., Matsumoto, K., and Okuda, Y., "Observation of new nonlinear phenomena in focused acoustic beam in pressurized superfluid helium-4", *Physica B*, **165/166**, 131-2, (1990).
[85] Kraki, K., Saito, T., Matsumoto, K., and Okuda, Y., "Nonlinear resolution improvement and second-harmonic generation of a pressurized superfluid ^{4}He acoustic microscope", *Appl. Phys. Lett.* **59(8)**, 908-10, (1991).
[86] Burov, V. A., Gurinovich, I. E., Rudenko, O. V., and Tagunov E. Y, "Nonlinear acoustical tomography in inhomogeneous media", *In Acoustic Image,* **22**, Plenum Press, New York, 125-130, (1996).
[87] Gong X., and Zhang, D., "Nonlinearity parameter tomography-a novel imaging method in tissue characterization", *In Acoustic Image* **23**, Plenum Press, New York, 601-5, (1997).
[88] Synnevag, J., and Holm, S., "Non-linear propagation of limited diffraction beam", *Proc. IEEE 1998 Ultraso. Symp.* 1885–8, (1998).
[89] Ohono, M., Miyasaka, C. and Tittmann, B. R., "Pupli function splitting method in calculating acoustic microscopic signals for elastic discontinuities", **33**, 309-20, (2001)
[90] A. Atalar, C. F Quate, and H. K. Wickramasinge, "Phase imaging in reflection with acoustic microscope", *Appl. Phys. Lett.*, 31, p. 791, (1977)
[91] J. Bereiter-Hahn, C. H. Fox, and B. Thorell, "Quantitative reflection contrast microscopy of living cells," *J. Cell Biol.* 82, pp. 767-779, (1979)

[92] R. A. Lemons and C. F. Quate, "Acoustic microscope-scanning version", *Appl Phys. Lett.,* 24, vol 24, no.4, pp. 163-165, (1974)
[93] R.Gr. Maev, "Scanning acoustic microscopy of polymeric materials and biological substances", Review. *Tutorial Archives of Acoustics* 13(1-2): 12-43 (1988)
[94] R.Gr. Maev, V.M. Levin, R.M. Piliar, E.Yu. Maeva, and T.A. Senjushkina, "Acoustic microscopy applications for observing microstructure of bones and bone-implant systems", *Acoustic Imaging* 22:323 (1995)
[95] R. Gr. Maev, O. V. Lolosov, V. M. Levin, O. I. Lobkis, "Transmission acoustic microscopy investigation", *Acoust Imaging* 19, 1992, pp. 679-683.
[96] R.N. Johnston, A. Atalar, J. Heiserman, V. Jipson, and C.F. Quate, "Acoustic microscopy: Resolution of subcellular detail", *Proc. Natl. Acad. Sci. USA*, vol. 76, no. 7, pp. 3325-3329 (1979)
[97] Kushibiki, J. and Chubachi, N., "Material characterization by line-focused-beam acoustic microscope", *IEEE. Trans. Sonics. Ultrason.*, SU-32, 132-135, (1985)
[98] Okawai, H., Tanaka, M., Chubachi, N., and Kushibiki, J., "Non-contact simultaneous measurement of thickness and acoustic properties of a biological tissue using focused wave in a scanning acoustic microscope", Jpn. J. Appl. Phys., 26, 52-54, (1987)
[99] J. A. Hildebrand, D. Rugar, R. N. Johnston, and C. F. Quate, "Acoustic microscopy of living cells", Proceedings of the National Academy of Sciences USA, 78(3), pp. 1656-1660 (1981)
[100] P. Anthony, N. Chandraratna, J. Gallet, J.P. Jones, Yung Do, "An investigation of possible effects of high-frequency ultrasound on cellular integrity of cultured fibroblasts", Ultrasound in Med. & Biol., vol. 24, no. 6, pp. 911-914 (1998)
[101] Y. Saijo, H. Sasaki, M. Sato, S. Nitta, and M. Tanaka, "Visualization of human umbilical vein endothelial cells by acoustic microscopy", Ultrasonics 38, pp. 396-399 (2000)
[102] Hildebrand, J.A., D. Rugar, R.N. Johnston, and C.F. Quate, "Acoustic microscopy of living cells", Proc. Natl. aci. USA. 78: 1656-1660 (1981)
[103] Hildebrand, J.A., D. Rugar, and C.F. Quate, "Biological acoustic microscopy-living cells at 37°C and fixed cells in cryogenic liquids", Proc. Elect. Microsc. Soc. Am. 40: 174-177 (1982)
[104] Hildebrand, J.A., and D. Rugar, "Measurement of cellular elastic properties by acoustic microscopy", J. Micros. 134: 245-260 (1984)
[105] J. Bereiter-Hahn, "Scanning acoustic microscopy visualizes cytomechanical responses to cytochalasin D", J. Microsc. 146: 29-39 (1987)
[106] J. Bereiter-Hahn, "Comparison of the appearance of cells observed using scanning acoustic microscopy with that obtained by interference and fluorescence microscopy", Scanning Imaging Technol. 809: 162-165 (1987)
[107] J. Litniewski, and J. Bereiter-Hahn, "Measurements of cells in culture by scanning acoustic microscopy", J. Microsc. 158: 95-107 (1990)
[108] K. Beck and J. Bereiter-Hahn, "Evaluation of reflection interference contrast microscopy images of living cells", Micros. Acta, 84, pp. 153-178 (1981)
[109] H. Lüers, K. Hillmann, J. Litniewski, and J. Bereiter-Hahn, "Acoustic microscopy of cultured cell: distribution of forces and cytokeletal elements", Cell Biophys. 18, pp. 279-293 (1992)
[110] J. Bereiter-Hahn and H. Lüers, In "Mechanics of Actively Locomoting Cells", (N. Akkas, ed.) ASI series 84, Springer, Heidelberg, New York, Berlin, pp.181 (1994)
[111] J. Bereiter-Hahn, J. Litniewski, K. Hillmann, A. Krapohl, and L. Zylberberg, "What can scanning acoustic microscopy tell about animal cells and tissues?" Acoust. Imaging 17, 1992, pp. 27-38.
[112] J. A. Hildebrand and D. Rugar, "Measurement of cellular elastic properties by acoustic microscopy", J. Microsc. 134, 1990, pp. 245-246.
[113] G. A. D. Briggs, J. Wang, and R. Gundle, "Quantitative acoustic microscopy of individual living human cells", J. Microsc. 172, 1993, pp. 3-12.
[114] R. Gr. Maev, "Acoustic microscopy of biological objects," Proc. Of the VII Intern. Symposium "UBIOMED-VII" WB 1986/73, Eisenach, DDR, pp. 55-58 (1986)
[115] J. Kushibiki, A. Ohkubo, and N. Chubachi, "Effect of leaky SAW parameters on V(z) curves obtained by acoustic microscopy", Electronics Lett. 18: 668-670 (1982)
[116] J. Kushibiki, Y. Matsumoto, and N. Chubachi, "Material characterization by acoustic microscope with line-focus beam", Acoust. Imaging. Plenum Press, Nyew York, 13: 193-202 (1983)
[117] R.D. Weglein, "Acoustic microscopy applied to SAW dispersion and film thickness measurement", IEEE (Inst. Electr. Electron. Eng.) Trans. Sonics Ultrason. SU-27: 82-86 (1980)
[118] R.D. Weglein, "Non-destructive film thickness measurement on industrial diamond", Electr. Lett. 18: 1003-1004 (1982)
[119] J. Kushibiki, A. Ohkubo, and N. Chubachi, "Material characterization by acoustic line-focus beam", Acoust. Imaging. Plenum Press, New York, 12: 101-111 (1982)
[120] C.M.W. Daft, J. M. Weaver, and G.A. Briggs, "Phase contrast imaging of tissue in the scanning acoustic microscope", J. Microsc. 139: RP3-RP4 (1985)
[121] K. Yamanaka, Y. Enomoto, and Y. Tsuya, "Application of scanning acoustic microscopy to the study of fracture and wear", Acoust. Imaging. Plenum Press, New York, 12: 79-87 (1982)
[122] K. Liang, B.T. Khuri-yakub, S.D. Bennett, and G.S. Kino, "Phase measurements in acoustic microscopy", Proc. Ultrasonics Symp. Atlanta USA, 2: 591-604 (1983)

[123]J.A. Hildebrand, and D. Rugar, "Measurement of cellular elastic properties by acoustic microscopy", J. Micros. 134: 245-260 (1984)
[124]P.K. Bhagat and W. Kerrick, "Ultrasonic characterization of aging in skin tissue", Ultrasound in Med. & Biol., vol. 6, pp. 369-375 (1980)
[125]N. Chubachi, J. Kushibiki, T. Sannomiya, N. Akashi, M. Tanaka, H. Okawaki, and F. Dunn, "Scanning acoustic microscope for quantitative characterization of biological tissues" Acoust. Imaging 16, 1987, pp. 1-9.
[126]V. Kolosov, V. M. Levin, R. Gr. Maev, T. A. Senjushkina, "The use of acoustic microscopy for biological tissue characterization," Ultrasound in Medicine & Biology, 13(8), 1987, pp. 477-483.
[127]R. Gr. Maev, "Scanning acoustic microscopy of polymeric and biological substances," Tutorial Archives of Acoustics, 13 (1-2), 1988, pp. 13-43.
[128]J. Bereiter-Hahn, J. Litniewski, K. Hillmann, A. Karapohl, and L. Zylberberg, "What can scanning acoustic microscopy tell about animal cells and tissues?", Acoust. Imaging 17, 1988, pp. 27-38.
[129]N. Akashi, J. Kushibiki, N. Chubachi, and F. Dunn, "Considerations for quantitative characterization of biological tissues by scanning acoustic microscopy", Acoust. Imaging 17, 1989, pp. 183-191.
[130]P. A. N. Chandraratna, M. I. Awaad, P. Chandrasoma, and M. Khan, "High frequency ultrasound: determination of the lowest frequency required for cellular imaging and detection of myocardial pathology", Am Heart J, 129, 1995, pp. 15-9.
[131]C. M. W. Daft and G. A. D. Briggs, "The elastic microstructure of various tissues", J. Acoust. Soc. Am. 85, 1989, p. 416.
[132]K. Itoh, G. Gosung, E. Jeno, K. Kasashara, and L. Zhao, "Studies of the relationship between acoustic patterns produced by liver carcinoma in ultrasonography and in scanning acoustic microscopy", Asian Medical J., 26(9), 1983, pp. 585-97.
[133]M. Marmor, H. Wickramasinghe, and R. Lemons, "Acoustic microscopy of the human retina and pigment epithelium", Invest. Opth. Vis. Sci., 16(7), 1977, pp. 660-66.
[134]F. D'Astous and F. Foster, "Frequency dependence of ultrasound attenuation and backscatter in breast tissue", Ultrasound in Medicine and Biology, 12(10) 1986, pp. 795-808.
[135]J. P. Jones, "Applications of acoustical microscopy in diagnostic medicine", Int J Imaging Syst Technol, 8, 1997, pp. 61–68.
[136]F. S. Foster, C. J. Pavlin, K. A. Harasiewicz, D. A. Christopher, and D. H. Turnbull, "Advances in ultrasound biomicroscopy". Ultrasound Med Biol; 26 2000, pp. 1–27.
[137]E. Maeva, I. Bruno, and M. Docker, "Method of acoustic microscopy for sex determination of sea lamprey, petromyzon marinus, larvae". J. Fish Biol, 65, 2004, pp. 148–156.
[138]R. E. Kumon, I. Bruno, Heartwell, and E. Maeva, "Breast tissue characterization with high-frequency scanning acoustic microscopy". J. Acoust Soc Am; 115, 2004, p. 2376(A).
[139]Barr, R.J., White, G.M., Jones, J.P., Shaw, L.B., and Ross, P.A., "Scanning acoustic microscopy of neoplastic and inflammatory cutaneous tissue specimens", J. Invest. Dermatol., 96, 38-42, 1991.
[140]Jones, J.P., "Applications of acoustical microscopy in dermatology", in Ultrasonic Tissue characterization, Dunn, F., Tanaka, M., Ohtsuki, S., and Saijo, Y., Eds., Springer-Verlag, Tokyo, 201-212, 1996.
[141]Saijo, Y., Tanaka, M., Okawai, H., and Dunn, F., "The ultrasonic properties of gastric cancer tissues obtained with a scanning acoustic microscope system", Ultrasound Med. Biol., 17, 709-714, 1991.
[142]Sasaki, H., Saijo, Y., Tanaka, M., Okawai, H., Terasawa, Y., Yambe, T., and Nitta, S., "Influence of tissue preparation on the high-frequency acoustic properties of normal kidney tissue", Ultrasound Med. Biol., 22, 1261-1265, 1996.
[143]Saijo, Y., Tanaka, M., Okawai, H., Sasaki, H., Nitta, S., and Dunn, F., "Ultrasonic tissue characterization of infracted myocardium by scanning acoustic microscopy", Ultrasound Med. Biol., 23, 77-85, 1997.
[144]Chandraratna, P.A.N., Whittaker, P., Chandraratna, P.M., Gallet, J., Kloner, R.A., and Hla, A., "Characterization of collagen by high-frequency ultrasound: Evidence for different acoustic properties based on collagen fiber morphologic characteristics", Am. Heart J., 133, 364-368, 1997.
[145]Saijo, Y., Sasaki, H., Okawai, H., Nitta, S., Tanaka, M., "Acoustic properties of atherosclerosis of human aorta obtained with high-frequency ultrasound", Ultrasound Med Biol., 24, 1061-1064, 1998.
[146]P.K. Bhagat and W. Kerrick, "Ultrasonic characterization of aging in skin tissue," Ultrasound in Med. & Biol., vol. 6, pp. 369-375 (1980)
[147]J.H. Cantrell, R.E. Goans, and R.L. Roswell, "Acoustic impedance variations at burn-nonburn interfaces in porcine skin," J. Acoust. Soc. Am., vol. 64, pp. 731-735 (1978)
[148]F.K. Forster, J.E. Olerud, M.A. Riederer-Henderson, and A.W. Holmes, "Ultrasonic assessment of skin and surgical wounds utilizing backscatter acoustic techniques to estimate attenuation," Ultrasound in Med. & Biol., vol. 16, pp. 43-53 (1990)
[149]J.E. Olerud, W. O'Brien, M.A. Riederer-Henderson, D. Steiger, F.K. Forster, C. Daly, D.J. Ketterer and G.F. Odland, "Ultrasonic assessment of skin and wounds with the scanning acoustic microscope," J. of Invest. Dermatol., vol. 88, pp. 615-623 (1987)
[150]J.E. Olerud, W.D O'Brien, M.A. Riederer-Henderson, D.L. Steiger, J.R Debel, and G.F. Odland, "Correlation of tissue constituents with the acoustic properties of skin and wound," Ultrasound in Med. & Bio., vol. 16, pp. 55-64 (1990)

[151]M.A. Riederer-Henderson, J.E. Olerud, W.D. O'Brien, F.K. Forster, D.L. Steiger, D.J. Ketterer and G.F. Odland, "Biochemical and acoustic parameters of normal canine skin," IEEE Transactions on Biomed. Eng., vol. 35(11), pp. 967-972 (1988)
[152]T. Baldeweck, P. Laugier, and G. Berger, "Ultrasound attenuation estimation in highly attenuating media: Application to skin characterization," Acoustical Imaging, vol. 22, pp. 341-348 (1996)
[153]J. Kushibiki, "Material characterization by Line-Focus-Beam acoustic microscope," IEEE Transactions on Sonics & Ultrasonics, vol. SU-32, no. 2, pp. 189-212 (1985)
[154]T. Gaertner, K.V. Jenderka, H. Schneider, and H. Heynemann, "Tissue characterization by imaging of acoustical parameters," Acoustical Imaging, Plenum Press, New York, vol. 22, pp. 365-370 (1996)
[155]Bruno, R.E. Kumon, B. Heartwell, E. Maeva, and R.Gr. Maev, "Ex Vivo breast tissue imaging and characterization using acoustic microscopy," Phys. & Astro., Acoustical Imaging, vol. 28, pp. 279-287 (2007)
[156]E. Maeva, F. Severin, C. Miyasaka, B.R. Tittmann, and R.Gr. Maev, "Acoustic imaging of thick biological tissue", IEEE Transactions on Ultrasonics, Ferroelectrics, and Frequency Control, vol. 56, no. 7, pp. 1352-1357 (2009)
[157]C. Miyasaka, B.R. Tittmann, R. Tutwiler, Y. Tian, E. Maeva, and D. Shum, "Systematic approach to study of thinly and thickly sectioned melanoma tissues with scanning acoustic microscopy," Proc. Of SPIE, vol. 7650, no. 2U, pp. 1-9 (2010)
[158]B. R. Tittmann, and C. Miyasaka, "Scanning Acoustic Microscopy". In Encyclopedia of Imaging Science and Technology, edited by Joseph P. Hornack, pp. 1228-1248. New York: Wiley. 2002.
[159]Wells, P.N.T., Biomedical Ultrasonics (Academic Press, London, 1977)
[160]B.T. Khuri-Yakub and C-H. Chou, (1986). "Acoustic microscope lenses with shear wave transducers", *IEEE Ultrasonics Symposium*, p. 741-744.
[161]C.-H. Chou, B. T. Khuri-Yakub, and K. K. Liang, (1987) "Acoustic microscopy with shear wave transducers," in *IEEE Ultrason. Proc.*, pp. 813-816.
[162]Atalar, A. (1978). "An angular spectrum approach to contrast in reflection acoustic microscopy". *J. Appl. Phys.* **49**, pp. 5130-5139
[163]Weglein, R. D. (1979). "A model for predicting acoustic materials signatures". *Appl. Phys. Lett.* **34**, 179-81.
[164]A. Atalar, (1979). "A physical model for acoustic signature", J. Appl. Phys., *50*, 12, p. 8237
[165]Parmon, W. and Bertoni, H. L. (1979). "Ray interpretation of the material signature in the acoustic microscope". *Electron. Lett.* **15**, 684-6.
[166]Kushibiki, J., Horii, K., and Chubachi, N., (1983). "Velocity measurement of multiple leaky waves on germanium by line-focus-beam acoustic microscope using FFT". *Electron. Lett.* **19**, 404-5.
[167]Liang, K., Kino, G. S., and Khuri-Yakub, B. T., (1985). "Material characterization by the inversion of V(z)". *IEEE Trans.* **SU-32**, 213-24
[168]Endo, T., Sasaki Y., Yamagishi, T., and Sakai, M., (1992). "Determination of sound velocities by high frequency complex V(z) measurement in acoustic microscopy". *Jpn. Appl. Phys.*, **31**, 160-2.
[169]Kulik, A., Gremaud, G., and Sathish, S., (1989). "Continuous wave reflection scanning acoustic microscope", *In Acoustic Imaging*, **17**, 71-8, Plenum Press, New York
[170]B. R. Tittmann and C. Miyasaka, "Imaging and quantitative data acquisition of biological cells and soft tissues with scanning acoustic microscopy," *Science, Technology and Education of Microscopy: An Overview.* Fomatex: Badajoz, Spain, 2003, p. 325
[171]B. R. Tittmann, C. Miyasaka, A. M. Mastro, R. R. Mercer, (2007) "Study of Cellular Adhesion with Scanning Acoustic Microscopy", *IEEE Transactions on Ultrasonics, Ferroelectics and Frequency Control.*, vol. 54, no. 8
[172]Atalar, A., Quate, C. F., and Wickramasinge, H. K., (1977). "Phase imaging in reflection with acoustic microscope", *Appl. Phys. Lett.*, 31, 791
[173]J. Kushibiki and N. Chubachi, (1985). "Material characterization by line-focus beam acoustic microscope", *IEEE Trans. SU-32*, p189,
[174]T. Kundo, J. Bereiter-Hahn, and, K. Hillmann, "Measuring elastic properties of cells by evaluation of scanning acoustic microscopy V(Z) values using simplex algorithm," *Biophsy. J. 56*, pp. 1194-1207, 1991
[175]Y. Sasaki, T. Endo, T. Yamagishi, and M. Sakai, (1992) "Thickness Measurement of Thin-Film Layer on an Anisotropic Substrate by Phase-Sensitive Acoustic Microscope", IEEE Trans. Ultrason., vol.39, No. 5, p. 638.
[176]T. Endo, C. Abe, M. Sakai, and M. Ohno, (1993). "Measurement of Dispersion Relation in Acoustic Velocities for the thin film on an anisotropic substrate using acoustic microscope", *IEEE Ultrason. Inter.* '93, Proc. p. 45
[177]C. Miyasaka, B. R. Tittmann, and S. Tanaka, (2002)."Characterization of Stress at a Ceramic/Metal Joint Interface by the V(z) Technique of Scanning Acoustic Microscopy," *Journal of Pressure Vessel Technology* Vol 124, No. 3, pp.336-342,
[178]C. Miyasaka, B. R. Tittmann, and S. Tanaka, (2002). "Stress Characterization of a Ceramic/Metal Jointed Interface Collimated X-Ray Beam Radiography and Scanning Acoustic Microscopy," *Nondestructive Testing and Evaluation,* Vol. 18, 3-4, pp.131-148
[179]T. Kundu, (1992), "A complete acoustic microscopical analysis of multilayered specimen", *J. Appl Mech*, **59**, pp.54-60

[180] M. Weichenthal, P. Mohr and E. W. Breitbart, (2001). "The velocity of ultrasound in human primary melanoma tissue-implications for the clinical use of high resolution sonography", *BMC Dermatology* 1:1

[181] K. Zell, J.I. Sperl, M.W. Vogel, R. Niessner and C. Haisch, (2007). "Acoustical properties of selected tissue phantom material for ultrasound imaging", *Phys. Med. Biol.* **52** N475-N484

[182] Inte Onsman, (2003). "In quest of events leading to pigmentary disorders in several mutants of the budgerigar; a light and electron microscopical survey", MUTAVI, Research & Advice Group, The Netherlands

VITA AUCTORIS

I was born in Baoding, Hebei, P.R.CHINA in 1984. I came to Canada on 2003 and enrolled at the University of Windsor as an international student and had my degree of BSc Honours in Physics and High Technology program in 2008. During the final year of my bachelor degree I was really keen into the research of acoustic microscopy application and it first brought me in contact with Dr. E. Maeva, who mentored me throughout my undergraduate research. In her lab there are a lot of relevant studies. I accomplished a study of breast cancer tissue with scanning acoustic microscopy under her guidance. Directly after that I applied for my Master's degree at the University of Windsor, continuing the research I had begun in my undergraduate program. It was under the supervision of Dr. E. Maeva and Dr. Miyasaka, who is a professor at Penn State University, that I completed the work presented here.